ERDC/CHL TR-23-9

US Army Corps
of Engineers®
Engineer Research and
Development Center

Houston Ship Channel Numerical Model Update and Validation

Jennifer McAlpin and Cassandra Ross

August 2023

Coastal and Hydraulics Laboratory

The US Army Engineer Research and Development Center (ERDC) solves the nation's toughest engineering and environmental challenges. ERDC develops innovative solutions in civil and military engineering, geospatial sciences, water resources, and environmental sciences for the Army, the Department of Defense, civilian agencies, and our nation's public good. Find out more at www.erdc.usace.army.mil.

To search for other technical reports published by ERDC, visit the ERDC online library at https://erdclibrary.on.worldcat.org/discovery.

ERDC/CHL TR-23-9
August 2023

Houston Ship Channel Numerical Model Update and Validation

Jennifer McAlpin and Cassandra Ross

US Army Engineer Research and Development Center
Coastal and Hydraulics Laboratory
3909 Halls Ferry Road
Vicksburg, MS 39180-6199

Final report

Prepared for US Army Corps of Engineers, Galveston District
Galveston, TX 77550

Under MIPR No. W45VAK11672077

Abstract

The Houston Ship Channel (HSC) is one of the busiest deep-draft navigation channels in the United States and must be able to accommodate increasing vessel sizes. The US Army Corps of Engineers, Galveston District (SWG), requested the US Army Engineer Research and Development Center, Coastal and Hydraulics Laboratory, update and revalidate a previously developed three-dimensional Adaptive Hydraulics (AdH) hydrodynamic and sediment model of the HSC, Galveston, and Trinity Bays. The model is necessary for analyzing potential impacts on salinity, sediment, and hydrodynamics due to alternatives designed to reduce shoaling in the HSC.

SWG requested an updated validation of the previously developed AdH model of this area to calendar years 2010 and 2017, utilizing newly collected sediment data. Updated model inputs were supplied for riverine suspended sediment loads as well as for the ocean tidal boundary condition. The updated model shows good agreement to field data in most conditions but also indicates potential issues with freshwater flow inputs as well as the ocean salinity boundary condition.

Contents

Figures and Tables

Figures

Tables

Preface

The model investigation was conducted for the US Army Corps of Engineers, Galveston District, under MIPR No. W45VAK11672077.

The work was performed at the US Army Engineer Research and Development Center (ERDC), Coastal and Hydraulics Laboratory (CHL), Vicksburg, MS, under the general direction of Dr. Ty V. Wamsley, director, and Mr. Keith Flowers, deputy director, ERDC-CHL. Direct supervision was provided by Dr. Cary A. Talbot, chief, Flood and Storm Protection Division, and Mr. Casey Mayne, acting chief, River and Estuarine Engineering Branch.

Portions of this report have been modified and reprinted from Jennifer, McAlpin, Cassandra Ross, and Jared McKnight, *Houston Ship Channel and Vicinity Three Dimensional Adaptive Hydraulics (AdH) Numerical Model Calibration/Validation Report,* ERDC/CHL TR-19-10 (Vicksburg, MS, US Army Engineer Research and Development Center, Coastal and Hydraulics Laboratory, 2019), http://dx.doi.org/10.21079/11681/33063. Public domain.

Portions of this report have been modified and reprinted from Jennifer, McAlpin, Jared McKnight, and Cassandra Ross, *Houston Ship Channel Expansion Channel Improvement Project (ECIP) Numerical Modeling Report,* ERDC/CHL TR-19-12 (Vicksburg, MS, US Army Engineer Research and Development Center, Coastal and Hydraulics Laboratory, 2019), http://dx.doi.org/10.21079/11681/33334. Public domain.

COL Christian Patterson was commander of ERDC, and the director was Dr. David W. Pittman.

1 Introduction

1.1 Background

Since the early 1800s, vessels have transited Galveston Bay both to and from Galveston and Houston (Galveston Bay Estuary Program 2002). Galveston Bay is a tidal estuary such that the effect of the tide on the water surface elevation is observed from the Gulf of Mexico to locations near Houston, Texas. The Houston Ship Channel (HSC) is a deep-draft navigation channel that allows for vessel passage from the Gulf to the City of Houston, approximately 53 mi* upstream. Since 1903, operations and maintenance dredging has been conducted in the bay portion to maintain authorized channel dimensions. Figure 1 shows the HSC as it passes through Galveston Bay from its entrance at Bolivar Roads to the Port of Houston.

Figure 1. Houston Ship Channel (HSC) area map.

* For a full list of the spelled-out forms of the units of measure and unit conversions used in this document, please refer to *US Government Publishing Office Style Manual*, 31st ed. (Washington, DC: US Government Publishing Office 2016), 248–52 and 345–347, respectively. https://www.govinfo.gov/content/pkg/GPO-STYLEMANUAL-2016/pdf/GPO-STYLEMANUAL-2016.pdf.

In 2005, The US Army Corps of Engineers (USACE), Galveston District (SWG), enlarged the HSC from a 40 ft depth by 400 ft width to a 45 ft depth by 530 ft width. Prior to the enlargement, a 3D numerical model study was implemented at the US Army Engineer Research and Development Center (ERDC), Coastal and Hydraulics Laboratory (CHL), to evaluate the salinity and circulation impact of this enlargement. In Berger et al. (1995a), the model was shown to represent the salinity and circulation in the earlier channel configuration. Berger et al. (1995b) used the model to predict the impact of the enlarged channel. Carrillo et al. (2002) used the model to evaluate the addition of barge lanes along the ship channel flanks. Tate and Berger (2006) looked into possible reasons for increased shoaling in the ship channel by analyzing vessel effects and sediment properties in the area. In Tate et al. (2008), the sediment model was validated using the same hydrodynamic model from 2006, and the results included the effects of vessel transport on the sedimentation patterns. The model was utilized again to investigate proposed changes to the Bayport Flare (Tate and Ross 2012).

The deep navigation channel acts as a natural pathway for salinity to travel upstream since high-saline water is denser than fresh water and tends to flow upchannel along the channel bottom. The residual velocity, or net drift, is flood in much of the channel (Tate and Berger 2006) (i.e., the tendency is for suspended material to move upstream into Galveston Bay.) The velocity magnitudes drop in the Atkinson Island reach due to tidal reflections from the bay boundaries. More stratification occurs as a result in this reach, and material from farther downstream in the estuary will tend to collect near Atkinson Island.

The behavior of the salinity and hydrodynamics in Galveston Bay during May through June is different than the remainder of the year due to a salinity drop in the northern Gulf of Mexico as the Mississippi, Sabine-Neches, Atchafalaya, and other northern Gulf river systems provide a significant influx of fresh water. When the salinity in the Gulf of Mexico drops, the salt water tends to evacuate from the bays (Berger et al. 1995a). A reduction in bay salinity is hypothesized to result in different suspended sediment concentrations. Therefore, fresh deposit characteristics may change during this time period when compared to data collected at other times during the year. If this is the case, sediment would tend to collect farther down the channel toward Red Fish Reef during this late springtime period.

1.2 Objective

In 2016, the SWG requested ERDC-CHL perform hydrodynamic and sediment transport modeling of proposed modifications along the HSC from its connection at the Gulf of Mexico to the Port of Houston (Figure 2). The modeling results are necessary to provide data for salinity and sediment transport analysis as well as ship-simulation studies in which pilots test the navigation effects of the modifications. The model results of project year zero (2029) and project year 50 (2079) with and without project results were documented in McAlpin et al. 2019a.

In early 2020, the Port of Houston Authority (PHA) requested modeling for two additional channel widths in the bay portion of the HSC (HSC Stations 138+000 to 0+000; labeled from 1 to 13 in Figure 2). These widths are necessary for ship simulation such that an adequate channel width can be determined for safe navigation. Previously, a 650 ft channel width was simulated. McAlpin and Ross (2020) include the analysis for channel widths of 700 ft and 750 ft.

Additionally, SWG requested simulations to analyze impacts on hydrodynamics, salinity, and sediment transport due to the closure of Rollover Pass (completed in September 2019 but remained opened in all previous model simulations), the addition of Bay Aquatic Beneficial Use System (BABUS) sites and proposed Bird Islands, as well as the combined impact of these additions with the Expansion Channel Improvement Project (ECIP) Project 11 modifications. Results from these simulations are provided in McAlpin and Ross (2021).

In 2021, SWG and the PHA sponsored a data collection effort by Texas A&M University–Galveston (TAMUG). This effort was to collect bed-sediment data as well as velocity transects, salinity, and suspended-sediment concentrations in the San Jacinto Bay west of Atkinson Island. The objective of the work presented in this report is to incorporate as much of these data as possible into the model by performing an update to the previous model-validation effort. Once updated and validated, the model will be used to analyze the impacts of proposed modifications to the area with the purpose of reducing the shoaling in the flare areas of the HSC—where the Bayport and Barbours Cut channels join the HSC.

Figure 2. Proposed modifications to the HSC (figure from Galveston District [SWG]).

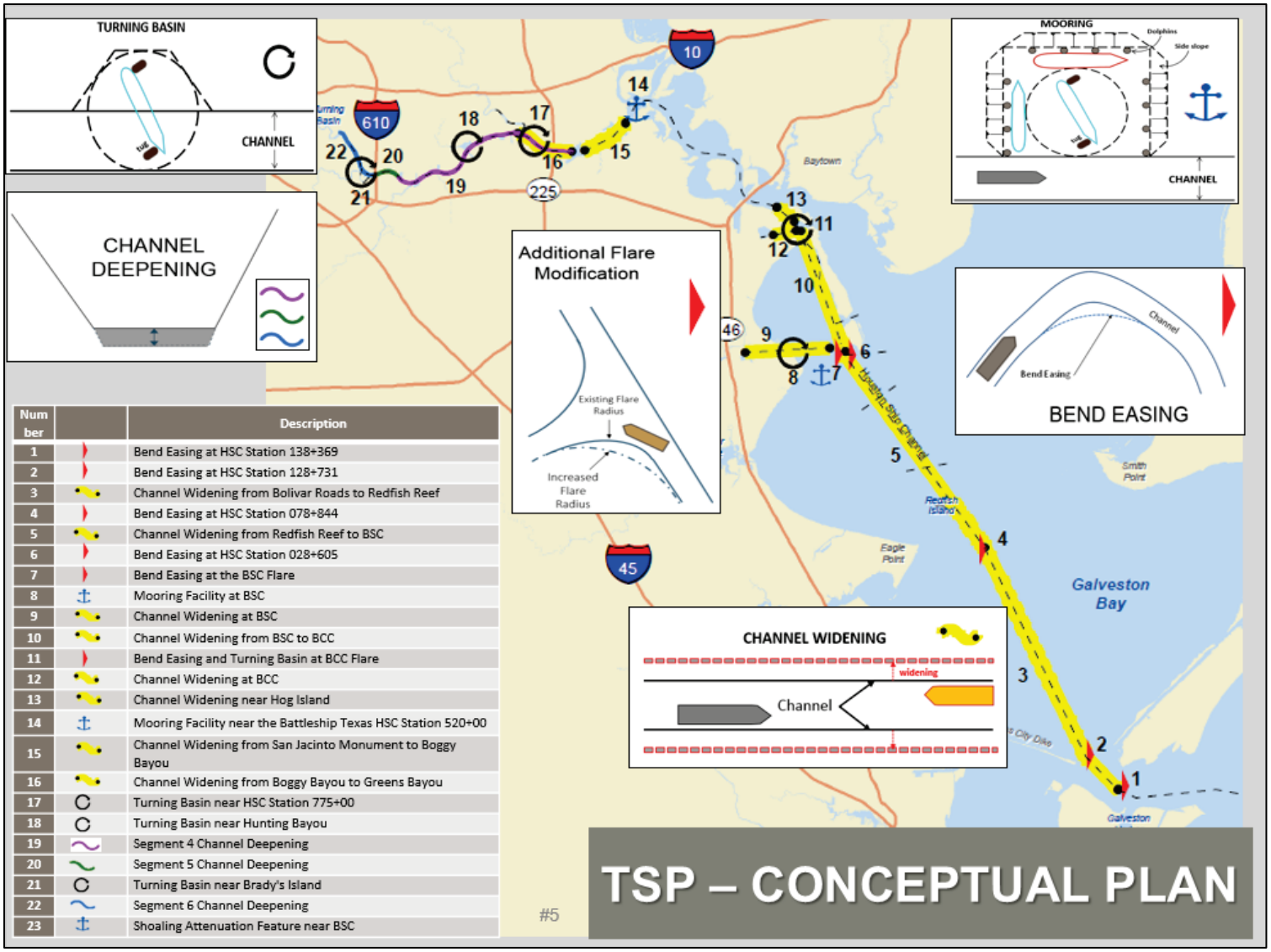

Number		Description
1		Bend Easing at HSC Station 138+369
2		Bend Easing at HSC Station 128+731
3		Channel Widening from Bolivar Roads to Redfish Reef
4		Bend Easing at HSC Station 078+844
5		Channel Widening from Redfish Reef to BSC
6		Bend Easing at HSC Station 028+605
7		Bend Easing at the BSC Flare
8		Mooring Facility at BSC
9		Channel Widening at BSC
10		Channel Widening from BSC to BCC
11		Bend Easing and Turning Basin at BCC Flare
12		Channel Widening at BCC
13		Channel Widening near Hog Island
14		Mooring Facility near the Battleship Texas HSC Station 520+00
15		Channel Widening from San Jacinto Monument to Boggy Bayou
16		Channel Widening from Boggy Bayou to Greens Bayou
17		Turning Basin near HSC Station 775+00
18		Turning Basin near Hunting Bayou
19		Segment 4 Channel Deepening
20		Segment 5 Channel Deepening
21		Turning Basin near Brady's Island
22		Segment 6 Channel Deepening
23		Shoaling Attenuation Feature near BSC

1.3 Approach

Previously, a 3D Adaptive Hydraulics (AdH) model was developed and validated for simulation of hydrodynamics, salinity, and sediment transport (Savant and Berger 2015). The AdH code solves the shallow-water equations to compute depth and velocity at node points defining the domain. AdH includes a linkage to the SEDLIB sediment transport library that computes cohesive and noncohesive erosion and deposition, which is then transported by the AdH code. Flocculation of sediment is not included in AdH but is somewhat accounted for by manipulation of sediment grain size and settling velocity. All models are limited by the data used to define them, and uncertainty in model boundary conditions must be considered when reviewing the model results and determining their applicability to the specific project. The model was validated to available field data for all parameters (McAlpin et al. 2019b) and then utilized to test project alternatives for present and future conditions (McAlpin et al. 2019a). For all simulations, the model was set up to run for 2 yr—the first year being a spin-up period to obtain an accurate initial salinity field as well as an accurate sediment bed, and the second year was used for all analyses. The same method is continued for all modeling presented in this report.

This document will address updates to the previous boundary condition development and validation process due to newly collected field data. Once validated, the model will be used to simulate both present and future boundary conditions (updated accordingly) as well as alternatives designed to reduce shoaling in the HSC, not presented in this document.

2 Model Development

A numerical model was developed to analyze alternative plans for the HSC and surrounding area as well as to provide hydrodynamic data for ship-simulation studies. The model was developed such that the natural driving forces of the system are included—winds, tides, salinity, freshwater inflows, friction effects, and sediment behavior. The model is compared to field data collected during the simulation period to ensure an accurate representation of nature. This model is validated using data from 2010 and 2017 (Hurricane Harvey).

2.1 Numerical Code

AdH is the numerical model code applied for the simulations in this study (Savant et al. 2014; Savant and Berger 2015). AdH is a finite element code that is capable of simulating 3D Navier-Stokes equations, 2D and 3D shallow-water equations, and groundwater equations. It can be used in a serial or multiprocessor mode on personal computers and high-performance computing systems. AdH can refine the domain mesh in areas where more resolution is needed at certain times due to changes in the flow conditions and then remove the added resolution when it is no longer needed, to minimize computational burden. The code also includes automatic time-step adaption, as needed. AdH can simulate the transport of conservative constituents, such as dye clouds, as well as simulate sediment transport, when used with SEDLIB, that is coupled to bed and hydrodynamic changes. This code has been applied to model riverine flow (Bell et al. 2017; Clifton et al. 2017) estuarine circulation (Tate et al. 2009; McAlpin et al. 2013), and sediment transport (Sharp et al. 2013; Heath et al. 2015; Letter et al. 2015).

SEDLIB is a sediment transport code that allows for the simulation of noncohesive (sand), cohesive (silt and clay), and mixed sediments. Each grain class is tracked separately yet allowed to mix as necessary in multiple bed layers. SEDLIB calculates erosion and deposition simultaneously and includes bed processes such as armoring, consolidation, and discrete depositional layer evolution.

For this study, the 3D shallow-water module of AdH is applied for all simulations. This code solves for depth and velocity throughout the model domain. More details of the 3D shallow-water module of AdH and its

computational philosophy and equations are available in Savant et al. 2014 and Savant and Berger 2015. AdH version 4.7 was applied for this study.

2.2 Mesh Development

Since the updated model validation was performed using 2010 and 2017, the previously developed model domain (McAlpin et al. 2019b) was adjusted only to smooth resolution or capture any missing features noted in the previous modeling efforts. Since 2017 includes Hurricane Harvey, which was a high rainfall and runoff event, the model domain had to be adjusted at the river inflow locations to account for the large amount of water entering the system. The 3D AdH code does not allow for wetting and drying of elements, so the full flow during the event must enter through the meshed channels, not extend into overbank areas. Forcing this high flow through the typically wet channel width created areas of supercritical flow that were not representative of the actual event. This modified mesh, though, will not be used for later alternative simulations since those will be simulating more average flow conditions (McAlpin et al. 2019a) as opposed to extreme flow conditions such as Hurricane Harvey. Although understanding how the alternatives perform under extreme conditions is important, initial design assessments should be made utilizing typical flow conditions for the region.

The domain is defined horizontally in Universal Transverse Mercator zone 15 coordinates with units of meters. Vertically it is based on North American Vertical Datum of 1988 (NAVD88) with units of meters. All data applied to the model are shifted to this datum and coordinate system.

Bathymetry data for the model were obtained from several sources: the National Geophysical Data Center, the Coastal Relief Model, sponsor-collected hydrographic surveys, and the National Elevation Dataset. These data sets were combined such that the latest data appropriate for the validation years were made a priority as well as data collected at finer resolution. Since the 3D AdH code cannot include areas that wet and dry, elevations above –2 m NAVD88 were set to –2 m to ensure the domain remains wet throughout the simulation period. Figure 3 shows most of the model domain and bathymetry. All areas have at least two vertical layers with most locations having a new layer every 2 m. The Gulf of Mexico has less vertical resolution with a new layer every 5 m. Figure 4 shows the vertical layering in a cross section of the HSC. Details of the mesh resolution are included in McAlpin et al. (2019b).

Figure 3. Model domain bathymetry.

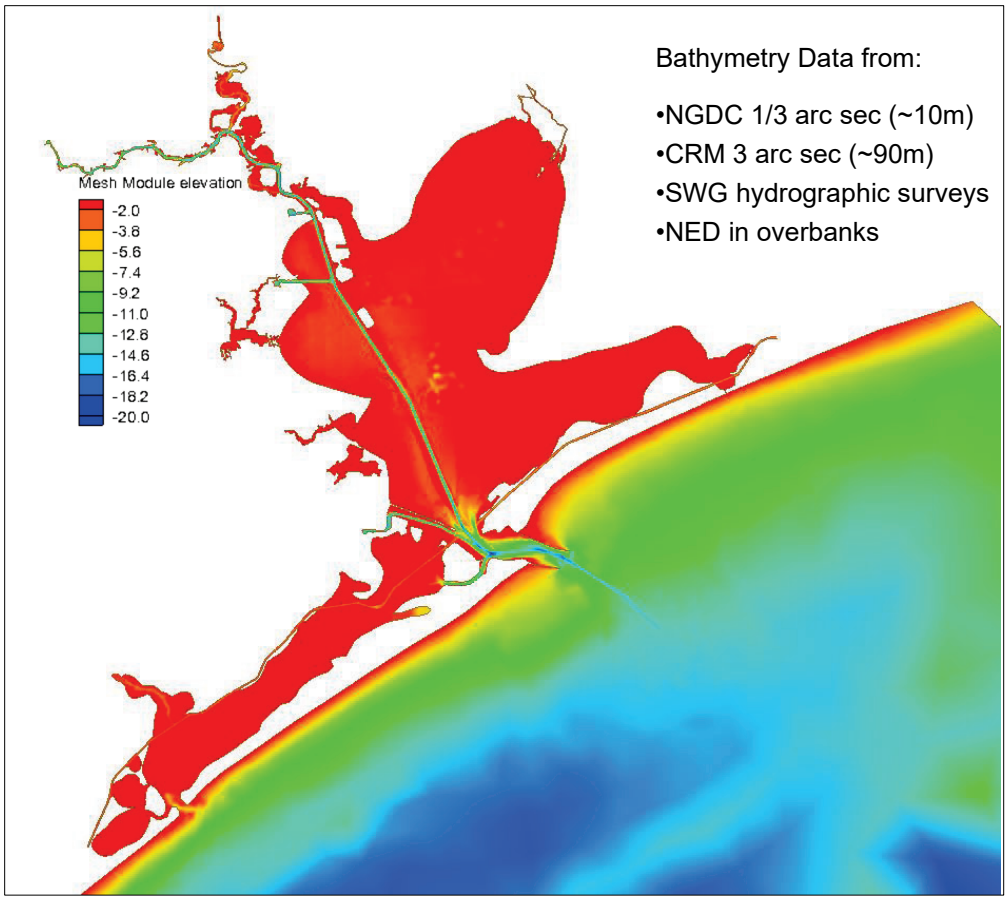

Figure 4. Vertical mesh resolution in HSC mesh. Colors represent Adaptive Hydraulics (AdH) 3D material regions.

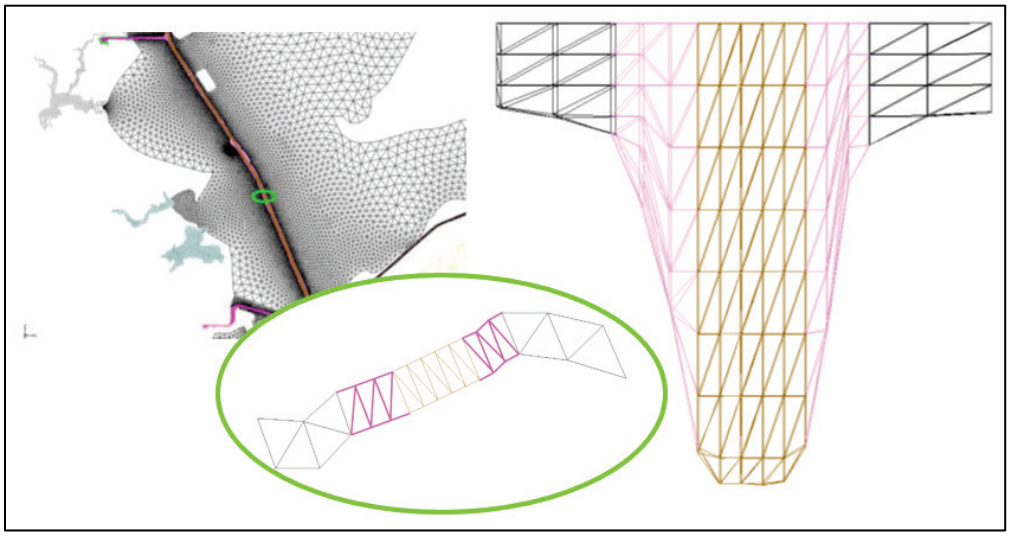

2.3 Boundary Conditions

The boundary conditions for this study are initially set up in the same manner as the previous work performed for this model domain (McAlpin et al. 2019b). Tidal water surface elevations and salinity are applied at the ocean boundary. Winds are included throughout the model domain. Freshwater inflow is applied for the Trinity River and the San Jacinto River as well as at other inflow locations to account for ungaged flows in the area. All inflow locations are labeled in Figure 5.

Figure 5. Inflow locations.

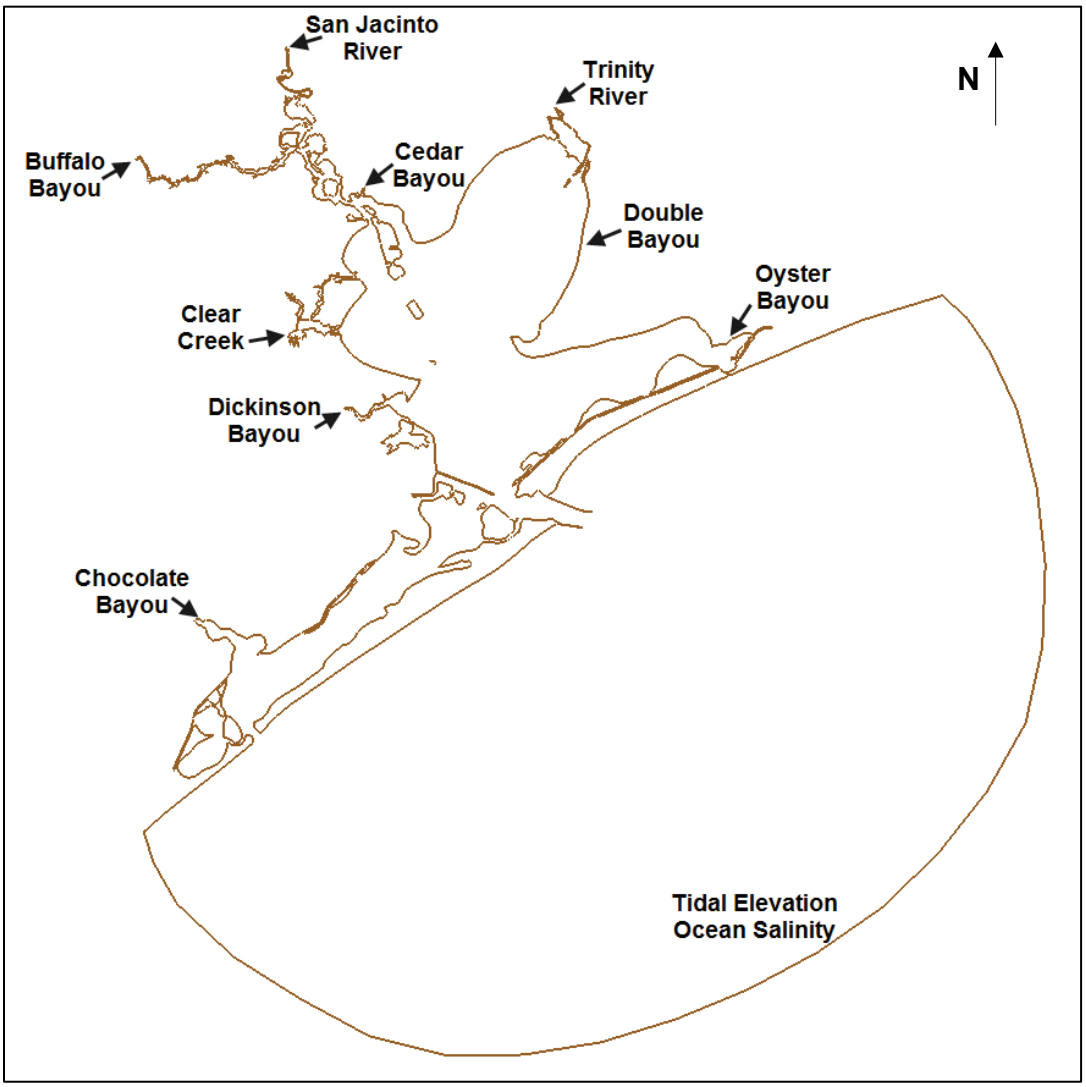

2.3.1 Freshwater Inflows

Figure 6 through Figure 8 show the inflow discharge for the two major rivers entering the bay—Trinity River and San Jacinto River—as well as the ungaged inflows at the seven remaining locations specified in Figure 5 for both flow years. These flows are computed through a hydrology model maintained by the Texas Water Development Board (Schoenbaechler and Guthrie 2012). All freshwater flow data are provided for calendar years 2010 and 2017 (please note that 2017 includes Hurricane Harvey).

Figure 6. River and ungaged inflows for 2010.

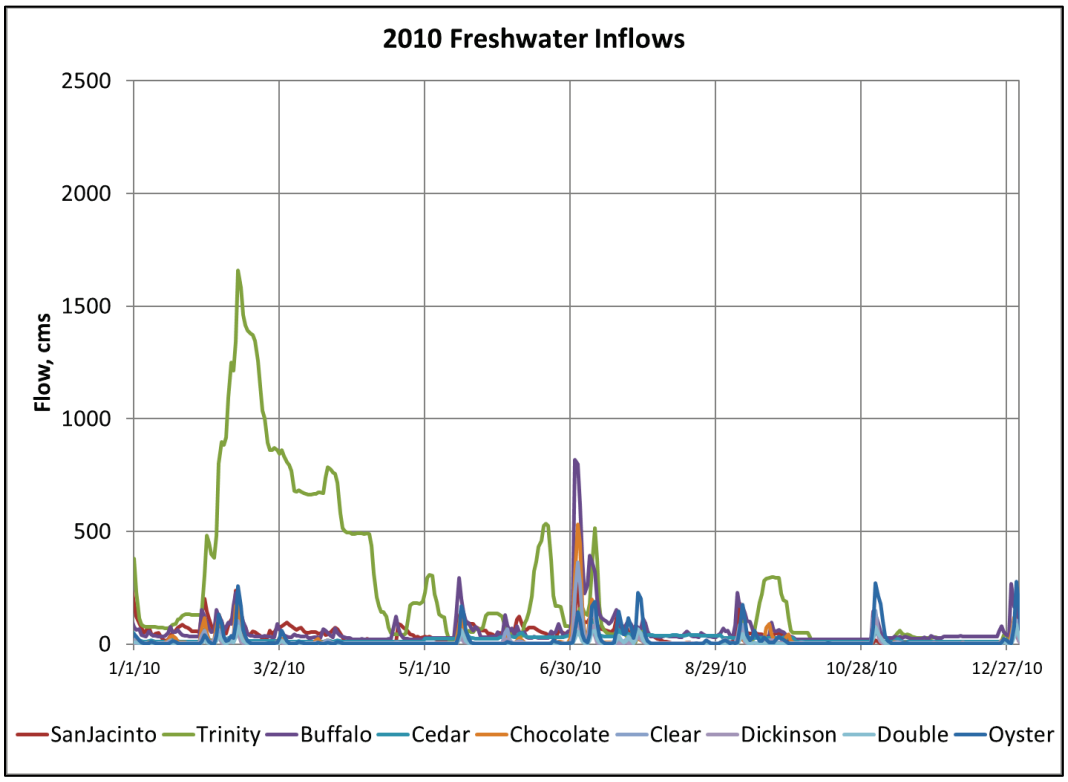

Figure 7. River and ungaged inflows for 2017 (please note that the total magnitude of Hurricane Harvey flows is not displayed).

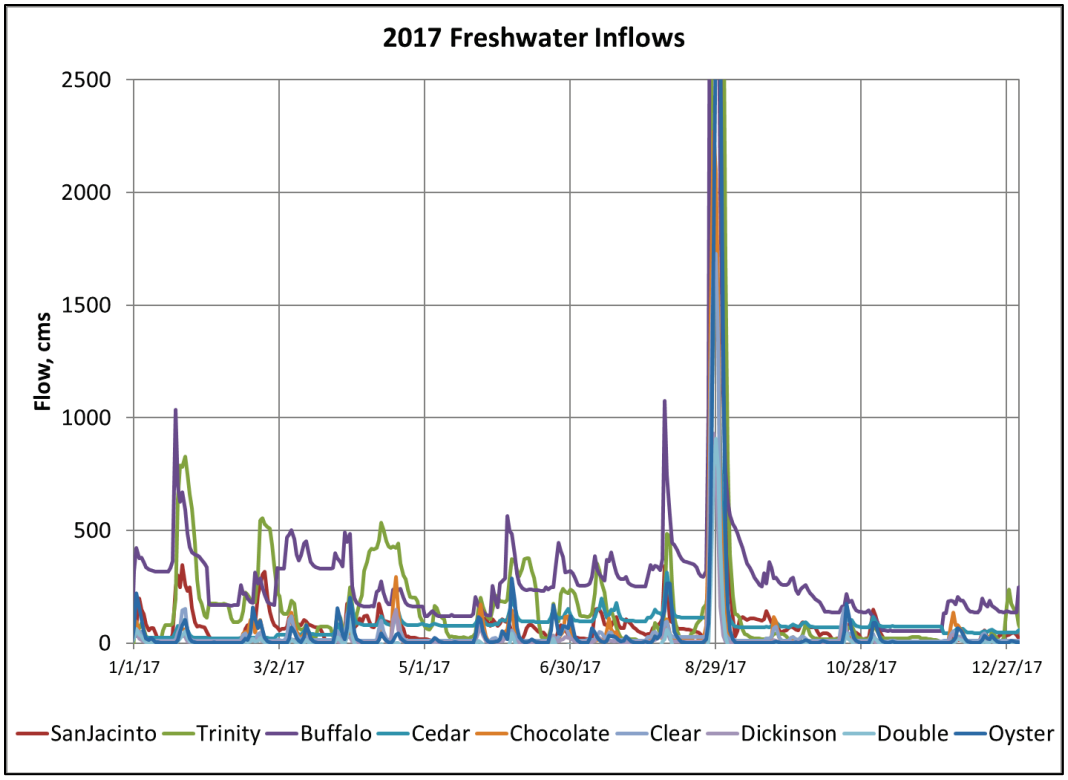

Figure 8. River and ungaged inflows for 2017, scaled to show Hurricane Harvey magnitude.

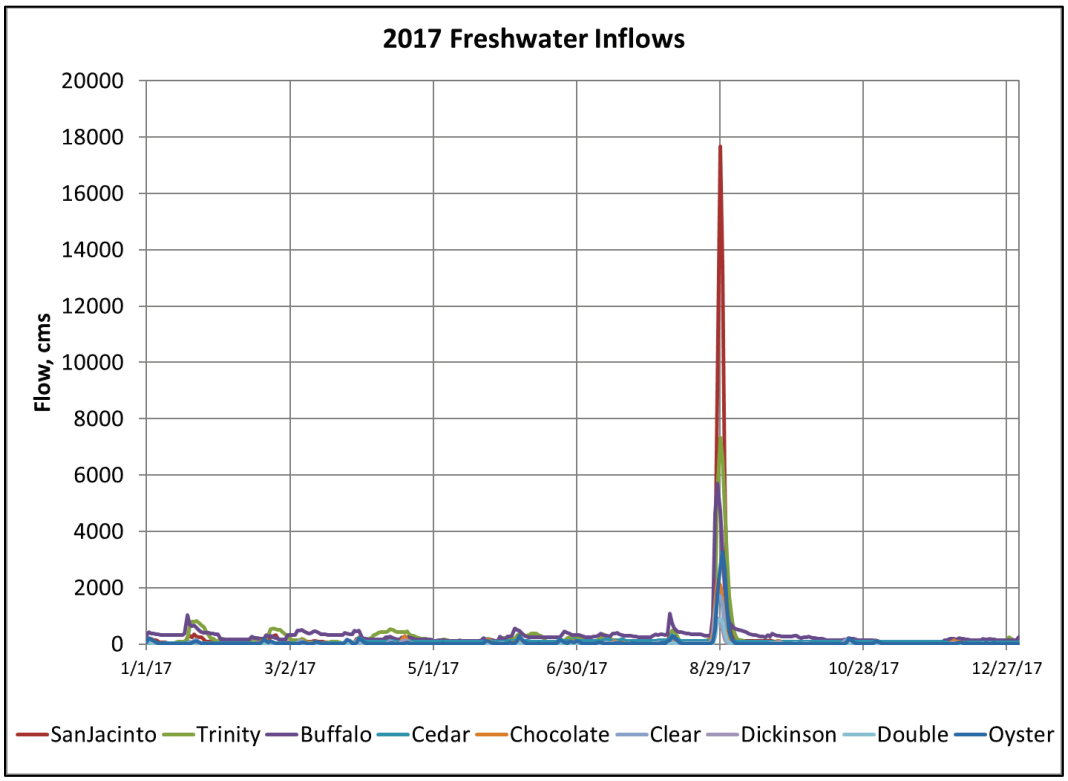

2.3.2 Tidal Boundary Conditions

2.3.2.1 Water Surface Elevation

In addition to freshwater inflows, a tidal boundary is applied at the ocean boundary of the mesh. The tidal boundary condition was developed differently for 2010 and 2017 since 2017 includes an extreme storm event.

For 2010, the tidal water surface elevation is based on harmonics for the area and measured data from National Oceanic and Atmospheric Administration (NOAA) gages at Freeport (8772447) and Sabine Pass (8770822), Texas. The harmonic constituents and the nonpredicted, or subtidal (nonharmonic), signal (the difference between the predicted value based on tidal constituents and the observed value, which includes winds and other factors) for each station are used to generate a tidal forcing or water surface elevation at each node along the tidal boundary for the simulation time period. The values for each node are determined by performing a linear interpolation of the gage amplitude and phase for each tidal constituent as well as for the nonpredicted signal. The tide is then reconstituted at each location along the boundary using these interpolated parameters.

For 2017, the Advanced Circulation model tidal database was used to obtain water surface elevation data for all points along the AdH model boundary. However, the database includes only the harmonic component of the tide, so a gulf-side gage with measured data is necessary to include the nonharmonic signal in the tide boundary. The NOAA gage at Galveston Bay Entrance, North Jetty (8771341), was used for the nonpredicted information (the difference between the predicted value based on tidal constituents and the observed value, which includes winds and other factors). This approach was not used for the 2010 simulation because there were no gulf-side gages collecting data at that time.

Initially, the water surface elevation is set to the average along the tidal boundary and is a flat surface throughout the model domain. A 1 yr spin-up period is executed, and the variable water surface from the end of that simulation is used as the initial condition for the analysis period model simulation.

2.3.2.2 Salinity

Salinity is also applied at the model's Gulf of Mexico tidal boundary. As with the previous model validation effort (McAlpin et al. 2019b), the salinity boundary condition is set based on monthly average salinity measurements over a 15 yr period (Cochrane and Kelly 1986).

Initially, the salinity throughout the domain is set to match values from an average time period. A 1 yr spin-up period is executed for each simulation year, and the salinity field from the end of that simulation is used as the initial conditions for the analysis-year model simulation.

2.3.3 Wind Conditions

The wind conditions applied to the model are obtained from the Wave Information Studies (WIS) computed wind field for points that lie in the vicinity of the model domain (Hubertz 1992). There are 26 WIS sites for this model (Figure 9). The WIS model is validated against measurement sites where applicable, and these wind data allow for variable wind conditions across the domain. The wind data are supplied to the AdH model as time series of x- and y-velocities. These wind components are then converted to a shear stress dependent on conditions set for each material—deeper water uses a Wu formulation (Wu 1969; Wu 1982) and shallow regions use a Teeter formulation (Teeter 2002). The wind rose for each data site for 2010 and 2017 is shown in Figure 10 and Figure 11, respectively.

Figure 9. Wind-data boundary condition locations.

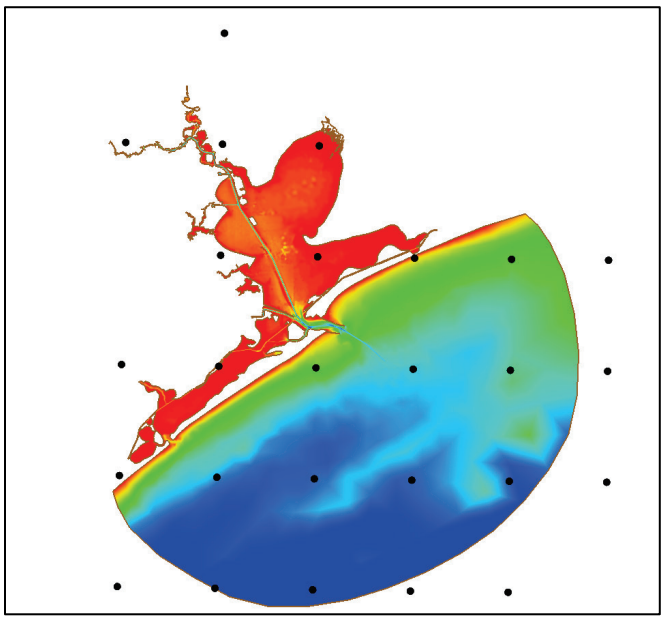

Figure 10. 2010 wind rose for all sites.

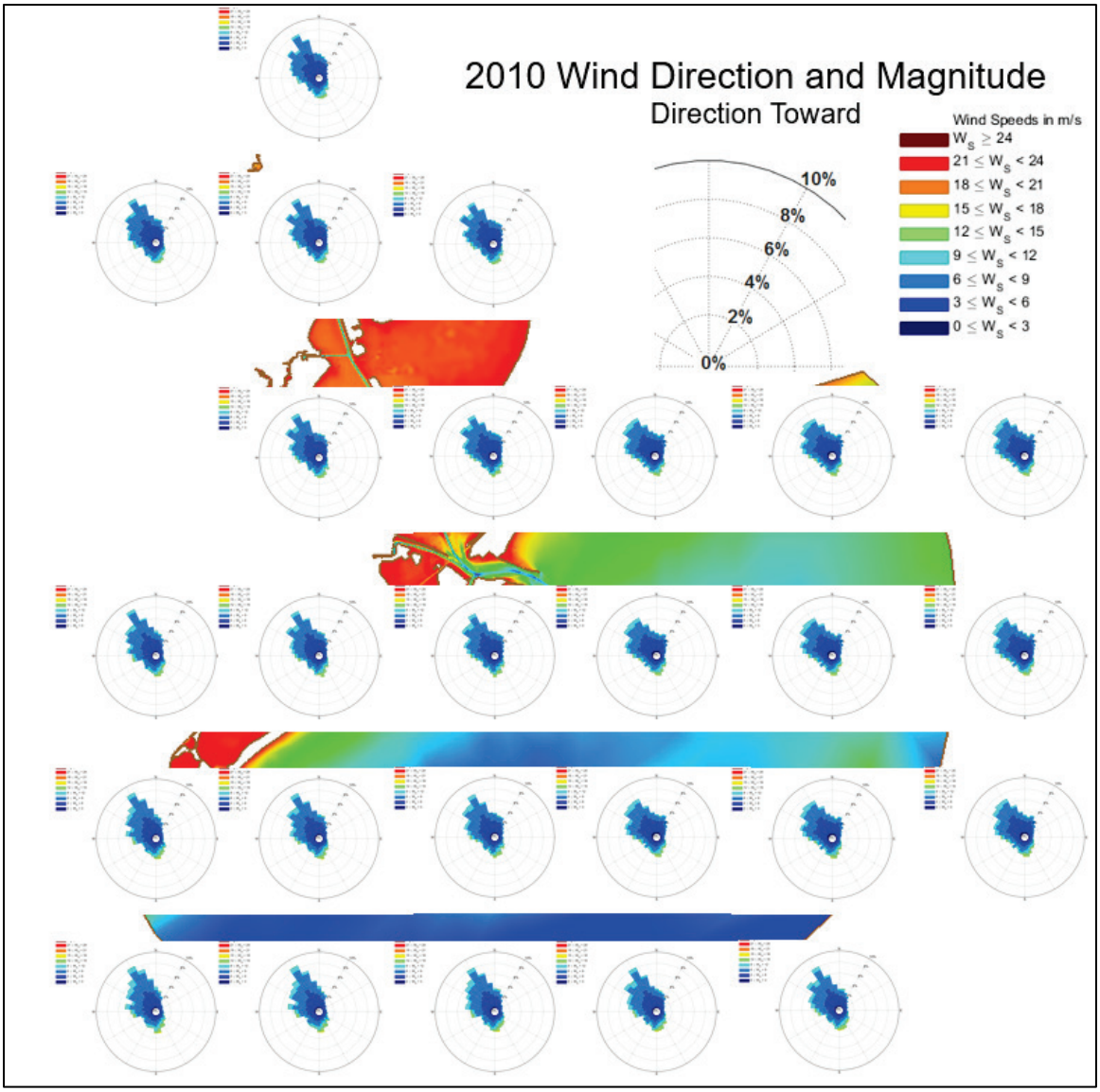

Figure 11. 2017 wind rose for all sites.

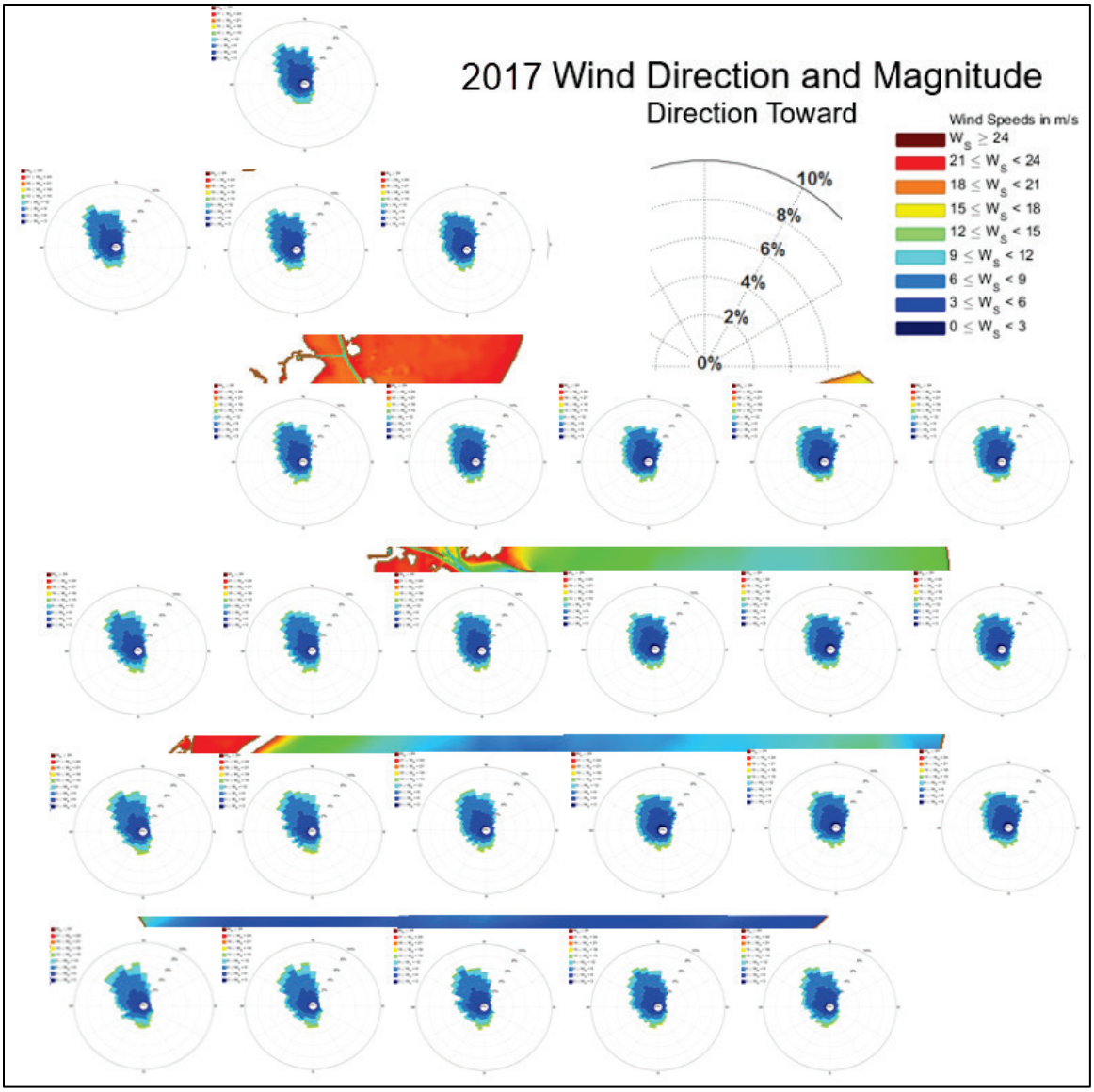

2.3.4 Meteorological Conditions

To accurately reproduce salinity values in Trinity Bay, evaporation and precipitation should be included in the model. These data (shown in Figure 12 and Figure 13) were also obtained from the Texas Water Development Board (TWDB), and the data are based on wind and temperature computations validated to several measurement locations using the Texas Rainfall Runoff Model. The combination of precipitation (rainfall only in south Texas) and evaporation is applied equally over the model domain. The heavy rainfall conditions of 2017 are visible in the meteorological data.

Figure 12. 2010 meteorological conditions.

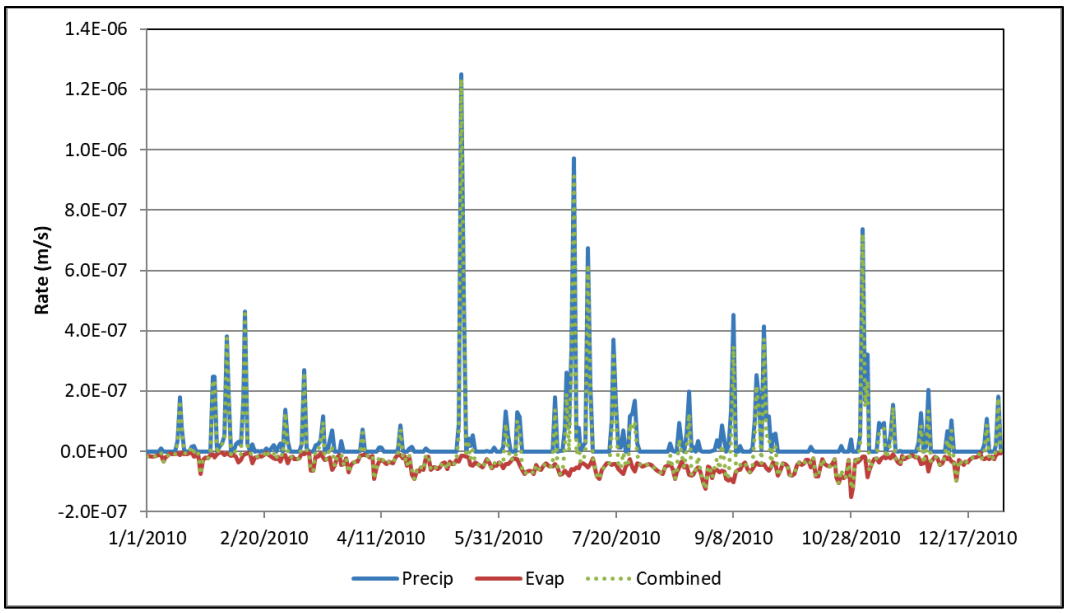

Figure 13. 2017 meteorological conditions.

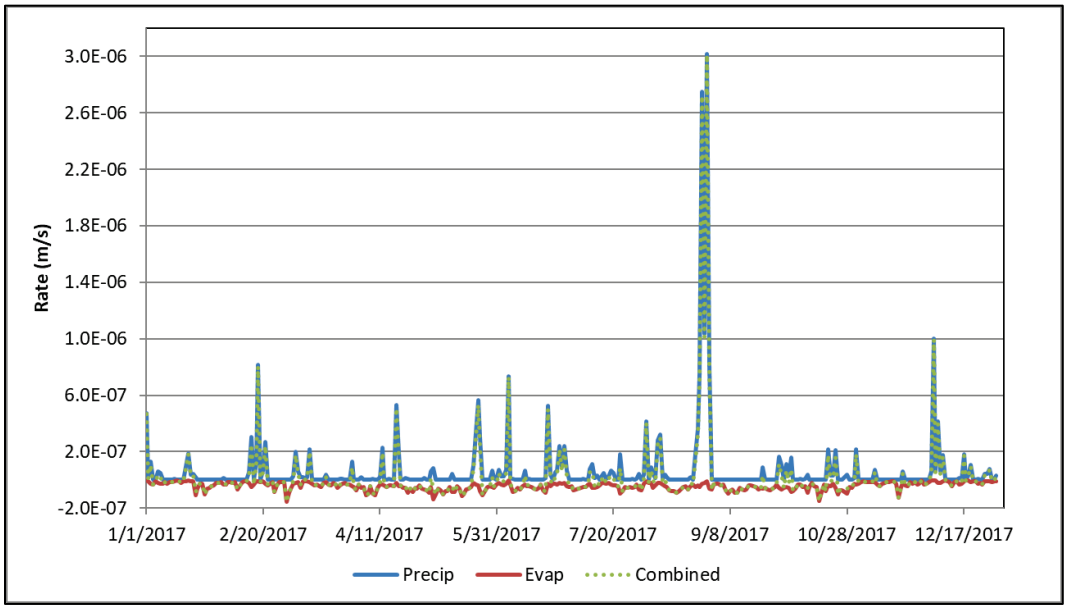

2.3.5 Sediment Model Boundary Conditions

The sediment model is fully coupled with the hydrodynamic model when simulating AdH with SEDLIB. The boundary conditions for the sediment model include grain characteristics, bed definitions, and sediment concentrations. As with the previous validation effort (McAlpin et al. 2019b), this model includes five fine sediment classes (sizes defined by the American Geophysical Union [AGU]), which encompasses the majority of the sediment present in the domain. Sand is dominant at the entrance at

Bolivar Roads, but it primarily remains in that area and therefore is not included in these simulations. It is known that sand-sized grains are included in the bed material and are in higher percentage in the HSC as well as along eroded shorelines and areas where vessel activity is high. These are areas where the fines have been pulled from the bed material due to high shear stresses on the bed and the bed has become armored. The sand-sized grains will not be of a high percentage in the suspended material in the upper bay regions (upstream of Red Fish Reef). The material that is being eroded and creating areas of high deposition is the fine grains, which this model is intended to track.

Texas A&M University at Galveston was tasked during this study to collect bed-sediment data throughout the region and provide grain-size fractions along with other data defining the bed sediment. From review of their 2021 and 2022 collected data, there is no reason to believe that the sediment parameters should be modified in the AdH model. Although their data show sand in the bed, this material is not what is being eroded and creating the large depositional problems in the Bayport and Barbours Cut flares.

The sediment-specific parameters for the model were initially established from the sediment-model validation documented in Tate et al. (2008) and were determined from field samples (although a small sample set) in Trinity and San Jacinto Bays. These parameters were then used as initial values for the previous AdH/SEDLIB sediment model and modified as necessary, within acceptable limits, for best results. The sediment-specific parameters used in the 3D AdH model documented here are given in Table 1. These parameters are utilized for suspended and newly deposited grains.

Table 1. Sediment parameters and values.

Grain Class (AGU)	Diameter (mm)	Specific Gravity	Porosity (kg/m^3)	Critical Shear for Erosion (Pa)	Erosion Rate Constant	Critical Shear for Deposition (Pa)	Settling Velocity (mm/s)
Clay	0.003	2.65	0.833	0.1	0.0000384	0.05	0.009
Very Fine Mud	0.006	2.65	0.833	0.2	0.0000384	0.06	0.036
Fine Mud	0.011	2.65	0.833	0.3	0.0000384	0.07	0.121
Medium Mud	0.023	2.65	0.833	0.4	0.0000384	0.08	0.529
Coarse Mud	0.045	2.65	0.833	0.6	0.0000384	0.10	2.025

Initially, the bed is defined as an equal mix of all grain sizes, and the hydrodynamics of the system are then used to sort the bed prior to validation and alternative simulations. This step is performed by setting the top-most defined bed layer to equal fractions for all of the grains (0.2 for all five grains). This layer is also defined as 0.2 m thick—selected because erosion beyond this value during the course of the simulation year is likely prevented due to bed armoring or nonerodable material; it is known that the bay system is not eroding at a significant rate (Nichols 1989). Three additional bed layers are defined to track deposition events and help define bed features that may change the erosion and deposition potential. The cohesive bed properties that help determine erosion potential of a bed layer are defined with porosity of 0.7576 kg/m^3 (wet bulk density of 1,400 kg/m^3), critical shear stress for erosion of 1.0 Pa, erosion rate constant of 0.000062, and erosion rate exponent of 1.0.

As the model runs and the bed begins to sort and change, the bed properties vary from these initially defined parameters. An initial 1 yr simulation is performed with no bed displacement allowed so that the bed can sort based on the erosion and deposition tendencies in each area. The results of this spin-up simulation are then used as the initial conditions for the analysis model run with the bed allowed to change due to computed erosion and deposition.

The sediment entrainment algorithm used in this model is Wright-Parker (Wright and Parker 2004) and the hiding factor algorithm is Egiazaroff (Egiazaroff 1965). Flocculation properties are not included in the AdH code and should be considered when defining the sediment grain properties. There is no bedload in the present 3D Shallow Water AdH code, and cohesive bed consolidation is not included in this model due to the short simulation time of 1 yr for each analysis model run.

Sediment concentrations are applied to the two major rivers in the area: the Trinity River and the San Jacinto River. These concentrations are determined from a rating curve correlating discharge with concentration generated using data from the US Geological Survey (USGS) as documented in Tate et al. (2008). However, additional sediment-concentration data for these locations have been collected, and the sediment-concentration rating curves updated for this revalidation effort. Trinity River sediment concentrations are based on data at Wallisville, Texas (USGS 08067252) (Equation 1). San Jacinto River sediment concentrations are based on data at Sheldon, Texas (USGS 08072050),

which is downstream of Lake Houston (Equation 2). A maximum value is set for each river based on the range of the field data.

$$C_{Trinity} = MIN\left(17.279 * e^{0.0056 * Q_{Trinity}},\ 100\right) \quad (1)$$

$$C_{SanJacinto} = MIN\left(-6.322 * 10^{-5} * Q_{Trinity}^{\ 2} + 0.161 * Q_{Trinity} + 13.661,\ 150\right) \quad (2)$$

These concentration estimates are not ideal. The Trinity River concentration is based on data collected between 2009 and 2019 at the Wallisville lock, which is the upstream model boundary for this river. The San Jacinto River concentration is based on only 15 samples over 10 yr from Sheldon, Texas, which is located downstream of Lake Houston. Previous sediment concentrations for the San Jacinto River were taken from data upstream of Lake Houston, which impacts the amount of sediment exiting the reservoir. The total sediment concentrations applied at each river for each of the validation years are shown in Figure 14 and Figure 15. The total concentration is then divided equally among the five grain classes being modeled. The concentration information for the ungaged inflows is unknown and therefore set to zero.

Figure 14. 2010 total sediment concentration for the Trinity and San Jacinto Rivers.

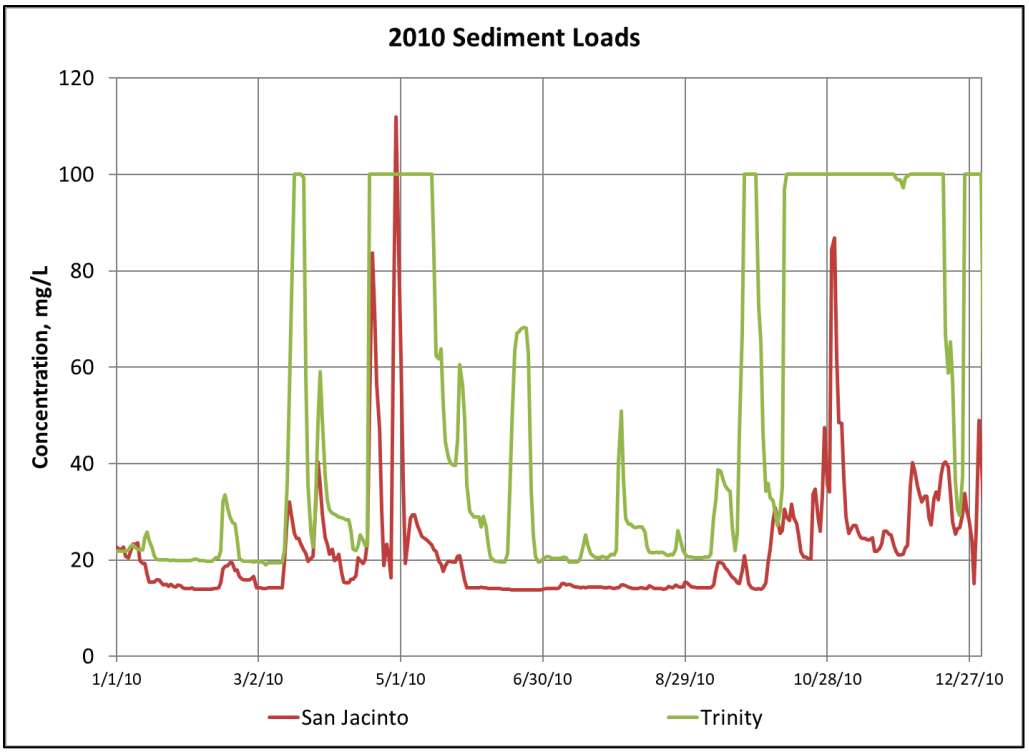

Figure 15. 2017 total sediment concentration for Trinity and San Jacinto Rivers.

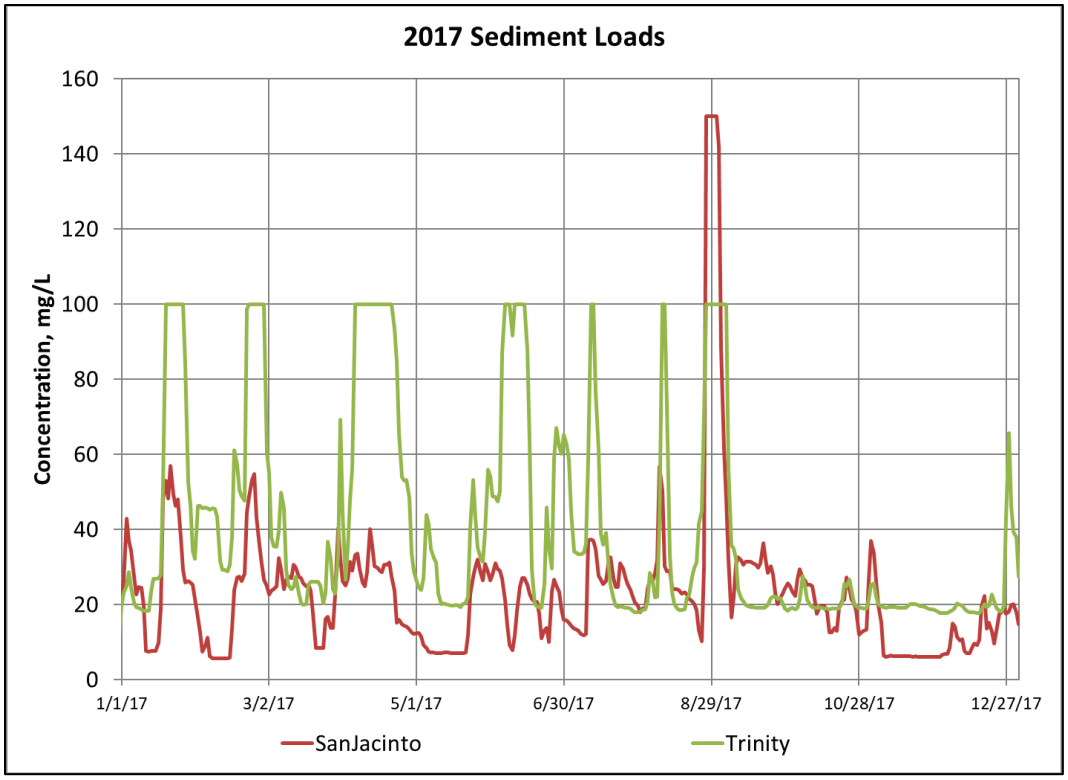

A sediment-concentration rating curve was computed for Buffalo Bayou based on data from 69th Street (USGS 08074700). Sediment concentrations for this site extend as high as 1,300 mg/L—much higher than the maximum measured value at the San Jacinto River (122 mg/L) and the Trinity River (854 mg/L). This rating curve and sediment concentration were included in initial model updates. However, it was determined that all of the material that was supplied at the Buffalo Bayou inflow location in the model immediately fell out in the HSC turning basin. Although this area is known to shoal, the magnitude of the shoaling is much higher than would be rational, and there is no mechanism in the model to resuspend the material in the turning basin, such as vessel movement, which is present in reality. Given these uncertainties and the scaling required for validation of the shoaling volumes, it was determined to not include sediment concentrations on Buffalo Bayou.

The sedimentation in the HSC and Trinity and Galveston Bays is influenced greatly by deep-draft vessel passages in the area (Tate et al. 2008; Tate et al. 2014). Figure 16 shows previous model-computed results indicating that vessel-induced shoaling can produce four times more shoaled volume in the HSC than other factors such as tidally driven sedimentation and river sediment loads. The model presented in this

report does not include vessel impacts indicating an expectation to underpredict the sediment volumes. Shoaling drivers not specifically in the model are incorporated as part of a scaling process performed during model calibration and validation.

Figure 16. Influences on HSC shoaling.

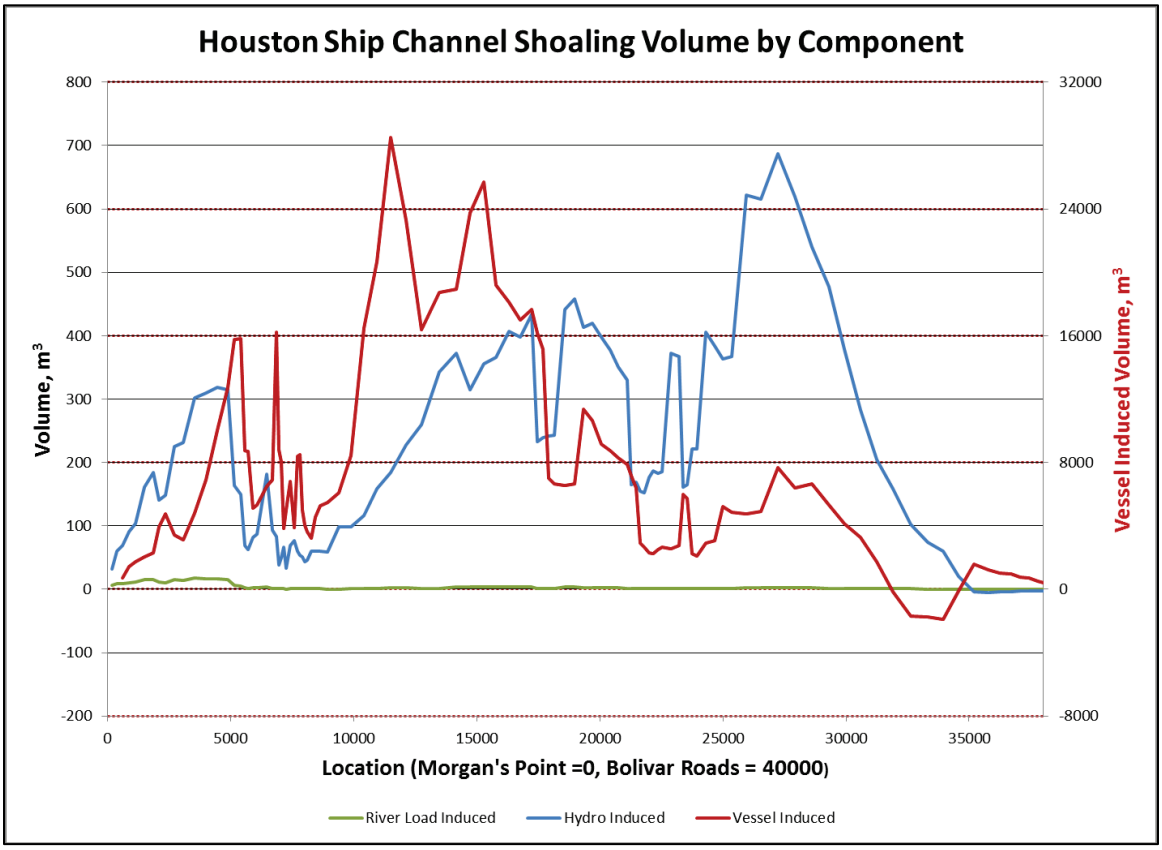

2.3.6 Adaptive Hydraulics (AdH) Model Parameters

The parameters used by AdH to achieve the validated model (discussed in the following sections) are provided in Table 2. This table provides the specific or range of values used for various model properties such as bed roughness, diffusion, eddy viscosity, and turbulence. The values vary by location (material designation) and sediment grain class. Large values of diffusion, viscosity, and turbulence coefficients (increased generally to maintain model stability) are associated with larger grain sizes and locations away from the immediate study area.

Table 2. Model parameters.

Parameter	Value
Turbulent Diffusion of Salinity	0.00005–10.0 m^2/s
Turbulent Diffusion of Cohesive Sediment	0.001–10.0 m^2/s
Eddy Viscosity	0.0001–5.0 m^2/s
Turbulence (Smagorinsky coefficient)	0.2–0.8
Bed Roughness (Manning's coefficient)	0.015
Time-Stepping	Second order
Time-Step Maximum	150 s
Convergence Maximum	0.5 (increment norm)

3 Model-to-Field Comparisons

The model is validated by comparing to measured field data over two different years—2010 and 2017. Since this effort is an update to a previously validated model, only 1 yr (2010) from the previous effort is being used for revalidation. The Hurricane Harvey year (2017) was included to model an extreme event. Limitations discovered while modeling 2017 are discussed in Chapter 2. Most field data for comparison to the model were obtained from publicly accessible data websites. For all comparison types—hydrodynamic, salinity, and sediment—a subset of the sites are provided in the body of the report with all site comparisons provided in the appendices.

3.1 Hydrodynamic Comparison

The model is compared to water surface elevation and velocity at several locations during the modeled years. Water surface elevation data were obtained from the NOAA Tides and Currents and the National Data Buoy Center. Velocity data were obtained from NOAA Physical Oceanographic Real-Time System (PORTS).

3.1.1 Water Surface Elevation

Water surface elevation results are compared to the field at six locations, although 2010 had data at only three of these sites. Figure 17 shows the location of the water surface elevation comparison sites. Statistical comparisons are provided in Table 3. Time-history and box-plot comparisons at Morgans Point, Eagle Point, and Pier 21 are shown in this section (Figure 18 through Figure 23). The full set of comparisons are provided in Appendix A.

For the time-history plots, the *red line* represents the measured field data and the *blue line* represents the model-computed values. Each comparison location also includes a box plot showing the relationship between the measured field data (x-axis) and the modeled data (y-axis). A perfect match would yield points on the *black 1:1 line*.

The 2017 comparison statistics are not as good as those for 2010. At least part of the reason for this is the modeled water level peak from Hurricane Harvey is higher than measured in the field. As noted previously, the model does not allow for any wetting and drying of elements, so all flow must stay within the model limits. In reality, some of the water that

enters at the rivers floods into overbank areas. This flooding will lower the water level downstream, which is what is seen in the field data but not included in the model.

Figure 17. Water surface elevation comparison locations.

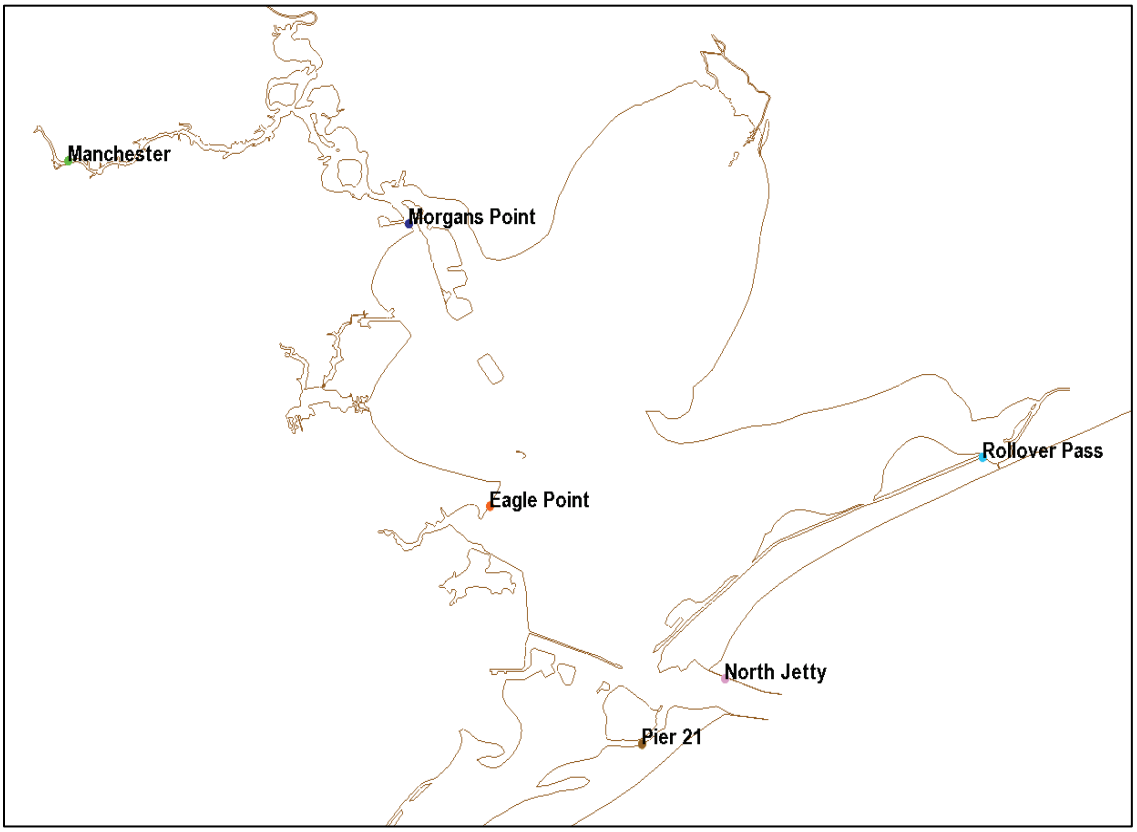

Table 3. Statistical model-to-field comparison of water surface elevation.

	Root Mean Square Error (m)		Correlation Coefficient	
	2010	2017	2010	2017
Manchester	—	0.15	—	0.95
Morgan's Point	0.08	0.11	0.96	0.92
Eagle Point	0.07	0.10	0.96	0.91
Pier 21	0.07	0.11	0.96	0.90
North Jetty	—	0.11	—	0.90
Rollover Pass	—	0.11	—	0.89

Figure 18. 2010 Water surface elevation comparisons over time and box plot for Morgans Point.

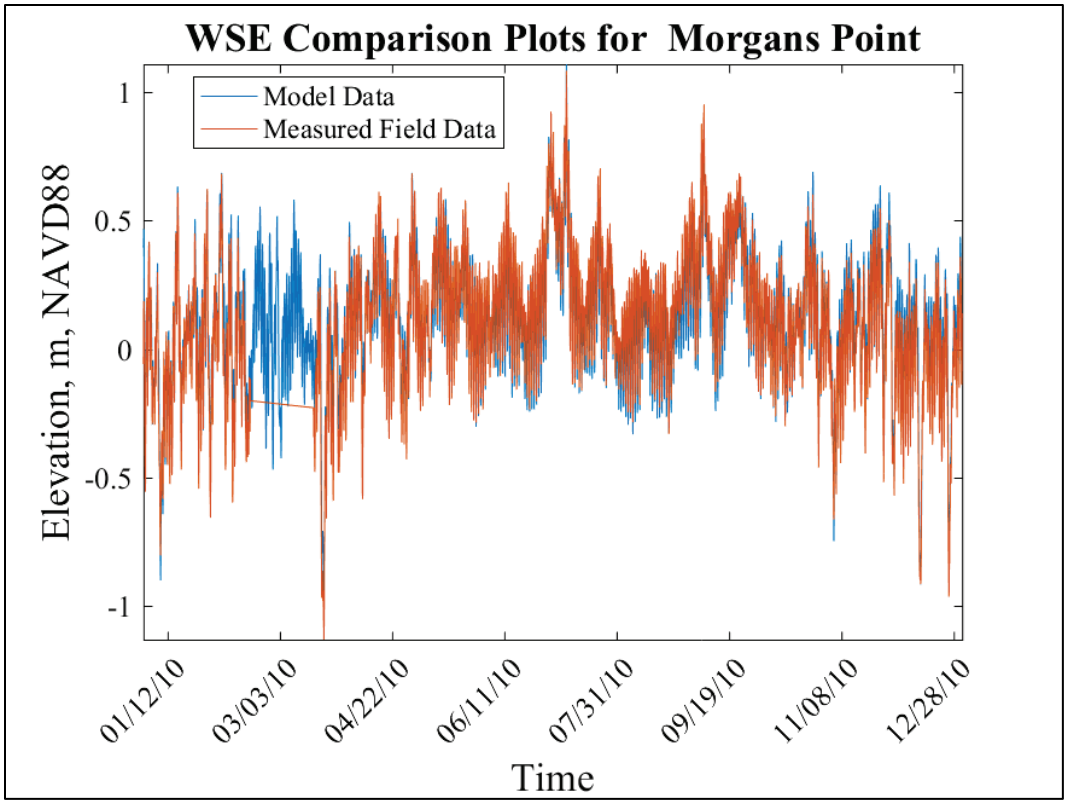

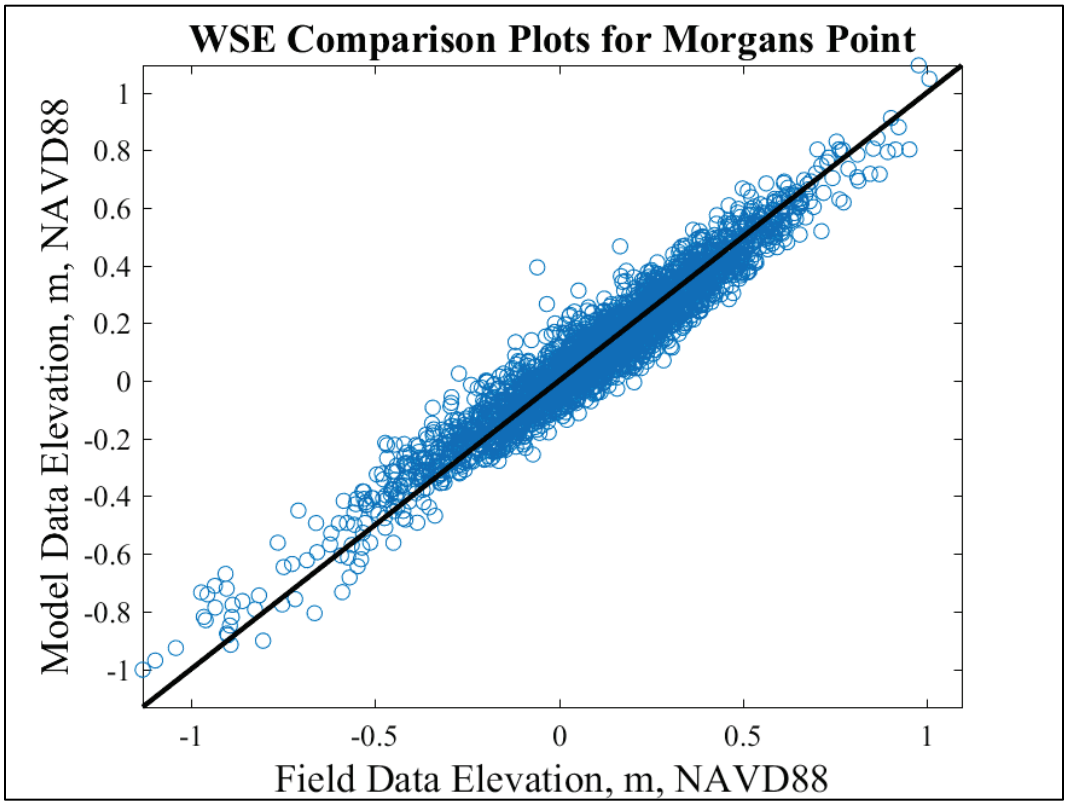

Figure 19. 2017 Water surface elevation comparisons over time and box plot for Morgans Point.

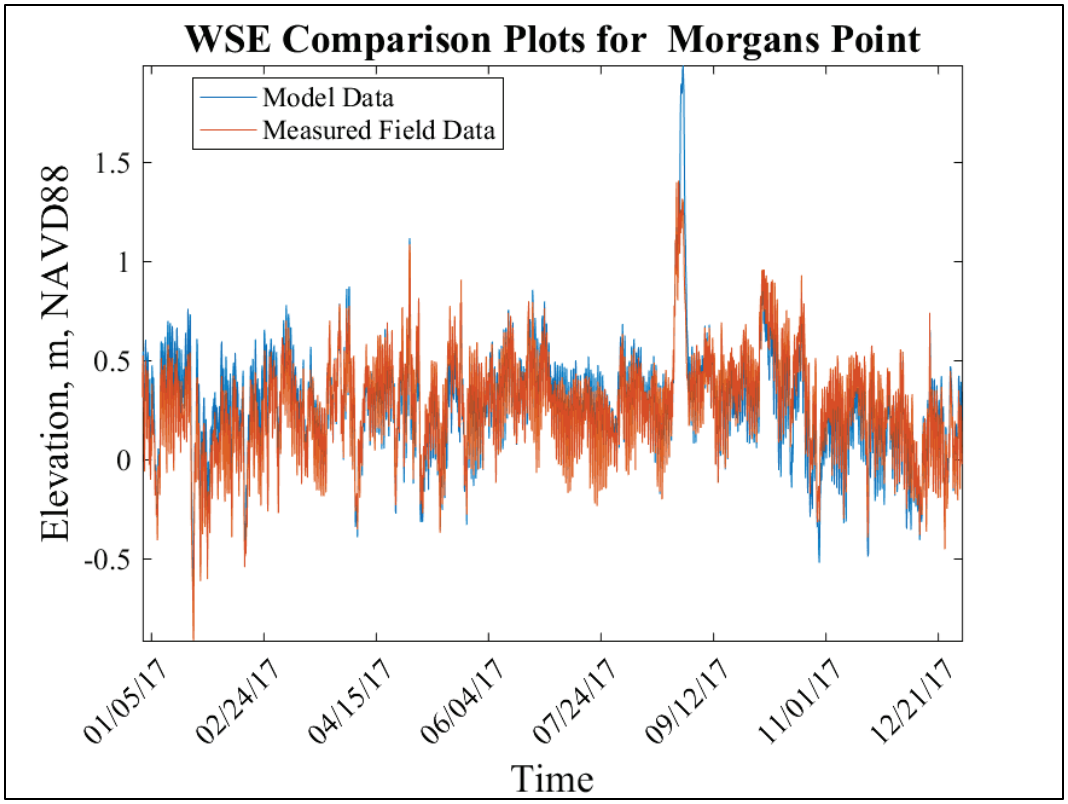

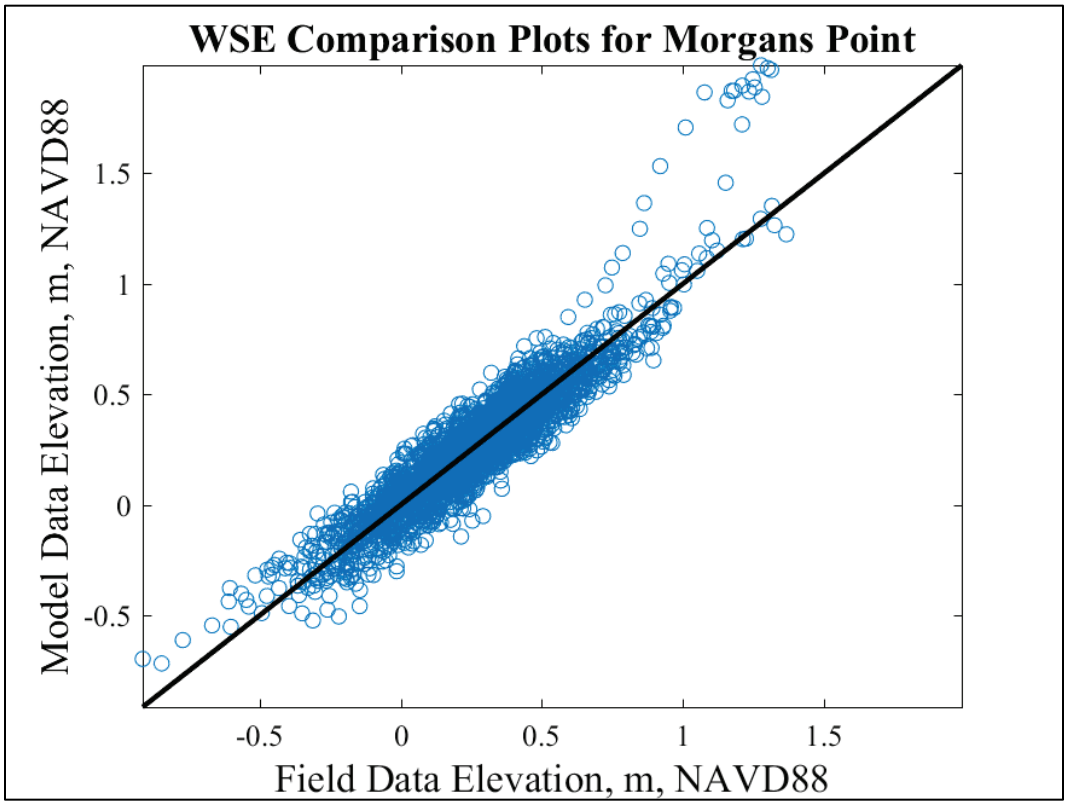

Figure 20. 2010 Water surface elevation comparisons over time and box plot for Eagle Point.

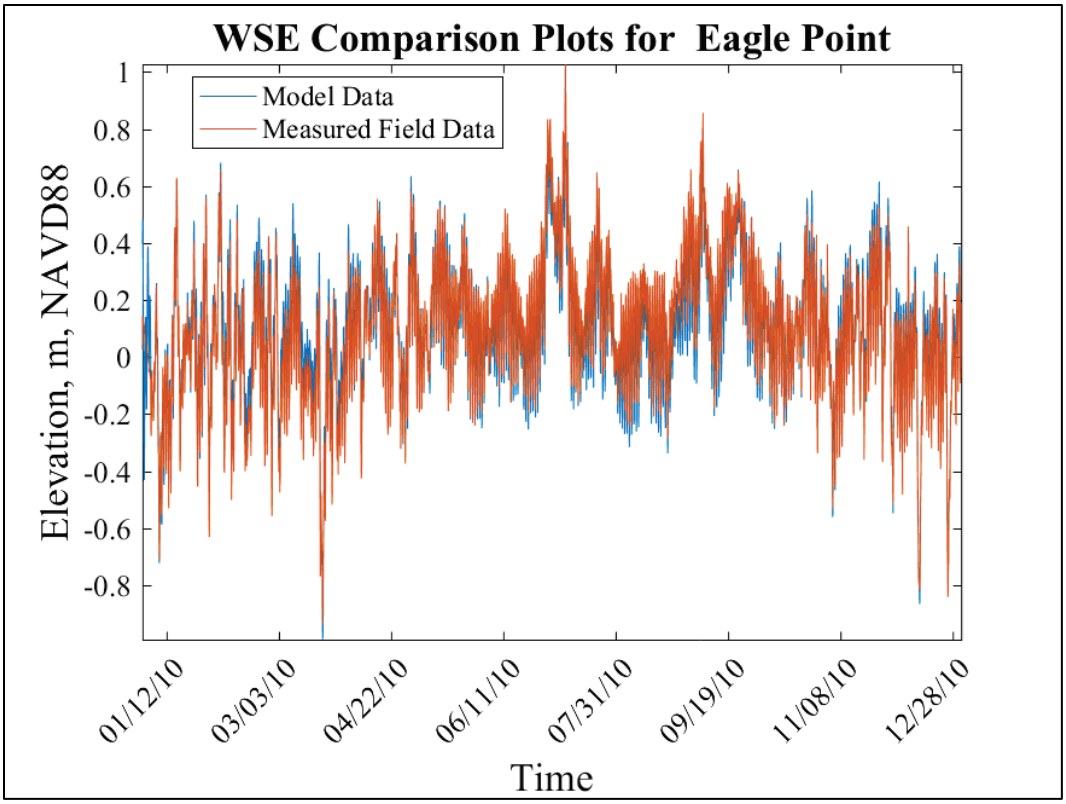

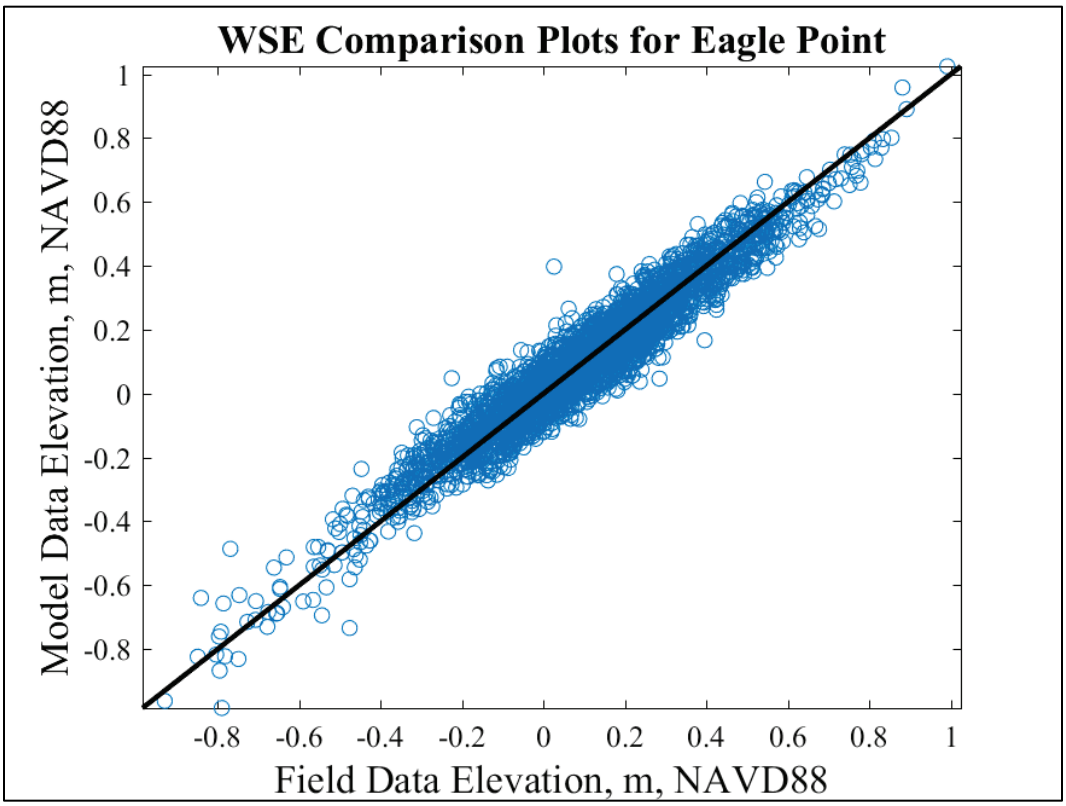

Figure 21. 2017 Water surface elevation comparisons over time and box plot for Eagle Point.

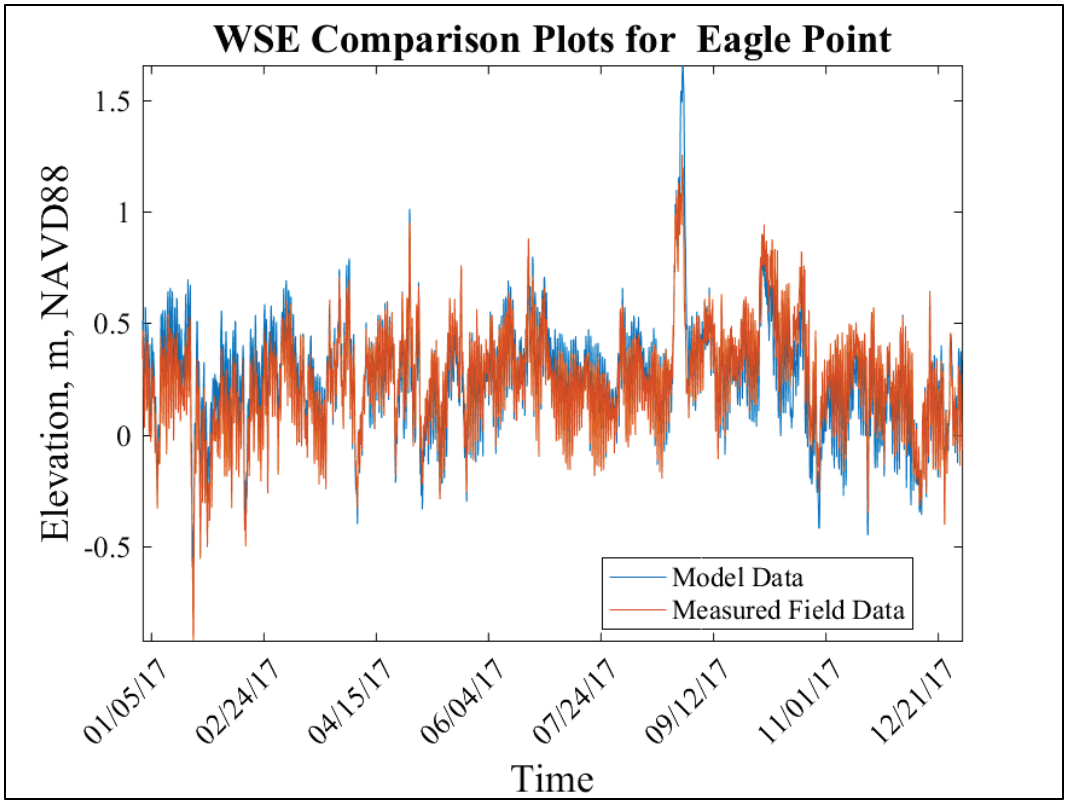

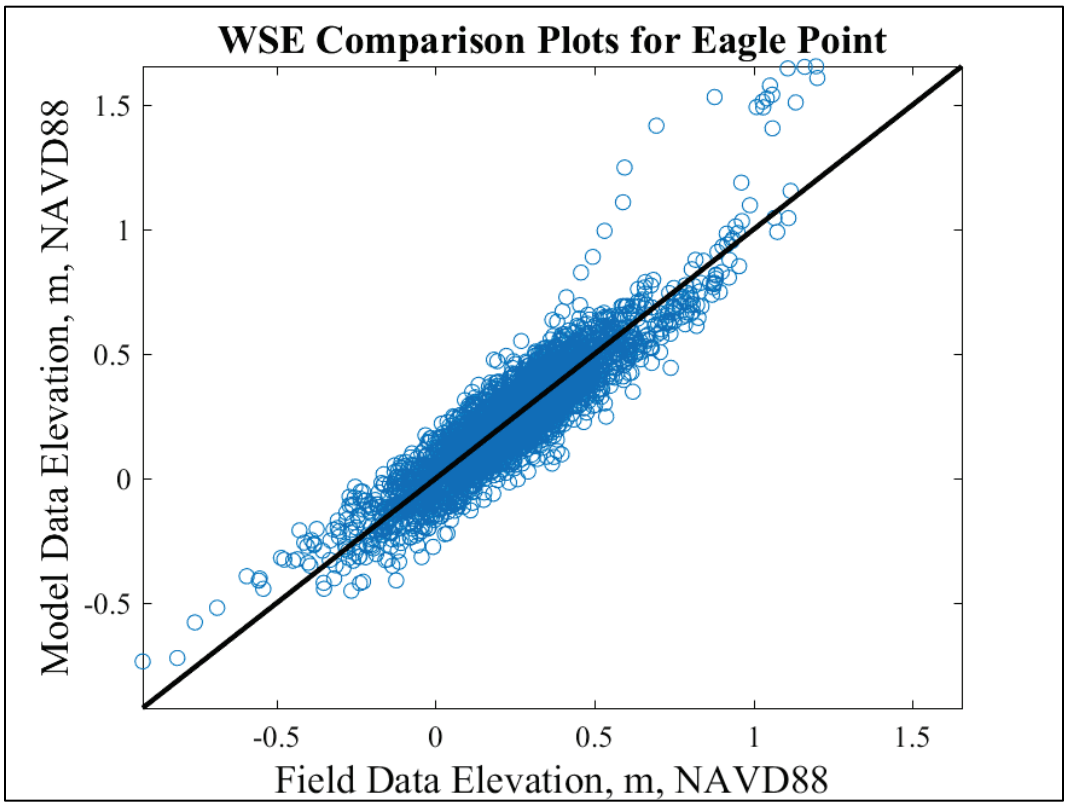

Figure 22. 2010 Water surface elevation comparisons over time and box plot for Pier 21.

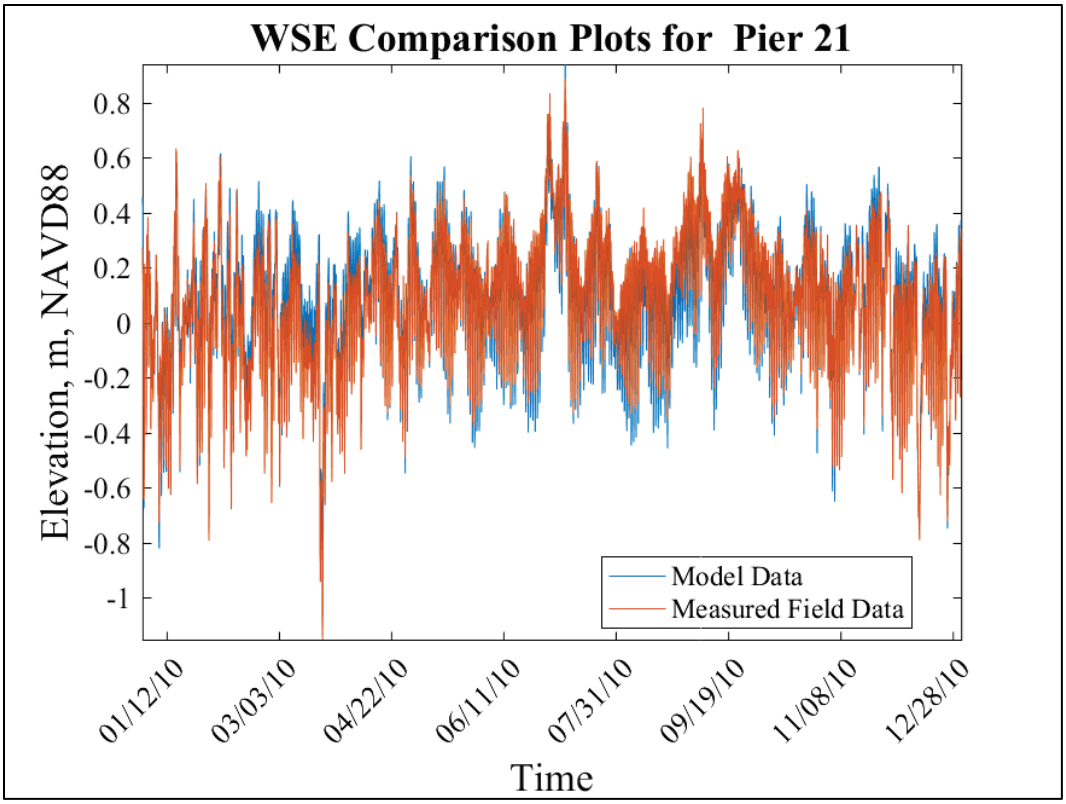

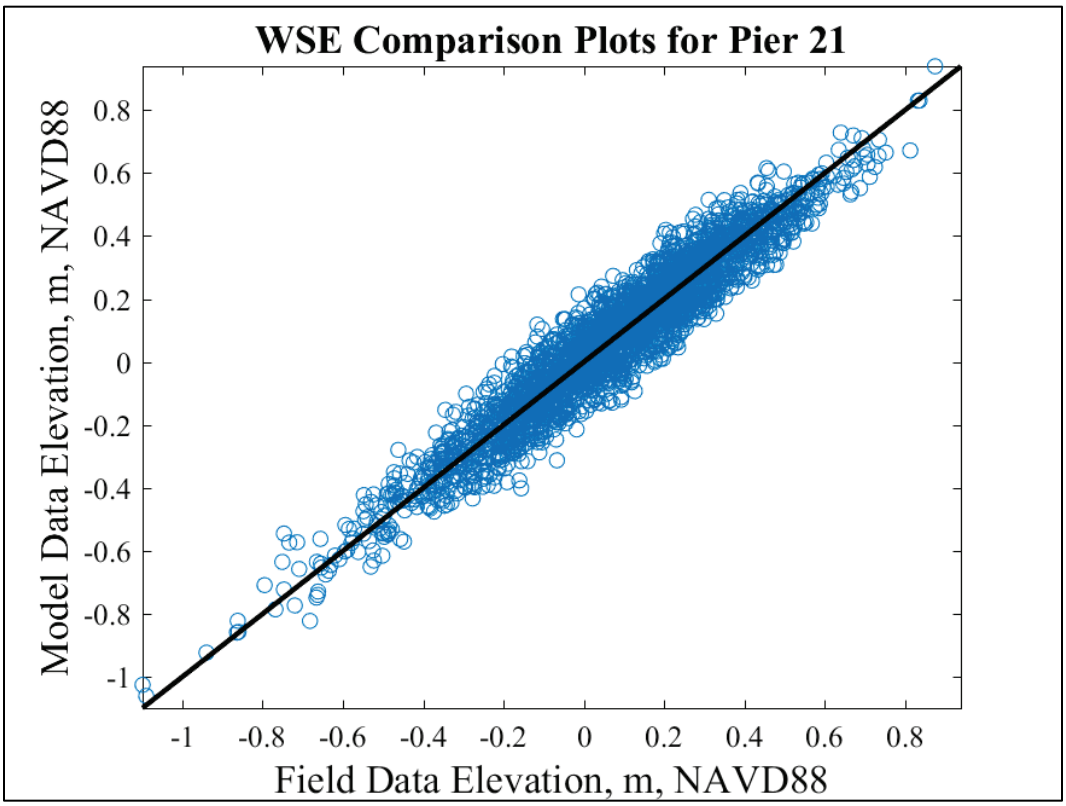

Figure 23. 2017 Water surface elevation comparisons over time and box plot for Pier 21.

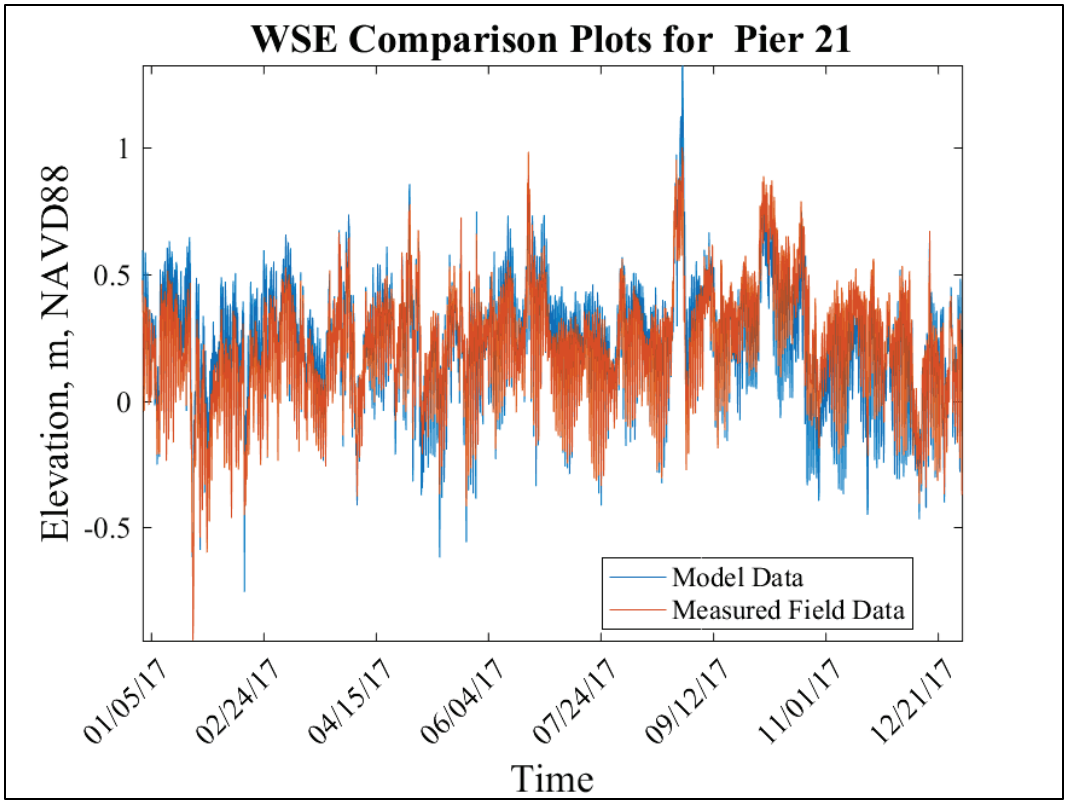

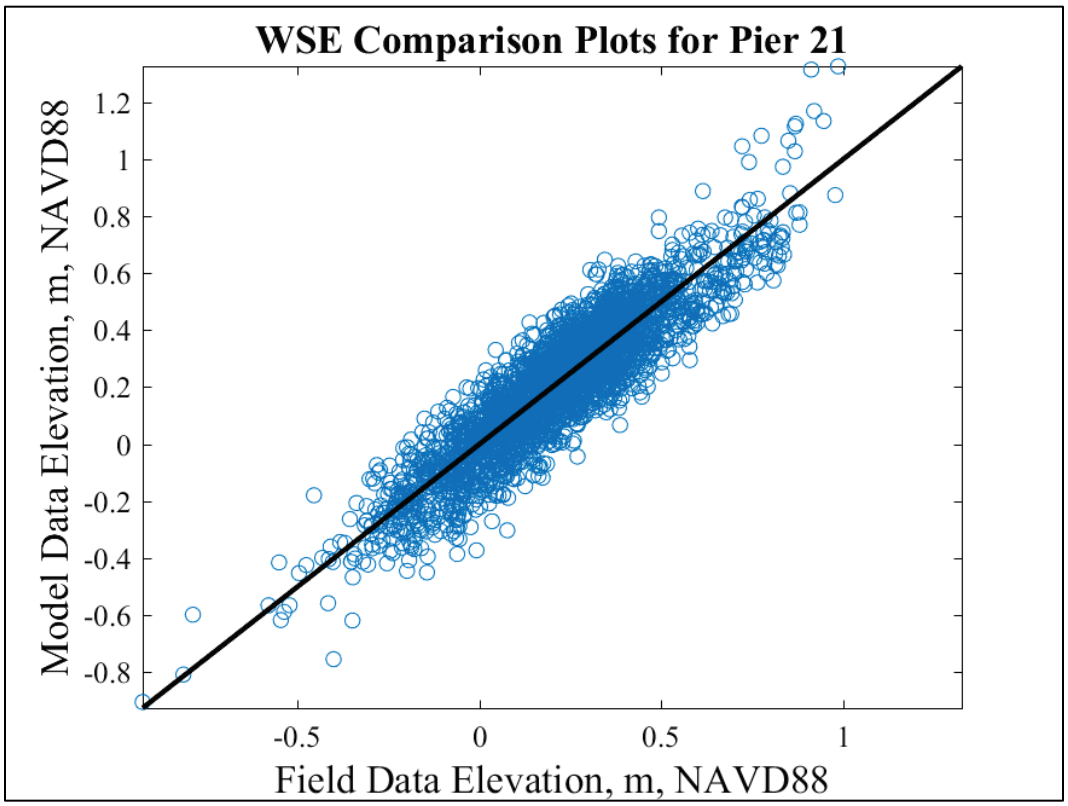

3.1.2 Velocity

Velocity validation comparisons are made at one location, Galveston Entrance for 2010, and two locations, Galveston Entrance and Fred Hartman Bridge for 2017—all data from NOAA PORTS (Figure 24). Comparisons are made to flood- and ebb-directed values using the flood angle, the angle that defines the upstream direction of flow at each location, provided by the data source.

Figure 24. Velocity-comparison locations.

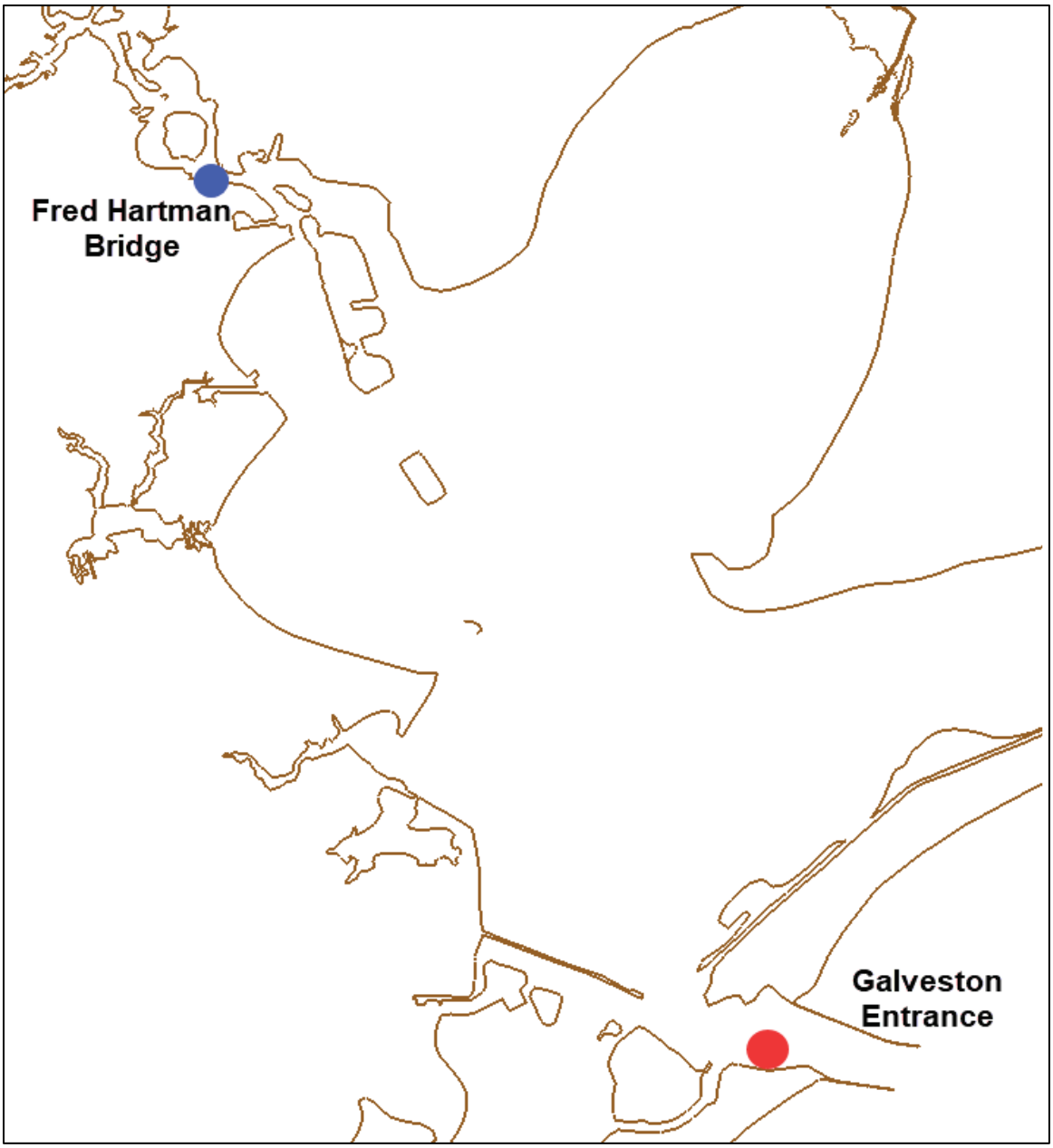

Figure 25 through Figure 29 show a time history of velocity magnitude and direction (positive: flood; negative: ebb) for these locations. Modeled surface velocities are shown in *blue* and bottom velocity in *red*. Field data are shown in *black*. The field data are sampled at varying locations in the water column depending on the site, but all are at an approximate middepth location.

Velocity datasets at the Galveston Entrance location are compared for both 2010 and 2017, although the time of data availability differs. Both years show good agreement to the measured field data—replicating the pattern and magnitude of the field data.

The Fred Harman Bridge velocity data are only available for a few periods during 2017, and the field data are extremely variable at this location. The same time period is plotted for the Galveston Entrance and Fred Hartman Bridge—15 October through 1 November—in Figure 26 and Figure 27.

It is obvious that there is much more variability in the field data at Fred Hartman Bridge than at the Galveston Entrance. The bridge location is a narrower flow location than the entrance channel location, and it is located in the HSC where numerous vessel passages are made daily. It is not unexpected that the vessels would impact the velocity patterns generated in the field at this location. This area also sees flow convergence around Alexander Island just to the north as well as flow impacts due to the large bridge pier to the west of the HSC. At this location, the model shows a reversal of flow direction from surface to bottom for much of the simulation period. At times the bottom velocity magnitudes are larger than the surface, which is atypical. However, given the nature of the converging flow and eddy formations around the geometric features, this variation in flow direction and magnitude is possible.

Figure 25. 2010 Galveston Entrance velocity comparison (positive: flood; negative: ebb).

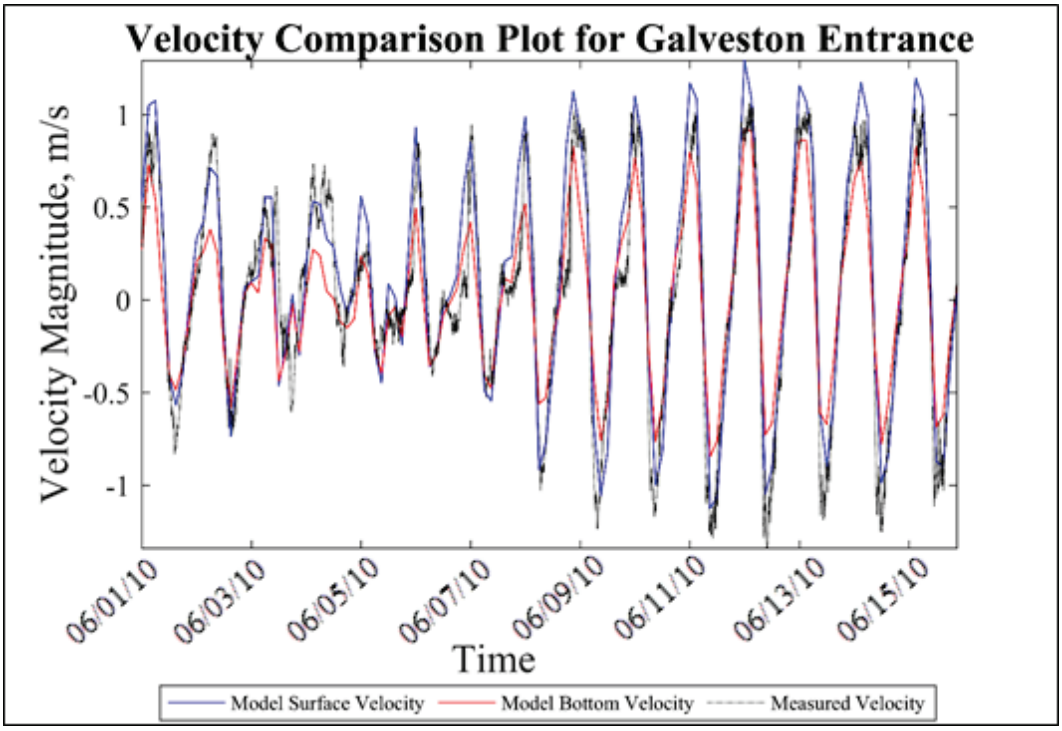

Figure 26. 2017 Galveston Entrance velocity comparison (positive: flood; negative: ebb).

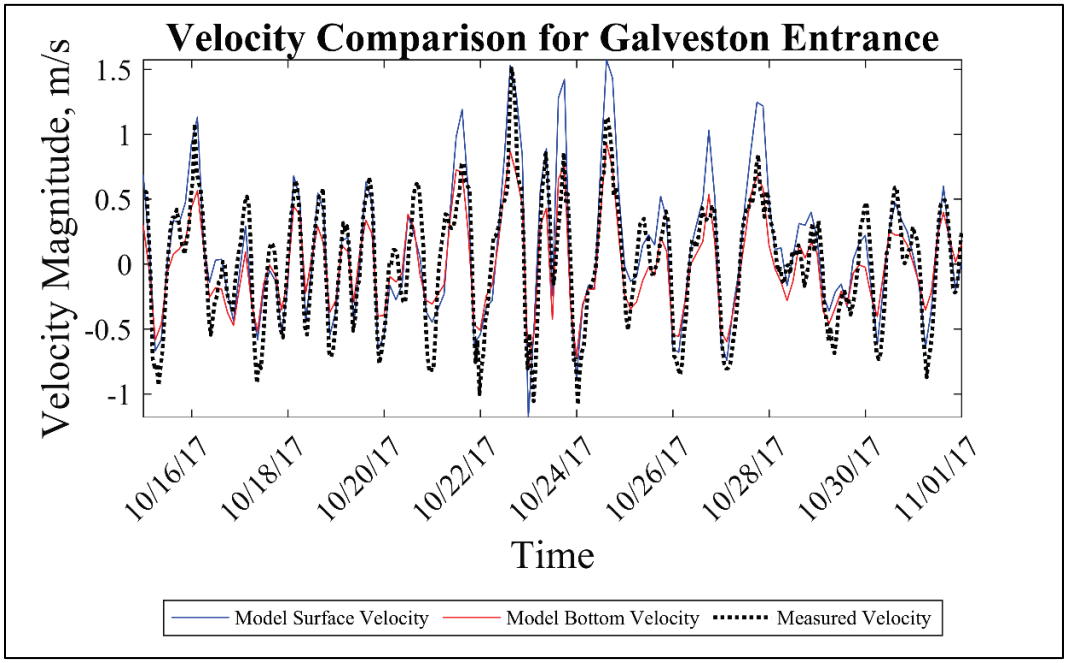

Figure 27. 2017 Fred Hartman Bridge velocity comparison (positive: flood; negative: ebb).

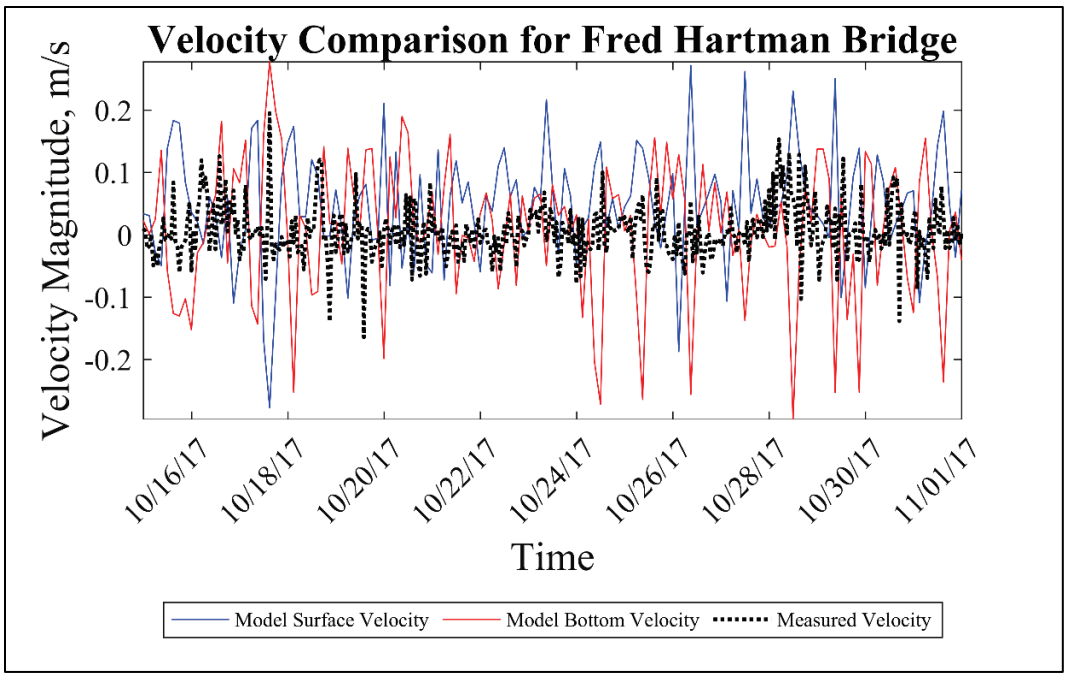

Figure 28 and Figure 29 are plotted at both locations for the time of Hurricane Harvey. The Galveston Entrance Channel velocity pattern is reproduced by the model although some peak magnitudes are not. Given that this measurement is taken at a middepth location, it would be expected that the model would show the field data between the surface and bottom velocity magnitudes. The Fred Hartman Bridge velocity is much higher in the model than in the field prior to the storm and then lower than the field after the storm. Figure 19 shows the water level in this general area also higher in the model than in the field. The model is forcing more flow in the channels since it cannot wet and dry, so this difference in not unexpected. There are also uncertainties in the inflow values that are being supplied from the TWDB watershed model (more details provided in Section 3.2).

Figure 28. Hurricane Harvey velocity comparison for Galveston Entrance (positive: flood; negative: ebb).

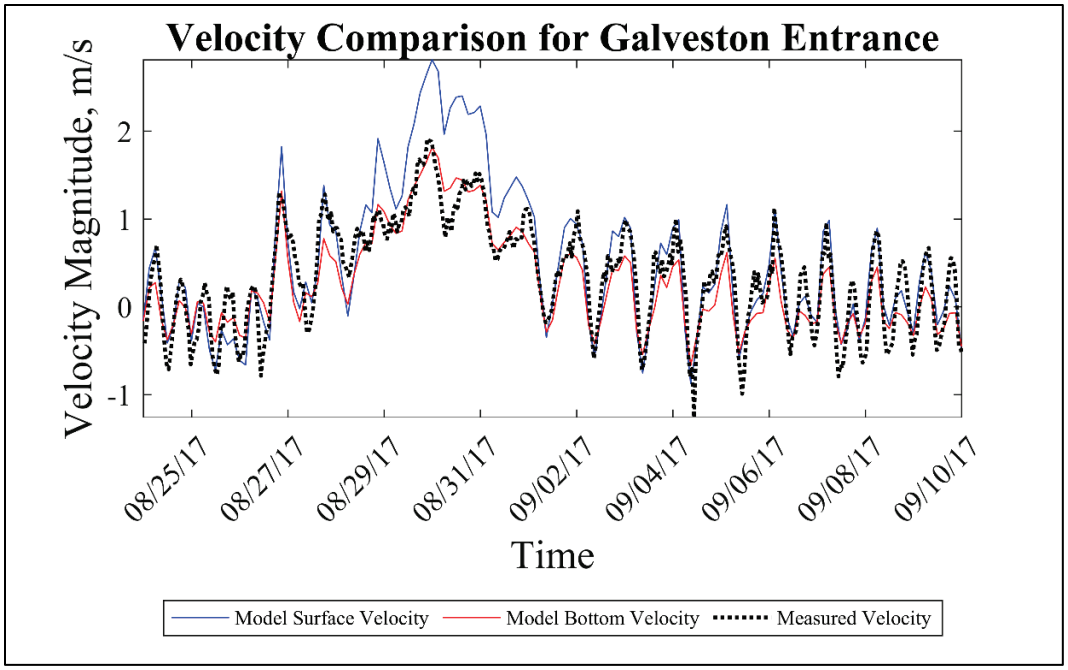

Figure 29. Hurricane Harvey velocity comparison for Fred Hartman Bridge (positive: flood; negative: ebb).

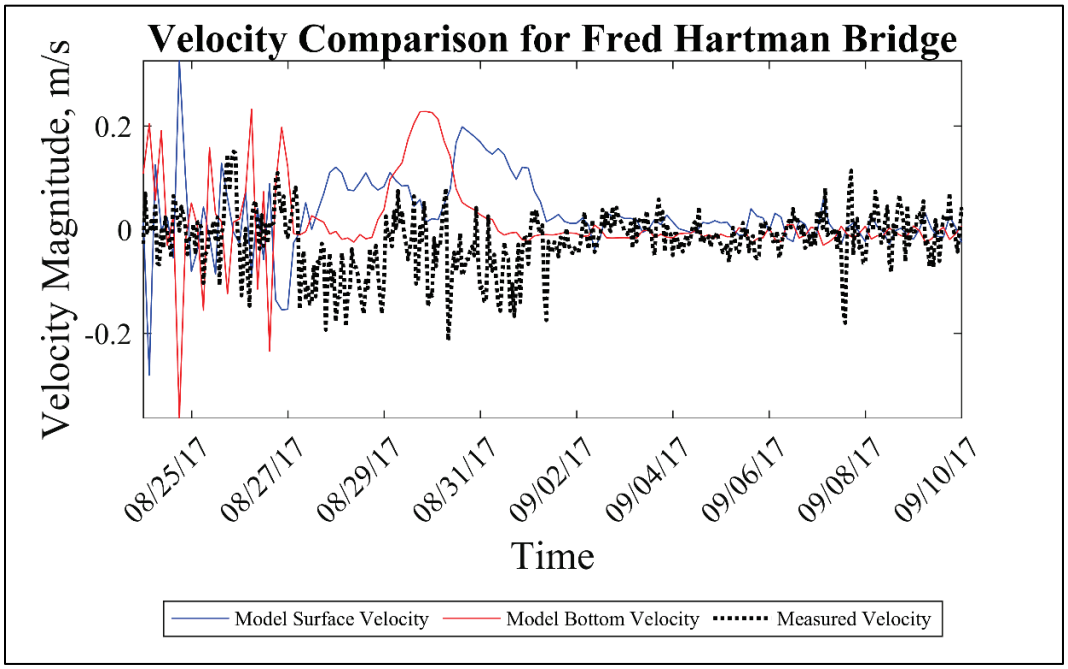

3.1.3 Texas A&M Galveston Acoustic Doppler Current Profiler (ADCP) Transects

TAMUG was contracted by SWG to collect vessel-mounted acoustic Doppler current profiler (ADCP) transects in areas along the HSC and San Jacinto Bay. They collected data in February and April 2022. Given that the AdH model validation period is several years prior to this recent field data collection, only a qualitative comparison can be made between the AdH model results and the field data. Figure 30 shows the field-data transects that will be used for comparison to model results.

Figure 30. Texas A&M University-Galveston (TAMUG) acoustic Doppler current profiler (ADCP) transects used for qualitative model-to-field comparison.

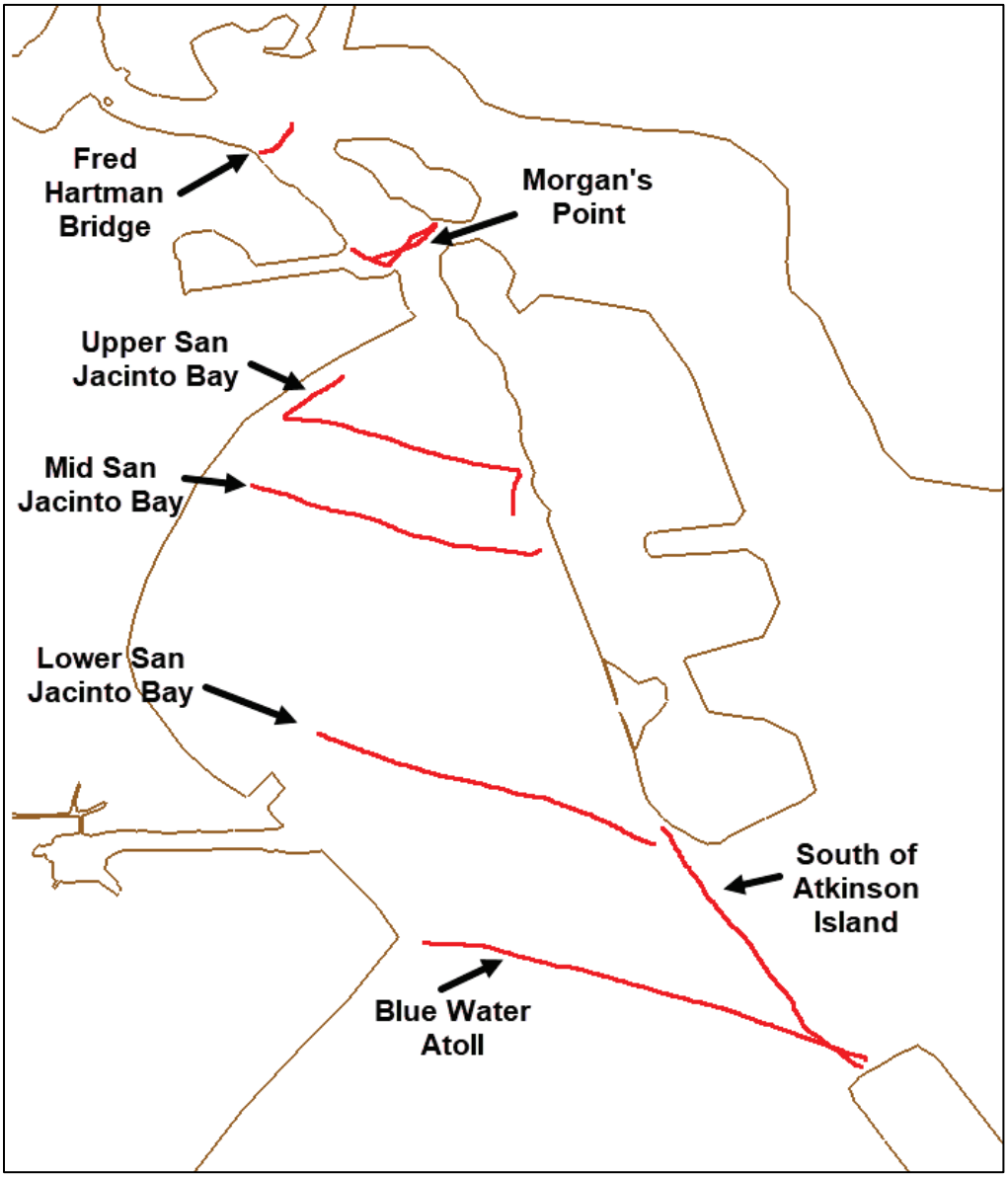

Figure 31 through Figure 39 show comparisons of field-data transect velocity (*red*) and model velocity (*black*). The results are not expected to be identical but to show a common trend in the model-to-field directions and magnitudes. Some comparisons for a single ADCP transect are shown for multiple model output times with *circles* indicating the areas along the transect showing better comparisons. Again, since the model was not run at the same time of the field data collection, identical results at a single time are not expected.

The upper San Jacinto River transect (Figure 34 and Figure 35) shows eddy formations in the bay in both the field data and the model results. The Figure 35 comparison shows eastward directed flow in the field data and in the model, although the model results show this to the west of where it is seen in the field. This difference of location could be due to many factors including local winds, tide strength, or river discharge. However, the comparison shows that the model is capable of producing this eastward directed flow in the same general area.

The Blue Water Atoll transect (Figure 39) shows some oscillating vector directions along the field-data transect. Some of this oscillation may be due to eddy formation or circulating flow, but vectors that reverse direction back and forth are often indicative of local instabilities or malfunctions in the field-data collection. However, along this transect, the model produces several velocity-direction results that are similar to the overall trend along sections of the transect (*circled* in the figure).

Figure 31. Fred Hartman Bridge model-to-field velocity comparison.

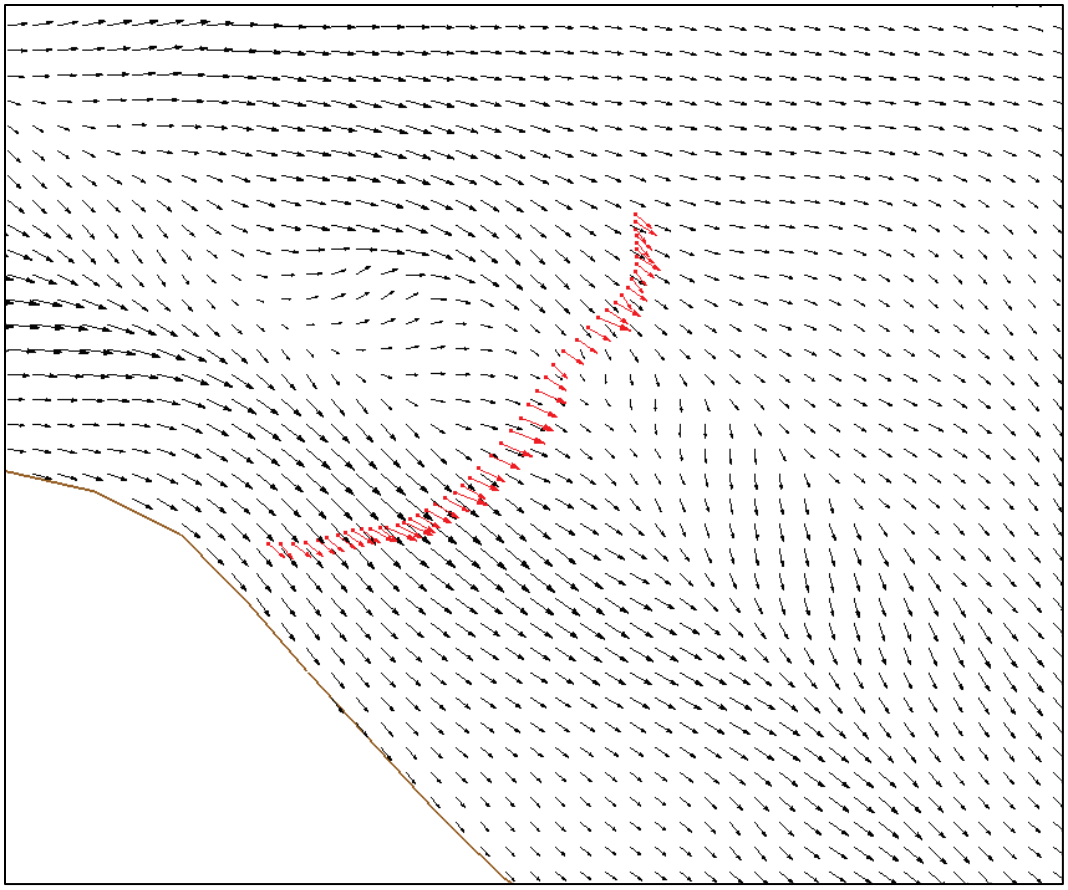

Figure 32. Morgan's Point model-to-field velocity comparison (model time 1).

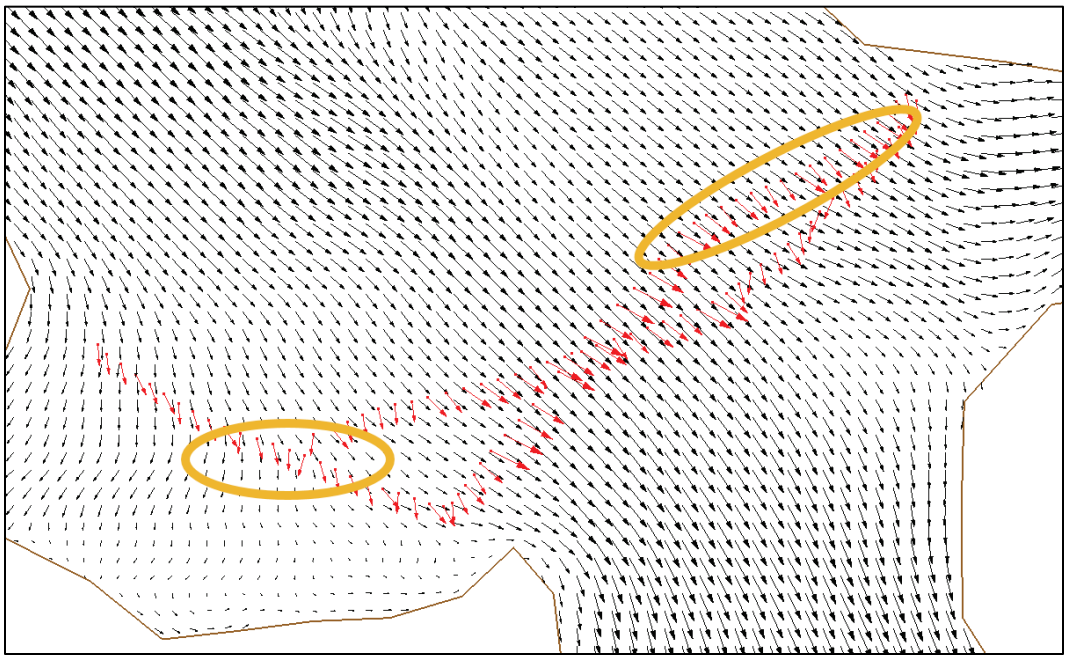

Figure 33. Morgan's Point model-to-field velocity comparison (model time 2).

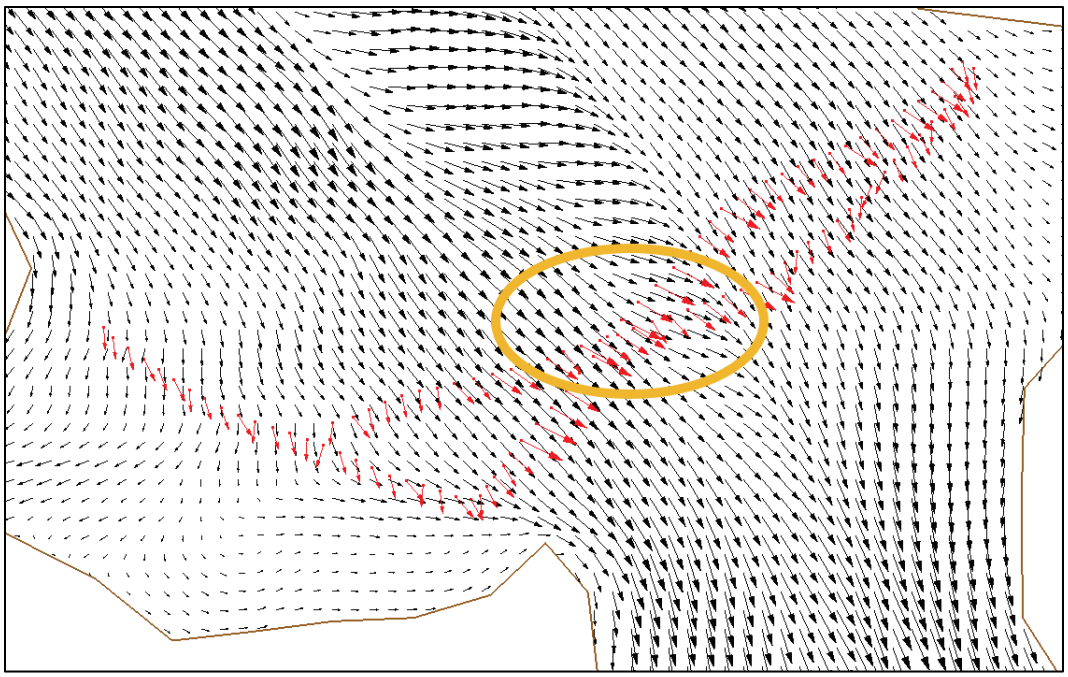

Figure 34. Upper San Jacinto Bay model-to-field velocity comparison (model time 1).

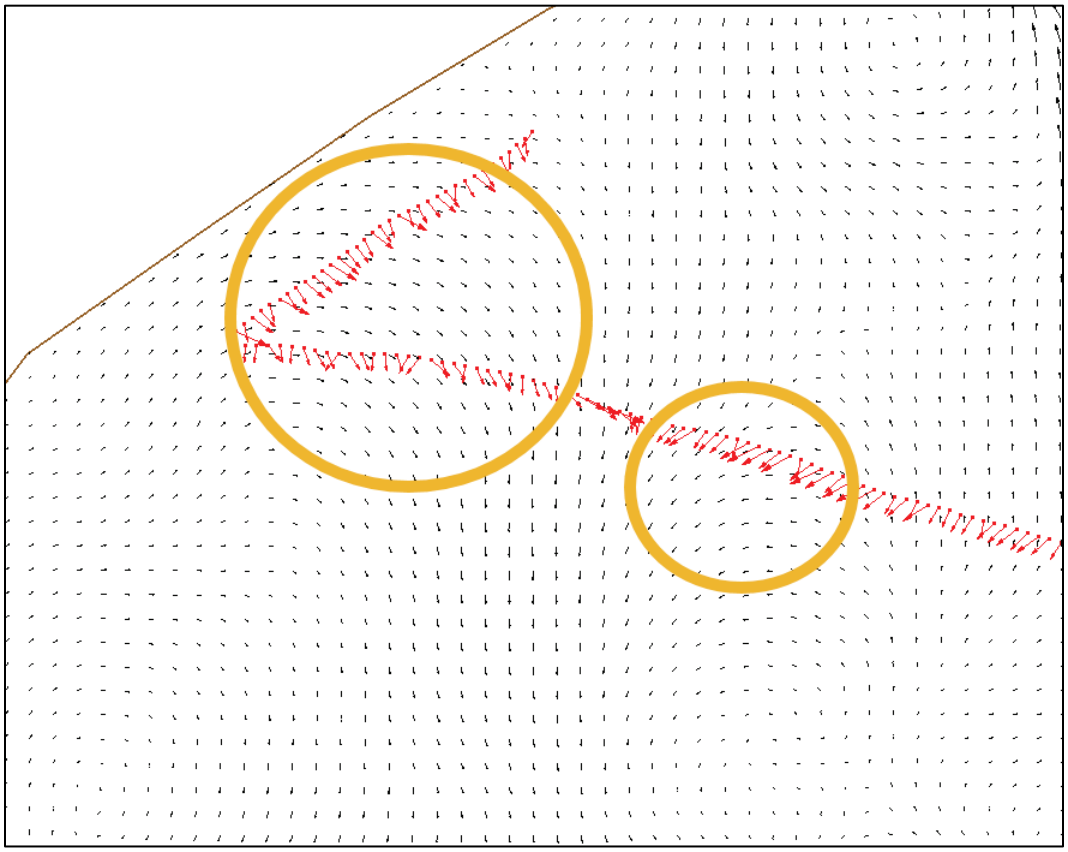

Figure 35. Upper San Jacinto Bay model-to-field velocity comparison (model time 2).

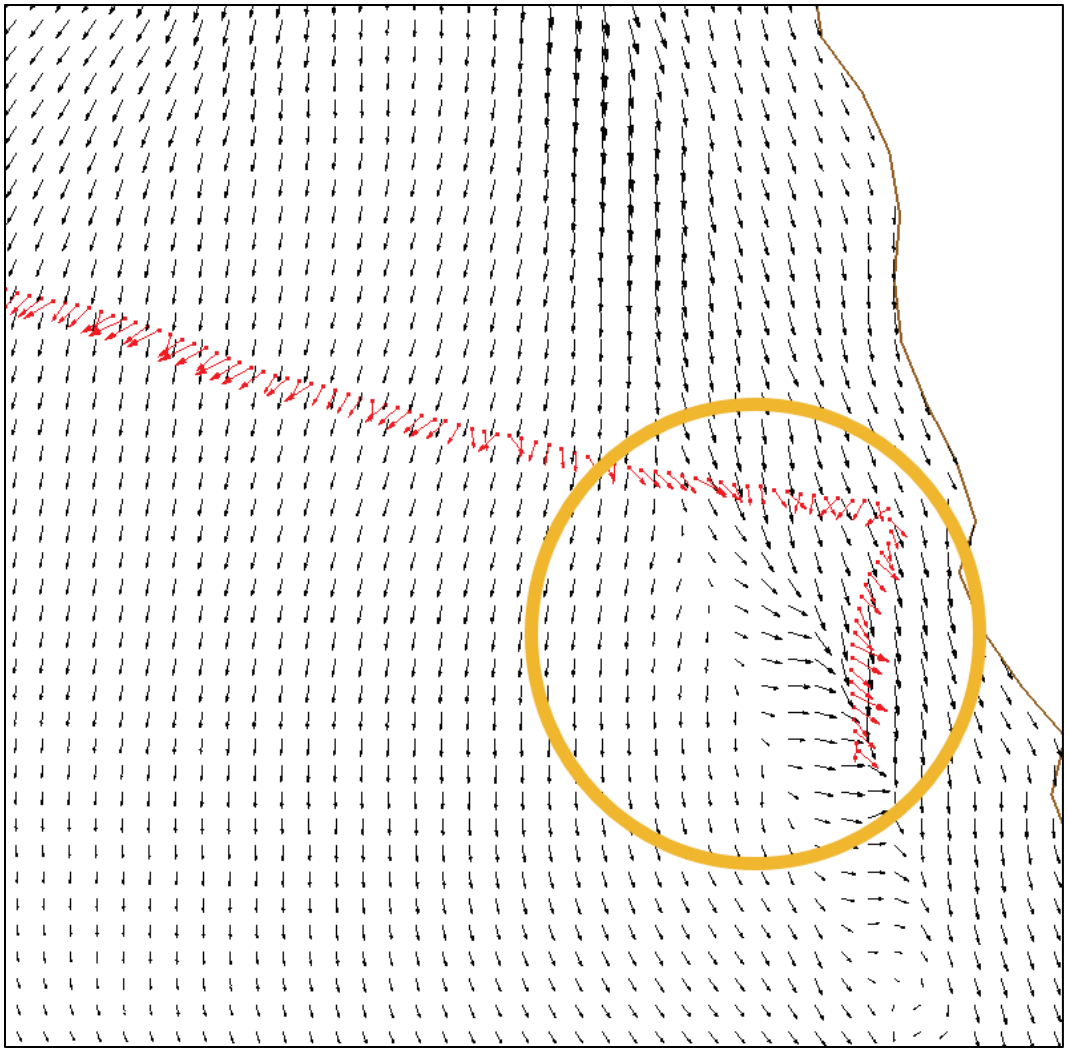

Figure 36. Mid San Jacinto Bay model-to-field velocity comparison.

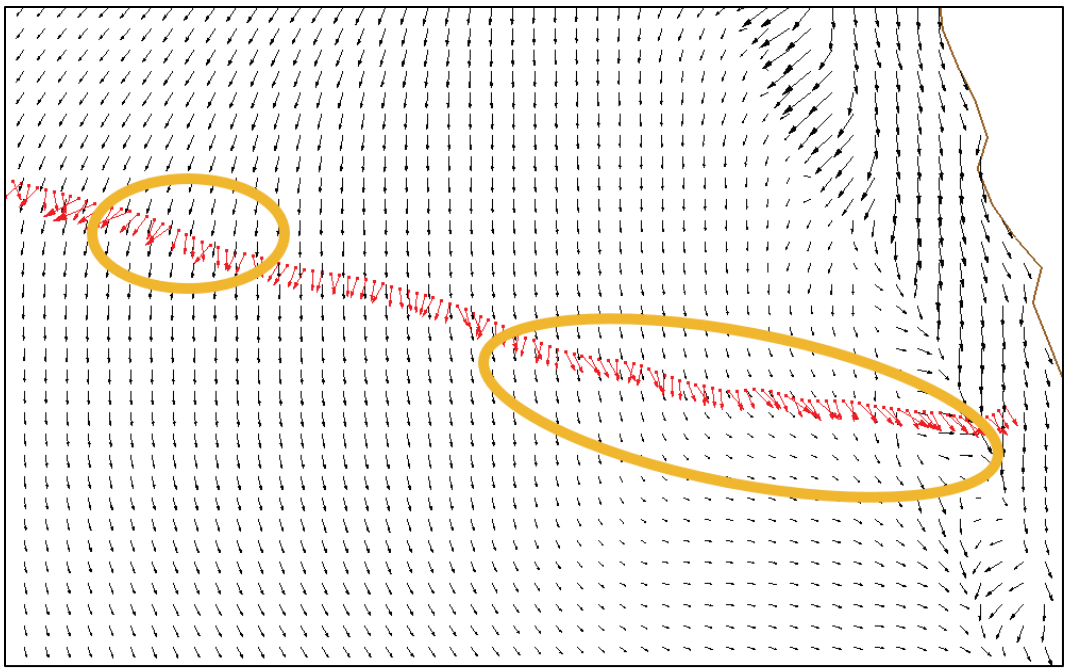

Figure 37. Lower San Jacinto Bay model-to-field velocity comparison.

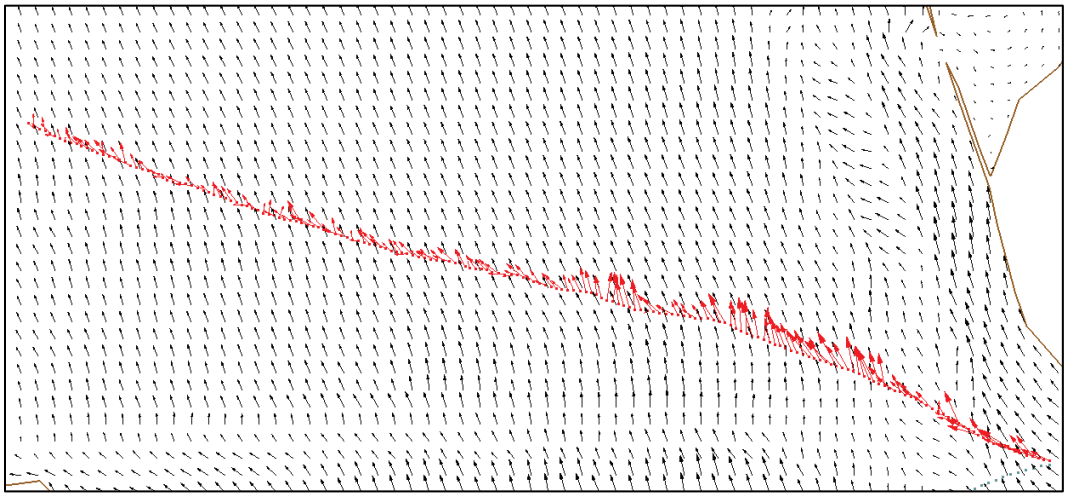

Figure 38. South of Atkinson Island model-to-field velocity comparison.

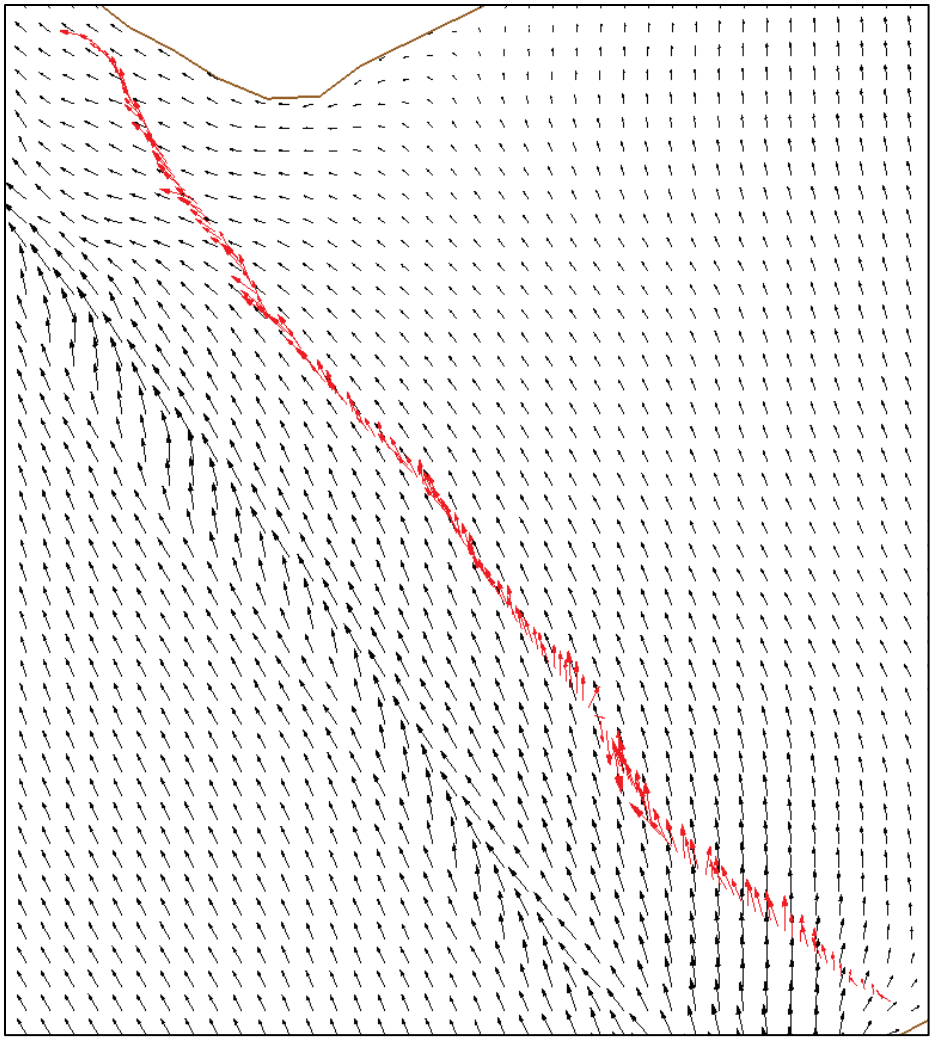

Figure 39. Blue Water Atoll model-to-field velocity comparison.

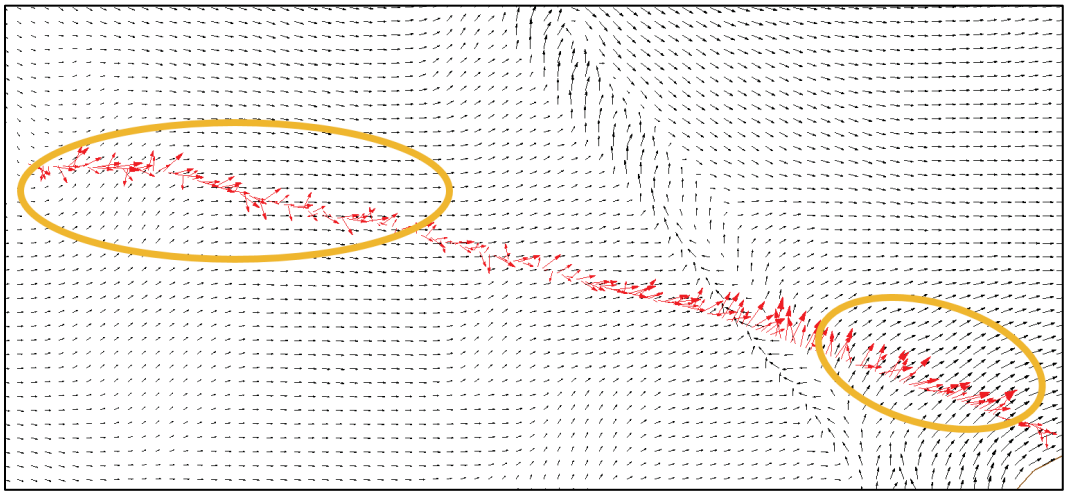

Comparisons to a 2-week data collection at fixed locations was also performed for the TAMUG fixed measurement sites. Figure 40 shows the bottom velocity field data collected by TAMUG during a 2-week spring tide period (15–28 April 2022). Figure 43 through Figure 48 show the AdH-modeled bottom velocity results in a similar fashion. The *left-side plot* includes the full 2010 simulation year. The *right-side plot* includes only a 2-week time period (28 June–11 July 2010) such that the water levels at Morgan's Point were similar to those during the field-data collection. It is known that a strong wind from the southeast was present during the field-data collection period (Figure 41). The wind speed during the 2 weeks of model data is lower than the field, on average, and does not show as strong of a southeastward direction (Figure 42). Although the comparison of the model to the field data is done under similar conditions, the two time periods are not identical.

Figure 40. TAMUG bottom velocity rose for fixed location measurements (from TAMU-G report, direction from which current originates).

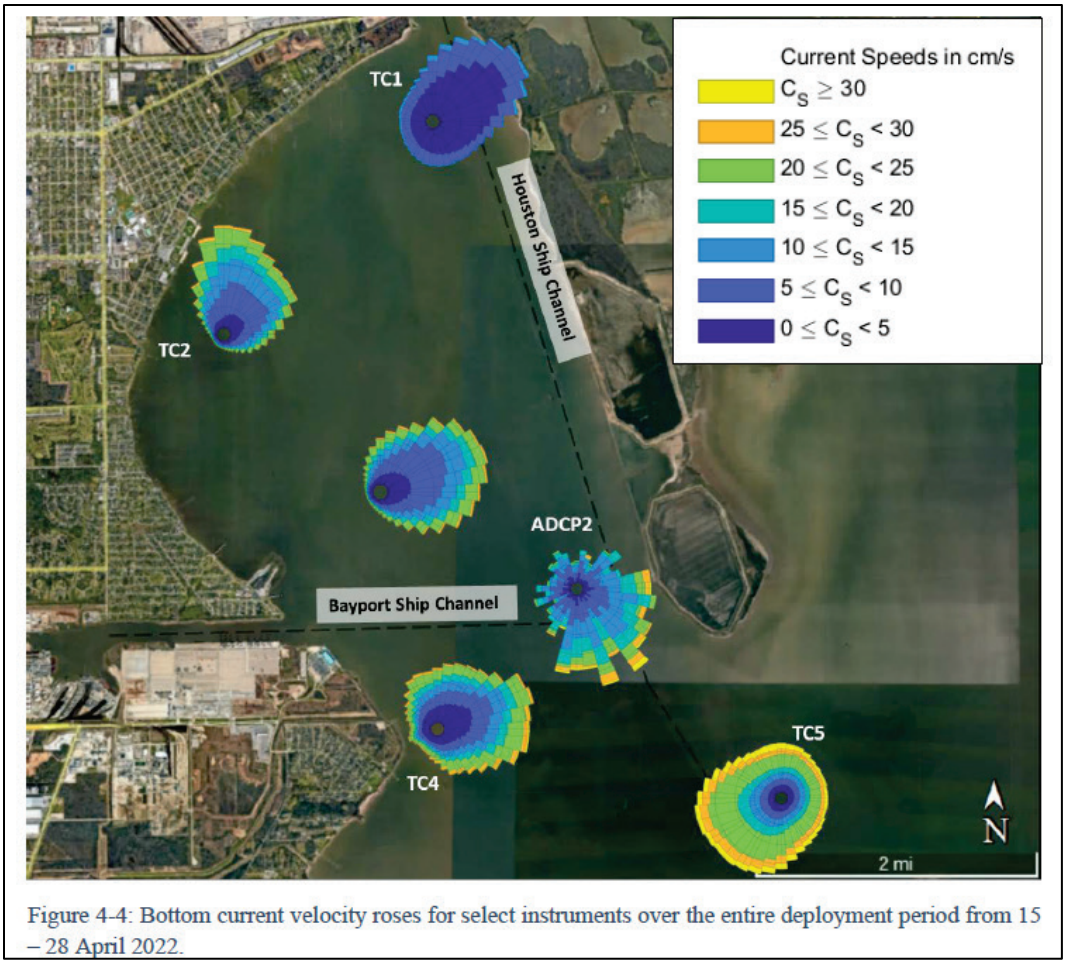

Figure 4-4: Bottom current velocity roses for select instruments over the entire deployment period from 15 – 28 April 2022.

Figure 41. National Oceanic and Atmospheric Administration (NOAA) plot of wind speed and direction for field data collection time period.

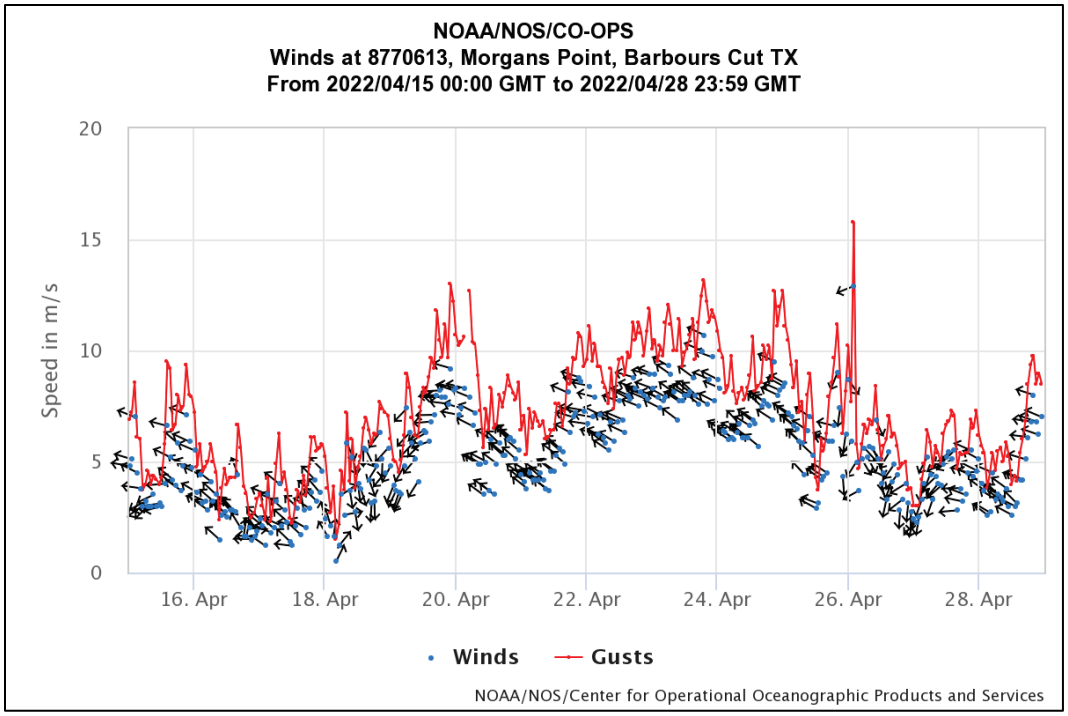

Figure 42. NOAA plot of wind speed and direction for model processed 2-week period.

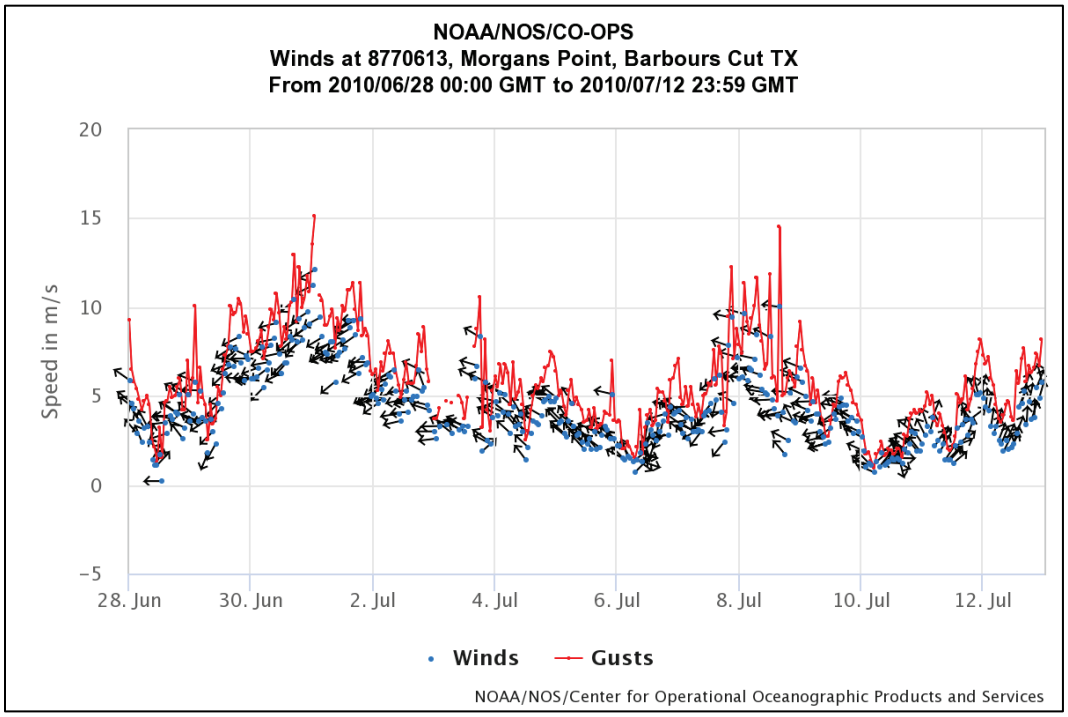

As with the previous set of comparisons, the model is not expected to replicate the field since the time periods analyzed are not the same. However, trends can be compared in a qualitative sense. In the case of these velocity comparisons, there are many local effects that can impact the results. The field data were collected during one time period that may not be indicative of average conditions. Vessel passages can greatly impact surface and bottom velocities, and these forces are not included in the AdH model.

The TC1 location shows good agreement between the model and the field data in the direction of flow. The TC2 location shows flows predominantly from the north-northeast, which is also indicated in the model results. The TC4 location in the field shows flows predominantly from the east whereas the model is showing flows predominately from the northwest and southeast. The TC 5 location shows model and field velocity coming from the southwest. The TC7 location is very different between model and field as is the ADCP2 location. These differences could be attributed to the difference in the time periods being compared as well as to local impacts of vessel traffic.

Figure 43. TC1 modeled bottom velocity roses (direction from, cm/s).

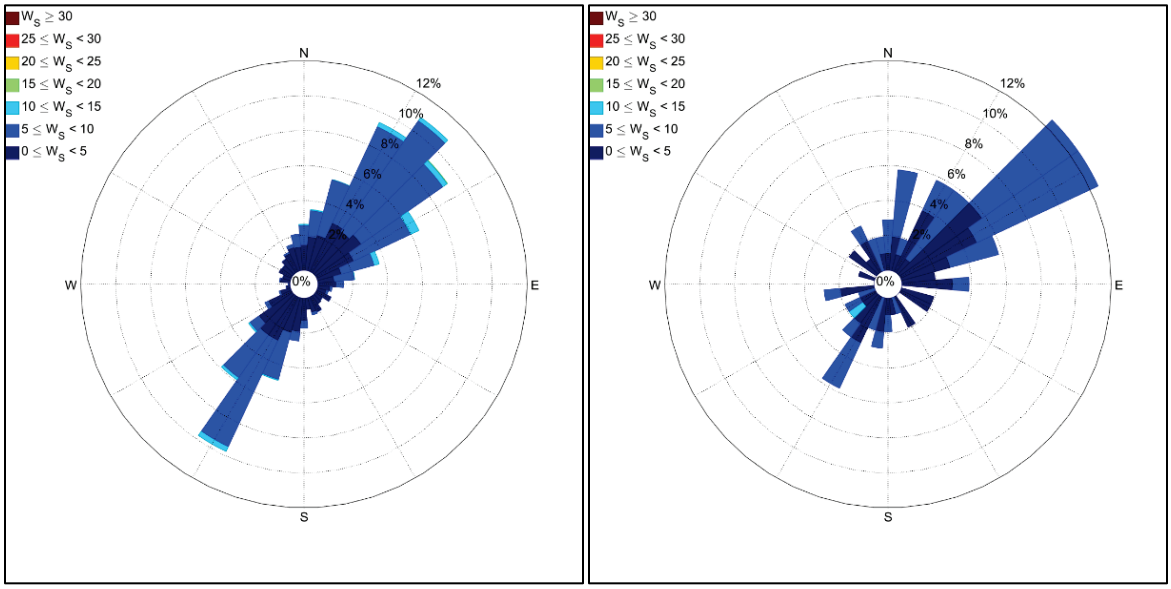

Figure 44. TC2 modeled bottom velocity roses (direction from, cm/s).

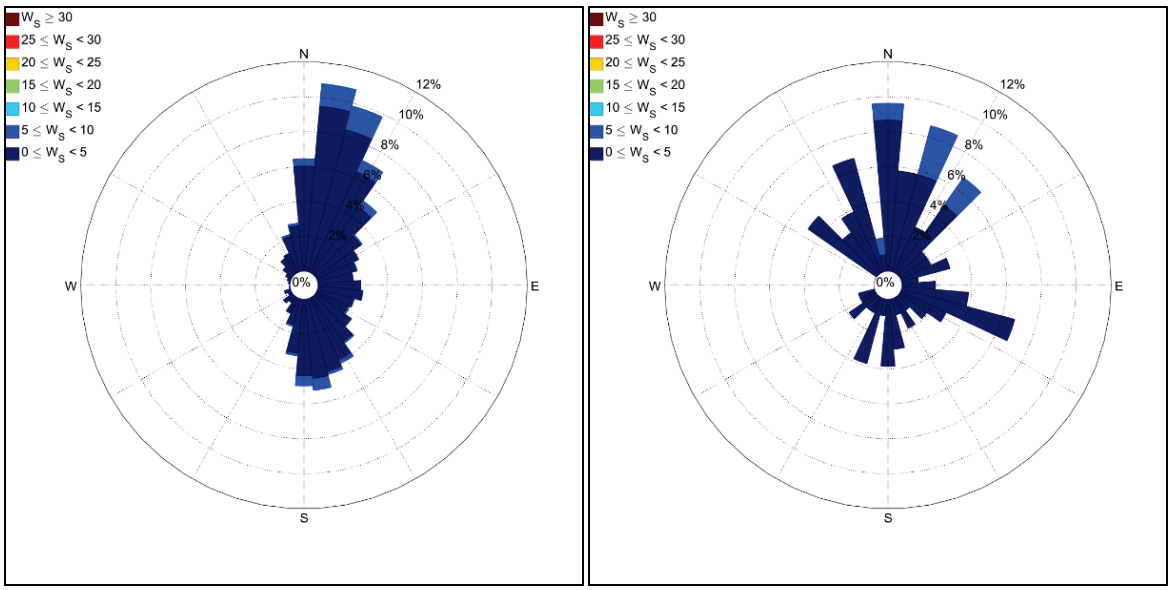

Figure 45. TC4 modeled bottom velocity roses (direction from, cm/s).

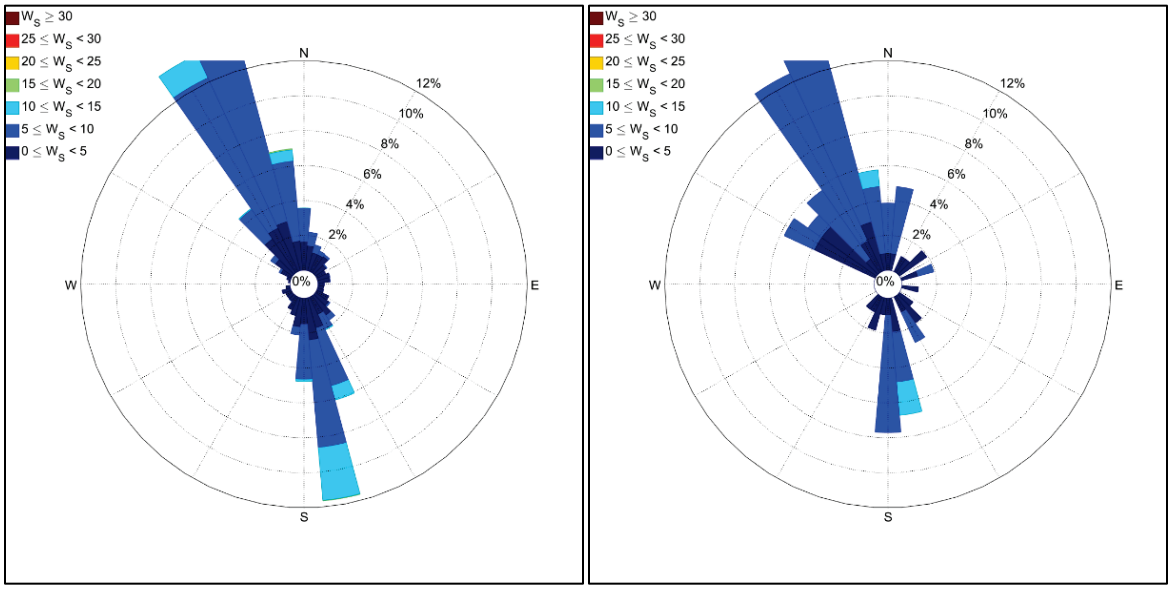

Figure 46. TC5 modeled bottom velocity roses (direction from, cm/s).

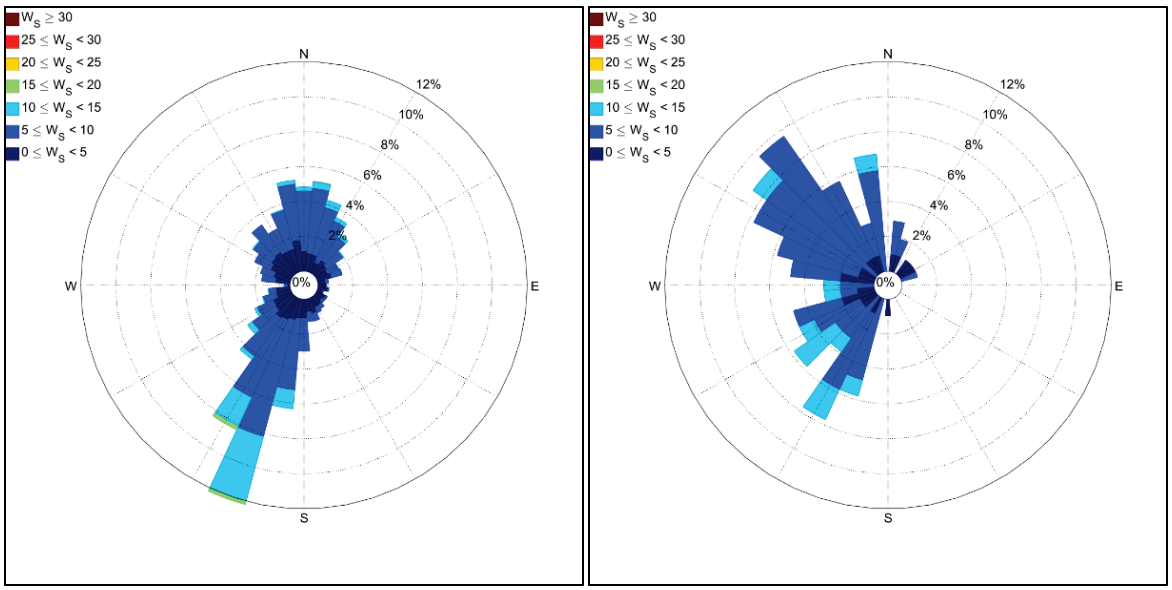

Figure 47. TC7 modeled bottom velocity roses (direction from, cm/s).

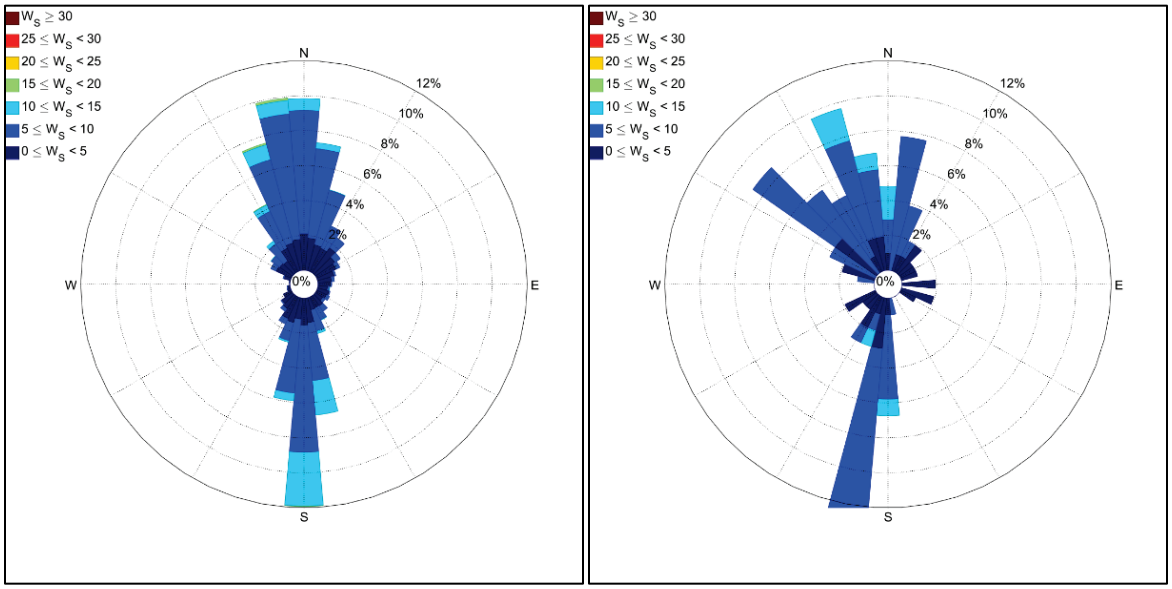

Figure 48. ADCP2 modeled bottom velocity roses (direction from, cm/s).

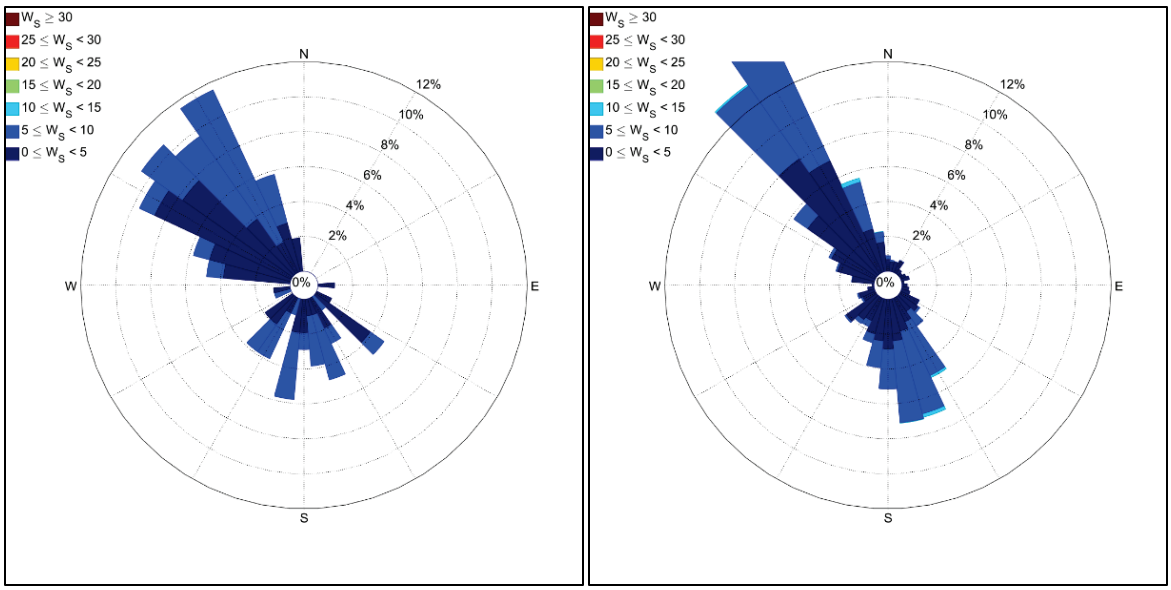

3.2 Salinity Comparison

Field salinity data were obtained for model validation from TWDB (Figure 49), Texas Commission on Environmental Quality (TCEQ) (Figure 50), Houston Advanced Research Center (HARC) (Figure 51), and Texas Automated Buoy System (TABS) (Figure 52). There are 29 salinity-comparison sites throughout the HSC and the surrounding bays. As with the previous data comparisons, some sites do not have data for both simulation periods.

Time-history comparisons at selected locations are shown in this section. The field data are represented by *black dots* whereas the model data are shown in *blue* for surface salinity and in *red* for bottom salinity. In deep, stratified regions, the bottom salinity is larger than the surface salinity. In well-mixed regions, the two should be approximately equal. The field-measured salinity is typically measured at the surface, but it is not specified for all data. A subset of comparisons is provided here for selected sites available for both comparison years with the full set of comparisons provided in Appendix B.

Figure 49. Texas Water Development Board (TWDB) salinity-validation comparison sites.

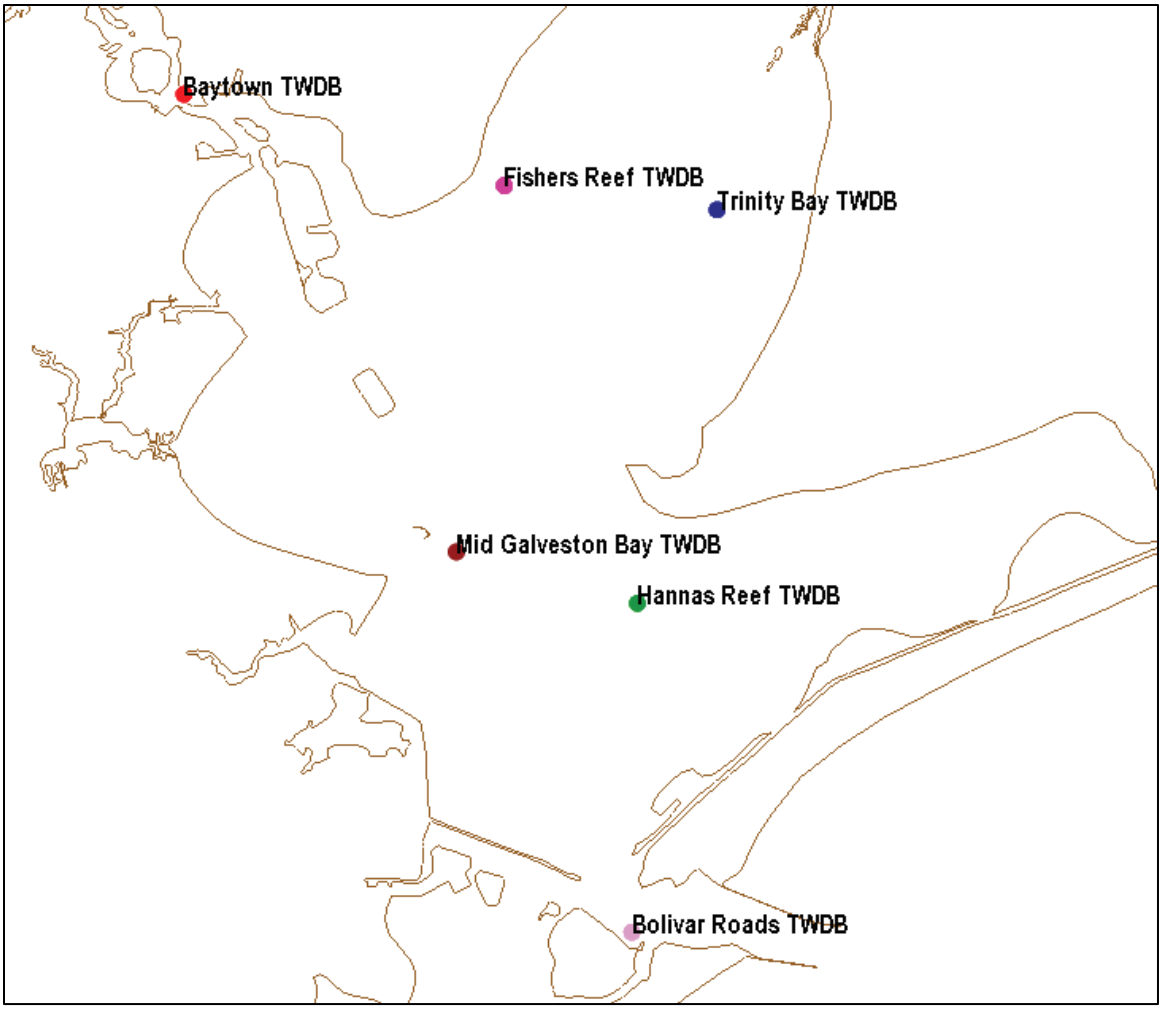

Figure 50. Texas Commission on Environmental Quality (TCEQ) salinity-validation comparison sites.

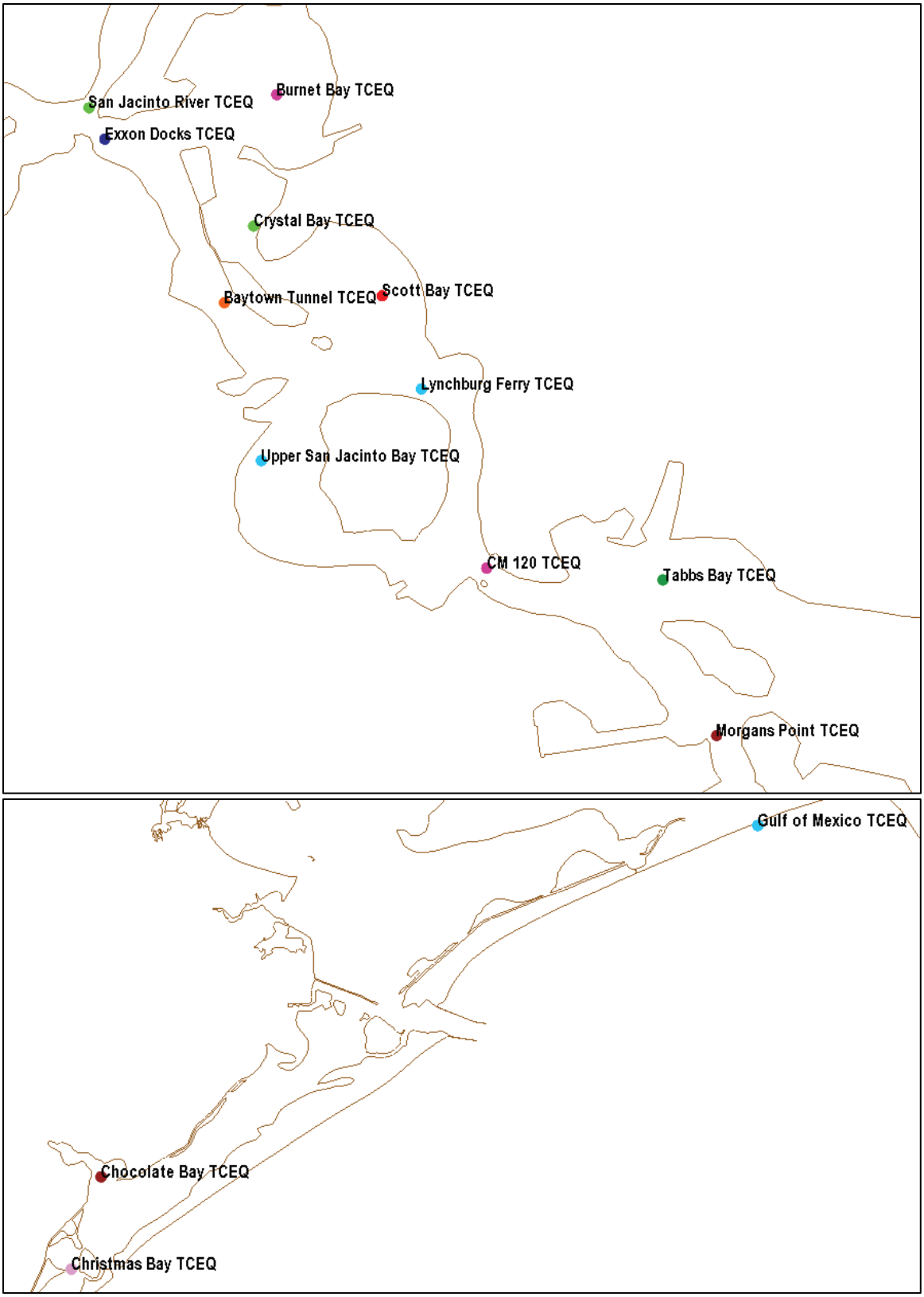

Figure 51. Houston Advanced Research Center (HARC) salinity-validation comparison sites (2010 only).

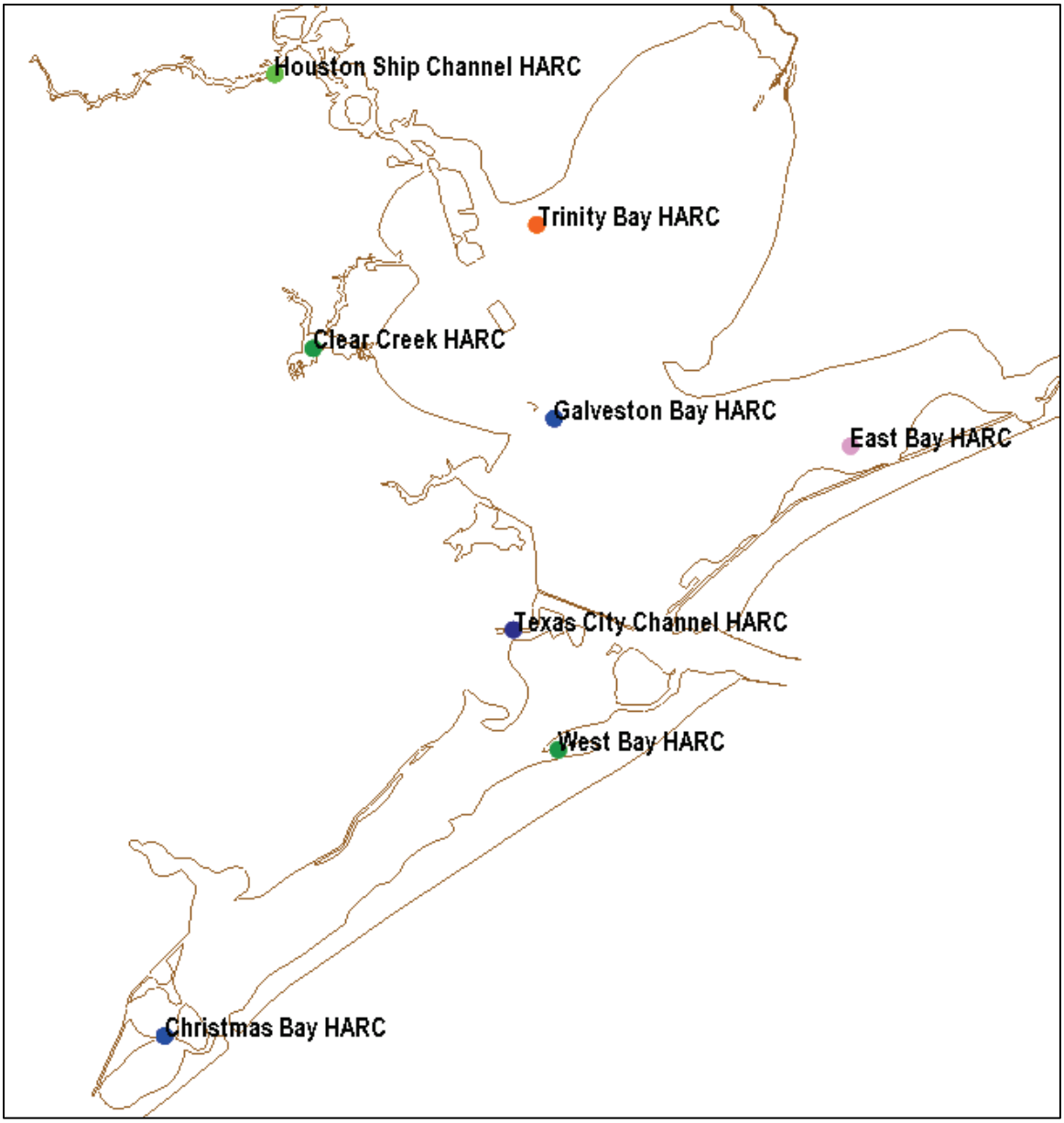

Figure 52. Texas Automated Buoy System (TABS) salinity-validation comparison site.

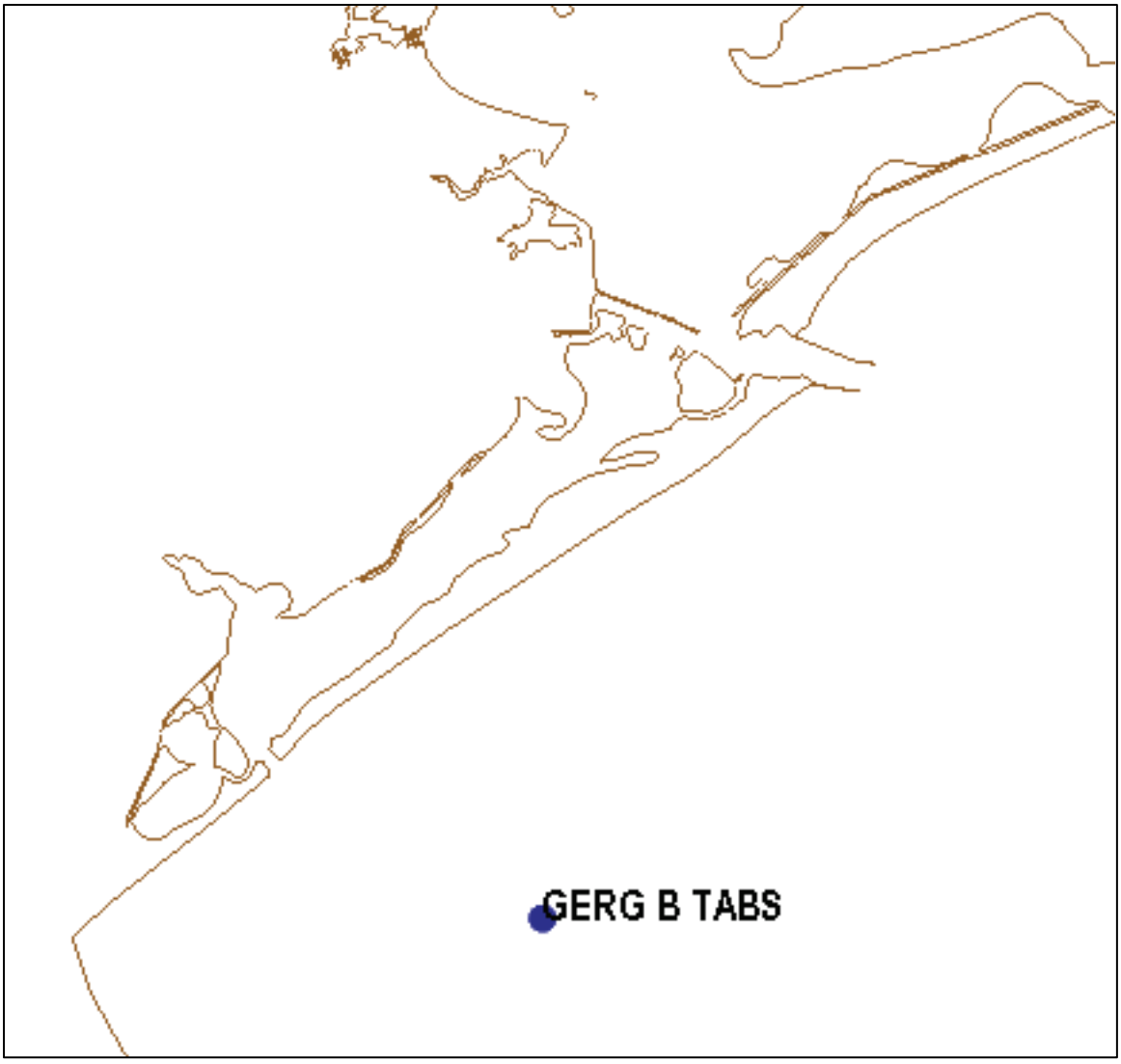

The upper HSC validation sites are primarily located in shallow regions outside of the ship channel. Model-to-field comparisons for the 2010 and 2017 years, from upstream to downstream, are shown in the following plots (Figure 53 through Figure 56) for four selected locations.

Figure 53. Tabbs Bay salinity comparisons.

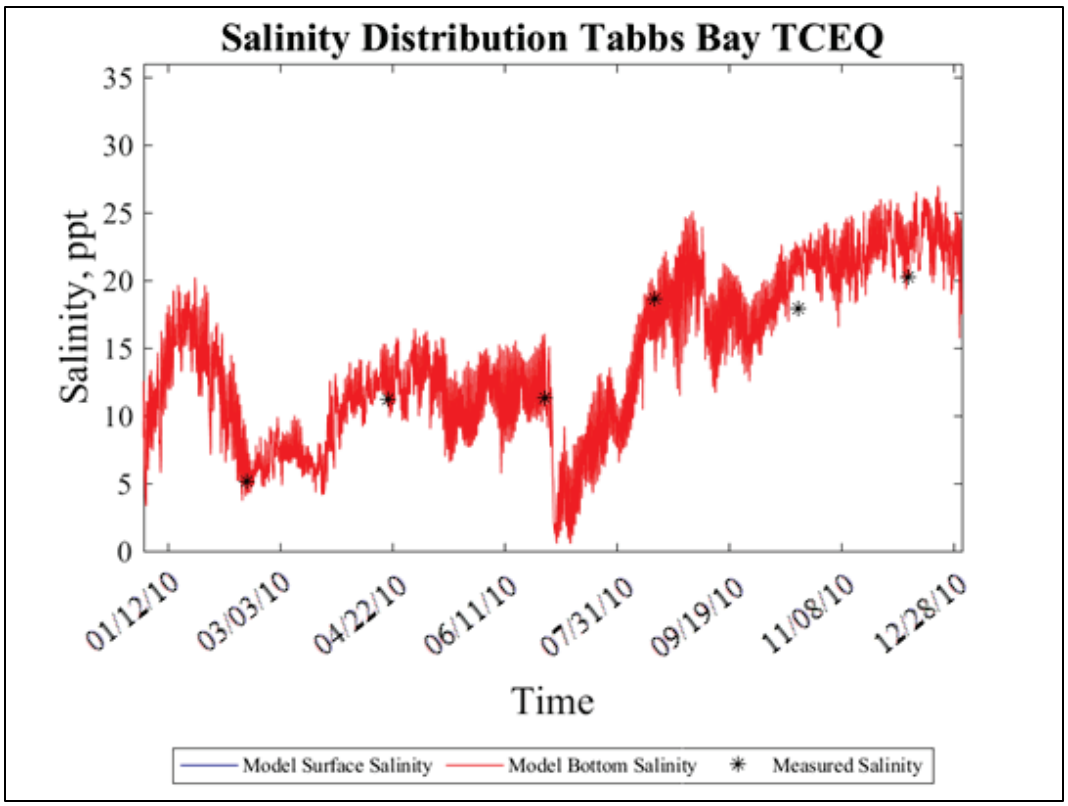

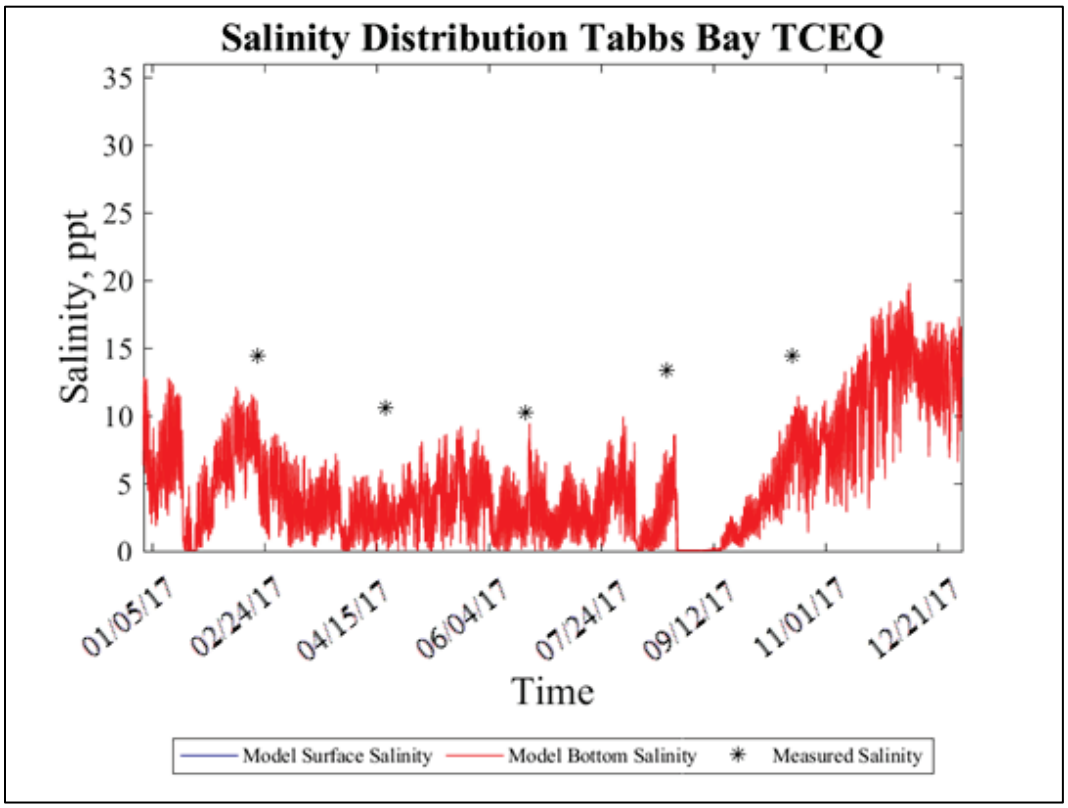

Figure 54. Fishers Reef salinity comparisons.

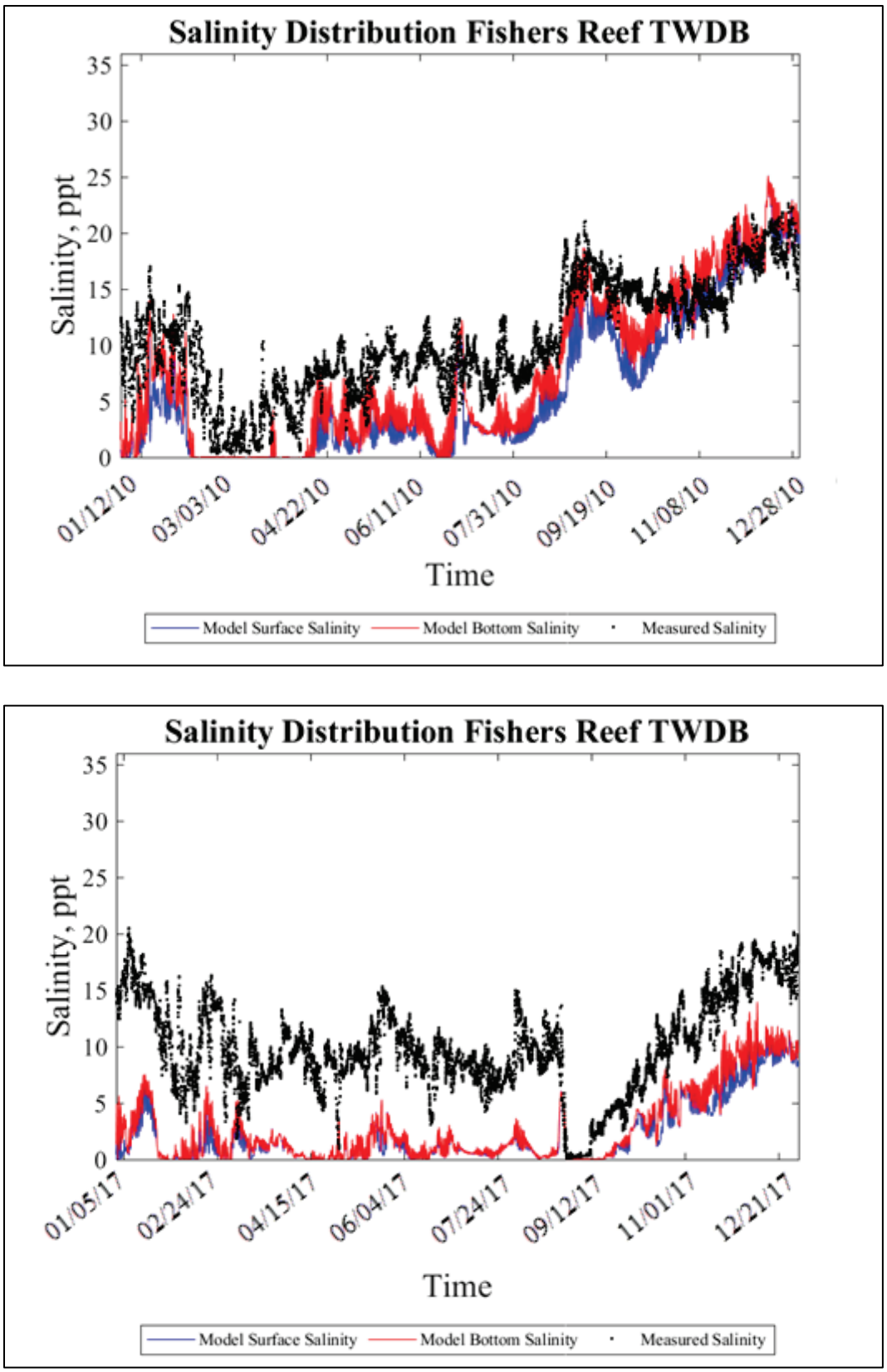

Figure 55. MidGalveston Bay salinity comparisons.

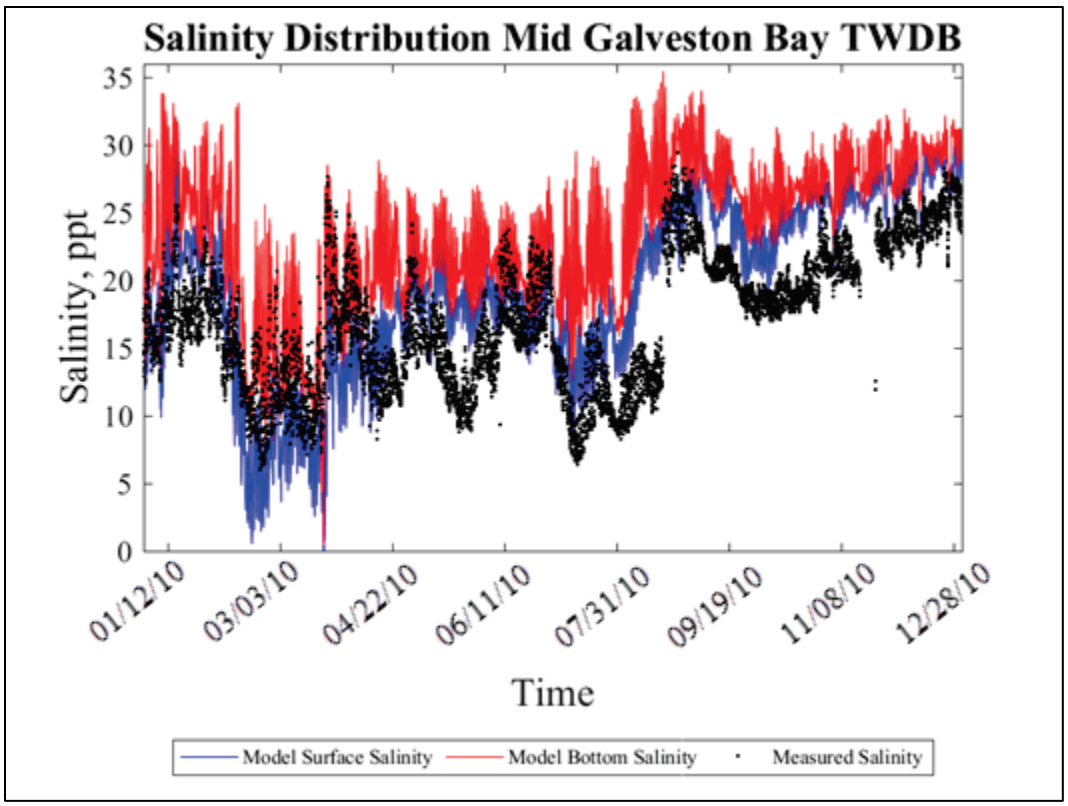

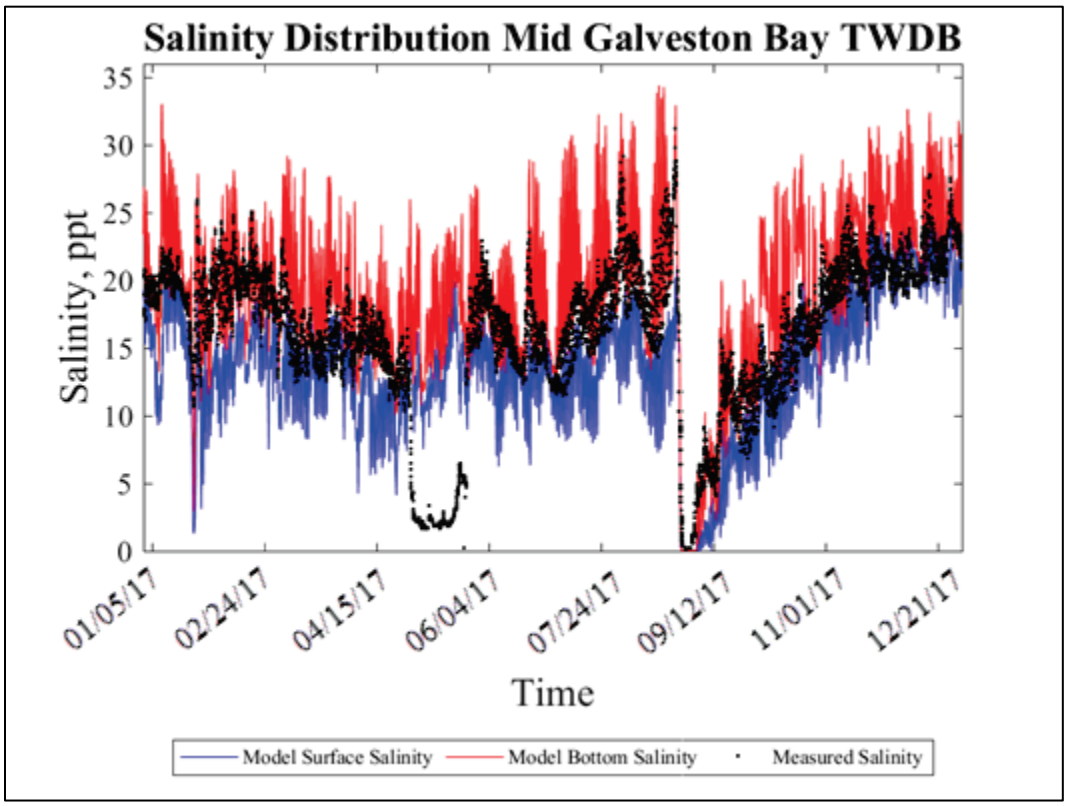

Figure 56. Bolivar Roads salinity comparisons.

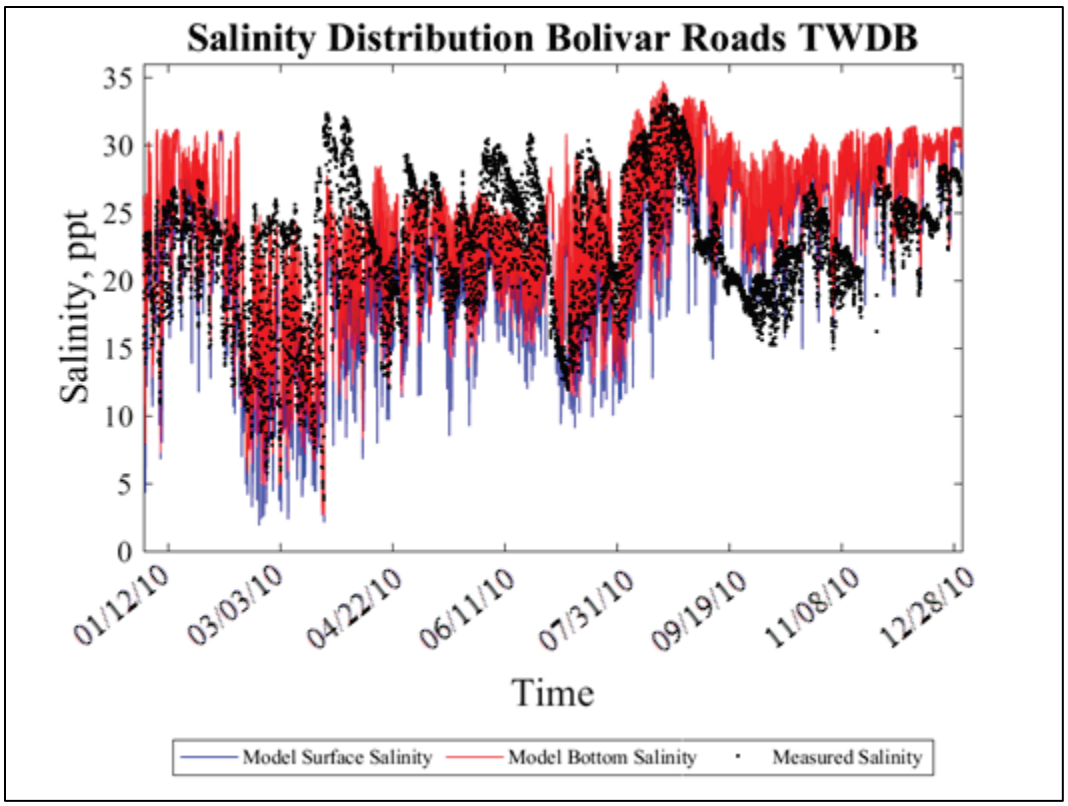

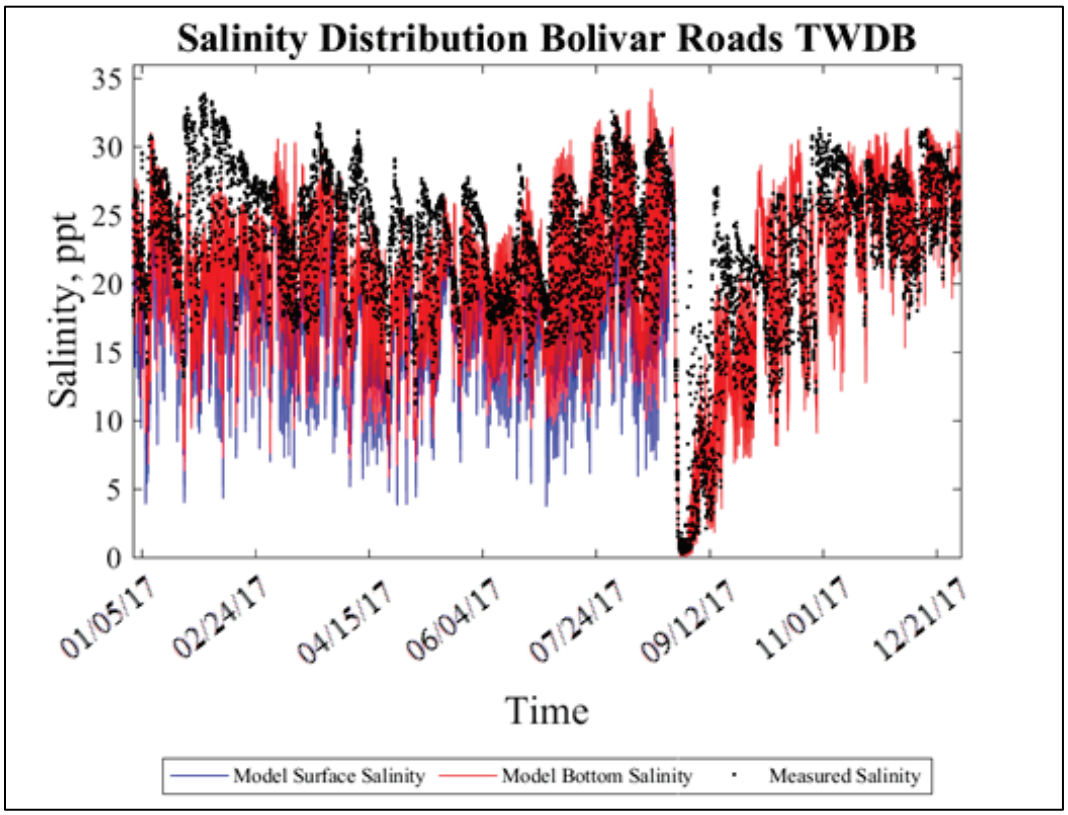

Review of the salinity results and the lower overall salinity produced by the model in 2017 indicated the need for a more detailed investigation of the freshwater inflow supplied to the model. More freshwater flow is supplied to the model in 2017 than in 2010 for most locations (Figure 6 and Figure 7 in Section 2.3.1), especially for the Buffalo and San Jacinto Rivers. Since the initial validation effort (McAlpin et al. 2019b), USGS has added flow gages on some of the waterways entering into this system. For 2017, measured-discharge data are available at the Trinity River at Wallisville (USGS 08067252). These data allow for a direct comparison of the measured flow to the freshwater flow supplied to the model based on TWDB values. Figure 57 shows this comparison. The inflows provided by the TWDB model are typically higher than the USGS-measured values. There does not appear to be a consistent shift in the measured vs. TWDB-computed values to support a direct scaling of the freshwater inflows. As more measurement gages are added to the system, better estimates of the input flows can be used to improve the model validation.

Figure 57. Comparison of measured and modeled supplied flow for the Trinity River.

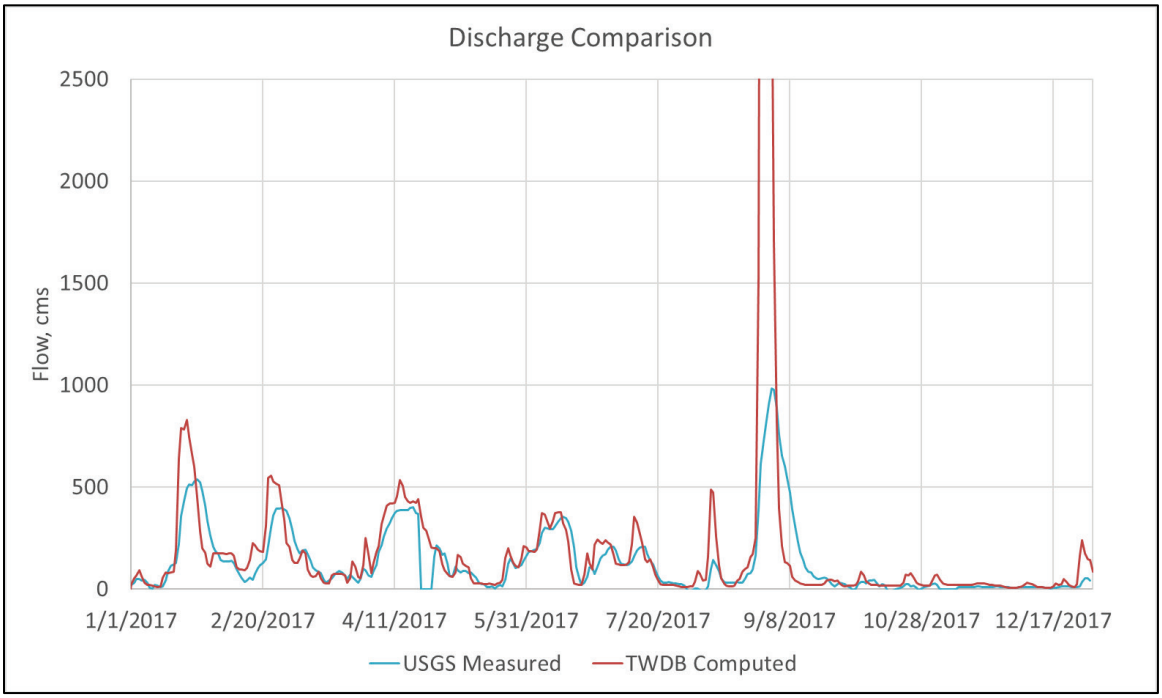

3.3 Sediment Comparison

Since it is known that sediment loads are unaccounted for from the ungaged freshwater inflows, from wind-generated wave erosion along the shallows, and from vessel-induced erosion in the bays, several methods to account for these missing sources were tested. A historical scaling method for each channel segment was determined to be the best option to account for the combined effect of the various unknown loads. The sediment model is compared to historic shoaling records from a Corps Shoaling Analysis Tool (CSAT) analysis of survey data from 2011 to 2020 for the HSC* (USACE 2020). Using the same HSC reaches as in the previous validation efforts (McAlpin et al. 2019b), a scale factor for each segment was computed so that the model is scaled to match the average yearly shoaling volume for each segment. The scale factor for each segment was then applied accordingly for the 2017 simulation results.

Figure 58 shows the shoaling comparison for 2010 and 2017 as compared to the CSAT shoaling volumes (*red columns*). The annualized historic maintenance dredging records for 1965 through 2012 (*blue columns*) are also included for comparison. The 2010 data were used to compute the scale factor based on the average of the CSAT volumes. The 2017 results are used to determine if these factors are reasonable. The preHurricane Harvey shoaling volumes generally lie in the range of the CSAT data. These data are taken from the model results at 1200 hr on 26 August. To compute an annualized shoaling volume, the preHarvey shoaling volumes were increased by 35%. The postHarvey data were taken from the final time-step of the 2017 year-long simulation. The postHarvey data do show a larger shoaling volume than any of the measured data sets for most reaches, not unexpected given the large amount of material that was moved around during the extreme storm event.

These results indicate that the model shoaling results, when scaled based on the CSAT 2010 data, should be appropriate for any base vs. plan comparisons made with the sediment model assuming the unaccounted for processes will not change with the plan alternative.

* USACE. 2020. Houston Ship Channel Expansion Channel Improvement Project. Houston, TX. Shoaling Analysis Report *U*sing CSAT [Draft]. USACE. Galveston, TX: US Army Corps of Engineers, Galveston District, Hydraulics and Hydrology.

Figure 58. Data and scaled shoaling volumes for HSC dredge reaches.

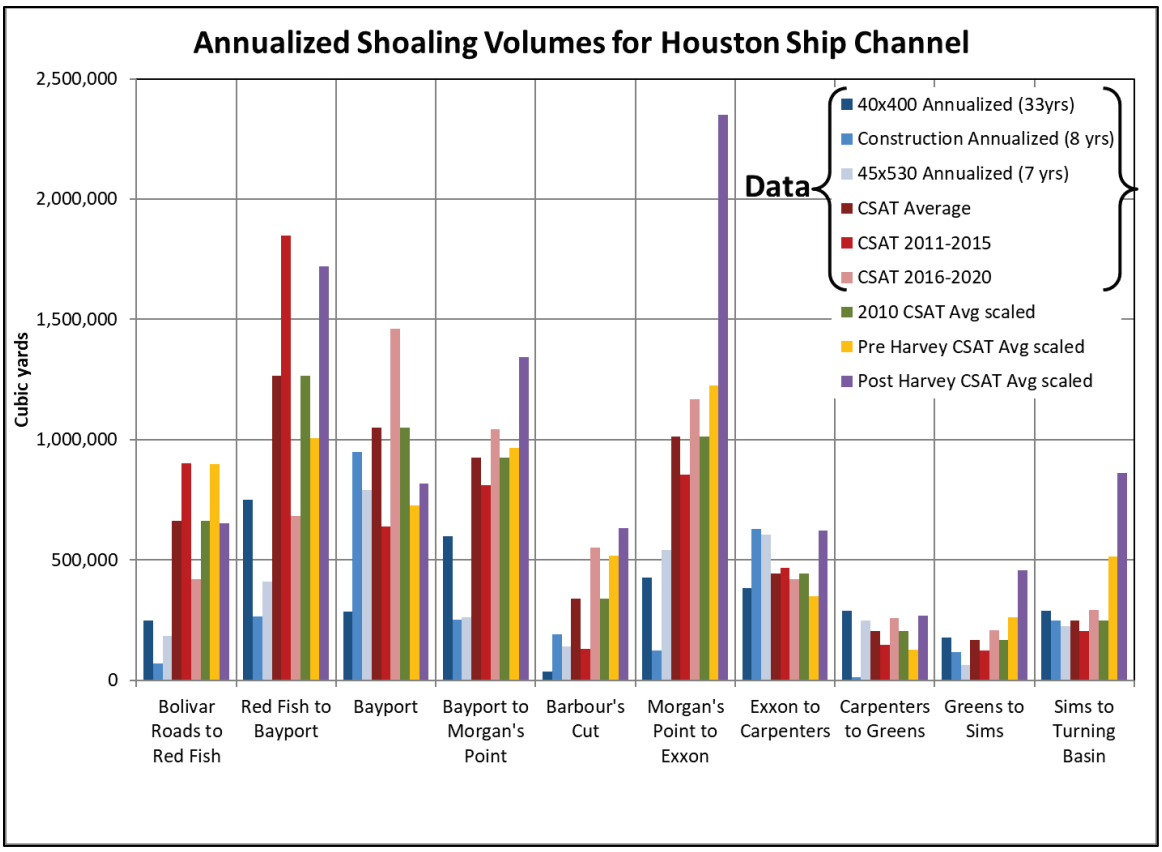

Figure 59 shows the bed displacement along a centerline of the HSC from the Gulf of Mexico to the Houston turning basin. The pattern of deposition along the HSC is replicated in both analysis years (prior to Hurricane Harvey). It is reasonable that 2017 would show lower deposition since the freshwater inflows are higher for 2017, allowing for higher shear stresses due to the flow and an increase in the time it takes suspended material to settle to the bed allowing it to move farther within the system. The postHarvey 2017 deposition pattern is very different than the others due to the extremely high flow conditions created by the excessive rainfall during the event. Much of the HSC is eroded, in some places down to the model bed thickness limit of 0.2 m. The same peaks in bed displacement in 2010 and prior to Hurricane Harvey are still evident after Hurricane Harvey, indicating that the places where sediment tends to collect are still behaving in that same manner. Below Red Fish Reef, the displacement pattern is similar for all three conditions and mostly erosional. This area is known to contain many more sand-sized particles, which are not included in the model. If sand were present in the model, it is likely that the modeled behavior in this area would be different. This model is defined to

best represent the upper portions (Red Fish Reef and upstream) of the bay and HSC that are dominated by cohesive bed properties.

Figure 59. Modeled bed displacement along the HSC for 2010, prior to Hurricane Harvey and for all of 2017.

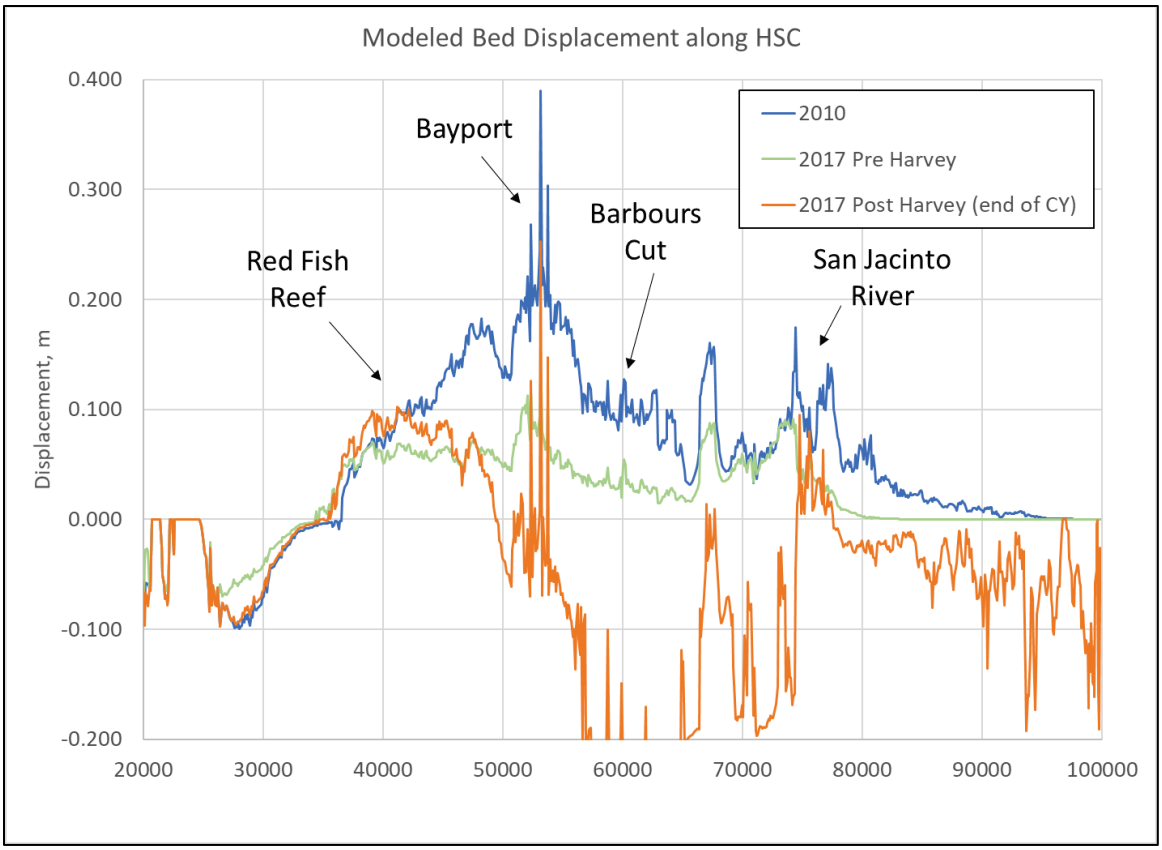

Figure 60 shows the modeled bed-change pattern at the end of the calendar year as *orange dots*. The difference in eHydro survey data pre- and postHurricane Harvey are shown as *grey stars*. Locations where survey data were unavailable pre- or poststorm are shown as values of 0.0. Due to several emergency dredging actions to maintain the navigation depths after the storm, the field-survey data were not able to be collected at the end of the calendar year. The magnitude of the bed change is not expected to be replicated due to many factors influencing the field that are not included in the model (e.g., vessel impacts). However, the overall pattern of areas of erosion and deposition are compared. Although not perfect, there are several areas of good agreement in the erosion and deposition pattern along the HSC.

Figure 60. Comparison of modeled bed change to measured bed change due to Hurricane Harvey.

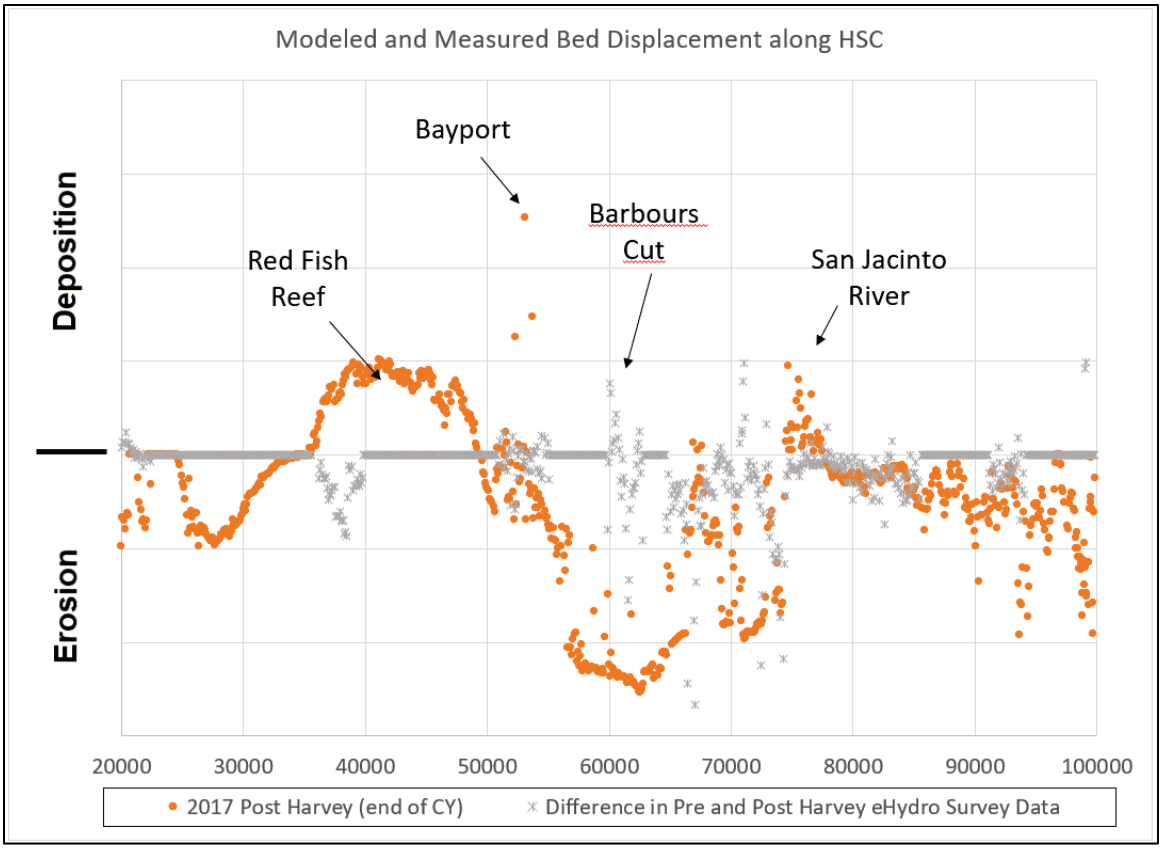

4 Conclusions

The model-validation effort documented in this report includes updated flow and sediment inputs based on recent data-collection efforts as well comparisons to Hurricane Harvey conditions. The model validation shows good agreement with field data from 2010—water surface elevation, velocity, and salinity. However, some concerns are raised over the approach used to obtain ungaged flow data, especially when simulating the Hurricane Harvey event. The sediment-model validation was performed using a scaling process since it is known that many sediment transport drivers are not included in the modeled parameters—including known sediment loads and vessel-induced sediment resuspension.

The model is validated for use in base-vs.-plan comparisons. As additional data for previously ungaged inflow locations becomes available, the model can continue to be updated and improved.

References

Bell, Gary L., N. D. Clifton, and D. D. Abraham. 2017. *Hydrodynamics in the Morganza Floodway Report 1: Phase 1–Model Development and Calibration*. MRG&P Report No. 13. Vicksburg, MS: US Army Engineer Research and Development Center.

Berger, R. C., R. T. McAdory, W. D. Martin, and J. H. Schmidt. 1995a. *Houston–Galveston Navigation Channels, Texas Project, Report 3, Three-Dimensional Hydrodynamic Model Verification*. Technical Report HL-92-7. Vicksburg, MS: US Army Engineer Waterways Experiment Station.

Berger, R. C., Robert T. McAdory, Joseph H. Schmidt, and William D. Martin. 1995b. *Houston-Galveston Navigation Channels, Texas Project, Report 4, Three-Dimensional Numerical Modeling of Hydrodynamics and Salinity*. Technical Report HL-92-7. Vicksburg, MS: US Army Engineer Waterways Experiment Station.

Carrillo, A. R., M. S. Sarruff, and R. C. Berger. 2002. *Effects of Adding Barge Lanes along Houston Ship Channel through Galveston Bay, Texas*. ERDC/CHL TR-02-23. Vicksburg, MS: US Army Engineer Research and Development Center, Coastal and Hydraulics Laboratory.

Clifton, N., D. Abraham, and D. Pridal. 2017. *Upper and Lower Hamburg Bend 2011 Flood Evaluation on the Missouri River near Hamburg, Iowa*. ERDC/CHL TR17-1. Vicksburg, MS: US Army Engineer Research and Development Center, Coastal and Hydraulics Laboratory.

Cochrane, J. D., and F. J. Kelly. 1986. "Low Frequency Circulation on the Texas–Louisiana Continental Shelf." *Journal of Geophysical Research* 91 (C9): 10645–10659.

Egiazaroff, I. V. 1965. "Calculation of Non-Uniform Sediment Concentrations." *Journal of Hydraulics Division*, *ASCE* 91 (HY4): 225–247.

Galveston Bay Estuary Program. 2002. *The State of the Bay: A Characterization of the Galveston Bay Ecosystem*, 2nd ed, edited by J. Lester and L. Gonzalez. Austin, TX: Texas Commission on Environmental Quality.

Heath, R. E., G. L. Brown, C. D. Little, T. C. Pratt, J. J. Ratcliff, D. Abraham, D. W. Perkey, N. B. Ganesh, S. K. Martin, and D. P. May. 2015. *Old River Control Complex Sedimentation Investigation*. ERDC/CHL TR-15-8. Vicksburg, MS: US Army Engineer Research and Development Center, Coastal and Hydraulics Laboratory.

Hubertz, J. M. 1992. *User's Guide to the Wave Information Studies (WIS) Wave Model: Version 2.0*. WIS Report 27. Vicksburg, MS: US Army Engineer Waterways Experiment Station. http://wis.usace.army.mil/.

Letter, J. V., G. L. Brown, R. T. McAdory, and T. C. Pratt. 2015. *Numerical Modeling of Trinity River Shoaling below Wallisville, Texas*. ERDC/CHL TR-15-1. Vicksburg, MS: US Army Engineer Research and Development Center, Coastal and Hydraulics Laboratory.

McAlpin, Jennifer N., and Cassandra G. Ross. 2020. *Houston Ship Channel Expansion Channel Improvement Project (ECIP) Numerical Modeling Report: Increased Channel Width Analysis*. ERDC/CHL TR-21-2. Vicksburg, MS: US Army Engineer Research and Development Center, Coastal and Hydraulics Laboratory.

McAlpin, Jennifer N., and Cassandra G. Ross. 2021. *Houston Ship Channel Expansion Channel Improvement Project (ECIP) Numerical Modeling Report: BABUS cell and Bird Island Analysis*. ERDC/CHL TR-21-12. Vicksburg, MS: US Army Engineer Research and Development Center, Coastal and Hydraulics Laboratory.

McAlpin, Jennifer N., C. Jared McKnight, and Cassandra G. Ross. 2019a. *Houston Ship Channel Expansion Channel Improvement Project (ECIP) Numerical Modeling Report*. ERDC/CHL TR-19-12. Vicksburg, MS: US Army Engineer Research and Development Center, Coastal and Hydraulics Laboratory.

McAlpin, Jennifer N., Cassandra G. Ross, and C. Jared McKnight. 2019b. *Houston Ship Channel 3D Adaptive Hydraulics (AdH) Numerical Model Validation Report*. ERDC/CHL TR-19-10. Vicksburg, MS: US Army Engineer Research and Development Center, Coastal and Hydraulics Laboratory.

McAlpin, T. O., G. Savant, G. L. Brown, S. J. Smith, and R. S. Chapman. 2013. "Hydrodynamics of Knik Arm: Modeling Study." *Journal of Waterway, Port, Coastal, and Ocean Engineering* 139(3).

Nichols, M. M. 1989. "Sediment Accumulation Rates and Relative Sea-Level Rise in Lagoons." *Marine Geology* 88 (3–4): 201–219.

Savant, G., R. C. Berger, T. O. McAlpin, and C. J. Trahan. 2014. *Three-Dimensional Shallow Water Adaptive Hydraulics (AdH-SW3): Hydrodynamic Verification and Validation*. ERDC/CHL TR-14-7. Vicksburg, MS: US Army Engineer Research and Development Center, Coastal and Hydraulics Laboratory.

Savant, G., and R. C. Berger. 2015. *Three-Dimensional Shallow Water Adaptive Hydraulics (AdH-SW3) Validation*: *Galveston Bay Hydrodynamics and Salinity Transport*. ERDC/CHL TR-15-3. Vicksburg, MS: US Army Engineer Research and Development Center, Coastal and Hydraulics Laboratory.

Schoenbaechler, Caimee, and Carla G. Guthrie. 2012. *Coastal Hydrology for the Trinity-San Jacinto Estuary*. Austin, TX: Texas Water Development Board.

Sharp, J. A., C. D. Little, G. L. Brown, T. C. Pratt, R. E. Heath, L. C. Hubbard, F. Pinkard, S. K. Martin, N. D. Clifton, D. W. Perkey, and N. B. Ganesh. 2013. *West Bay Sediment Diversion Effects*. ERDC/CHL TR-13-15. Vicksburg, MS: US Army Engineer Research and Development Center, Coastal and Hydraulics Laboratory.

Tate, J. N., and R. C. Berger. 2006. *Houston*-Galveston *Navigation Channels, Texas Project: Navigation Channel Sedimentation Study, Phase 1*. ERDC/CHL TR-06-8. Vicksburg, MS: US Army Engineer Research and Development Center, Coastal and Hydraulics Laboratory.

Tate, J. N., R. C. Berger, and C. G. Ross. 2008. *Houston-Galveston Navigation Channels, Texas Project, Navigation Channel Sedimentation Study, Phase 2*. ERDC/CHL TR-08-8. Vicksburg, MS: US Army Engineer Research and Development Center, Coastal and Hydraulics Laboratory.

Tate, J. N., J. P. McKinney, T. C. Pratt, F. C. Carson, M. W. Tubman, G. L. Brown, K. M. Barry, R. T. McAdory, and M. J. Briggs. 2009. *Salinas de San Pedro (Cabrillo) Wetland Restoration Project*. Vol. 1, Main Text. ERDC/CHL TR-09-14. Vicksburg, MS: US Army Engineer Research and Development Center, Coastal and Hydraulics Laboratory.

Tate, Jennifer N., and Cassandra G. Ross. 2012. *Bayport Flare Hydrodynamic Study for Ship Simulation*. ERDC/CHL TR-12-13. Vicksburg, MS: US Army Engineer Research and Development Center, Coastal and Hydraulics Laboratory.

Tate, J. N., B. Gunkel, J. Rosati, E. Wood, A. Sanchez, R. Thomas, N. Ganesh, and T. Pratt. 2014. *Monitoring Completed Navigation Projects Program; Houston–Galveston Navigation Channel Shoaling Study*. ERDC/CHL TR-14-14. Vicksburg, MS: US Army Engineer Research and Development Center, Coastal and Hydraulics Laboratory.

Wright, S., and G. Parker. 2004. "Flow Resistance and Suspended Load in Sand-Bed Rivers: Simplified Stratification Model." *Journal of Hydraulic Engineering* 130 (8): 796–805.

Wu, J. 1969. “Wind Stress and Surface Roughness at Air-Sea Interface.” *Journal of Geophysical Research* 74 (2): 444–455.

Wu, J. 1982. “Wind-Stress Coefficients Over Sea Surface from Breeze to Hurricane.” *Journal of Geophysical Research* 87 (C12): 9704–9706.

Appendix A: Water Surface Elevation Comparisons

The following plots include all of the model-to-field water surface elevation comparisons for the available field data during the two comparison years—2010 and 2017. Data are not available for both years at all sites. Figure 17 in the main text shows the locations of all water surface elevation comparison sites. For the time-history plots, the *red line* represents the measured field data and the blue line represents the model-computed values. Each comparison location also includes a box plot showing the relationship between the measured field data (x-axis) and the modeled data (y-axis). A perfect match at all times would yield points on the *black 1:1 line*.

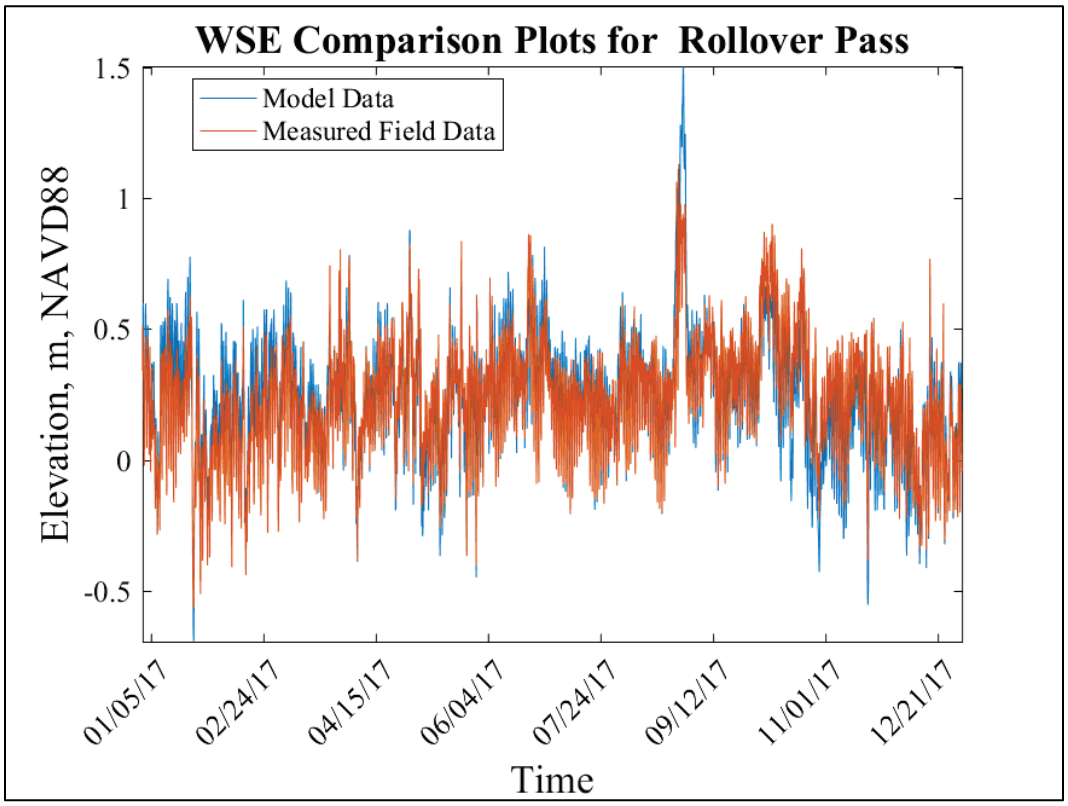

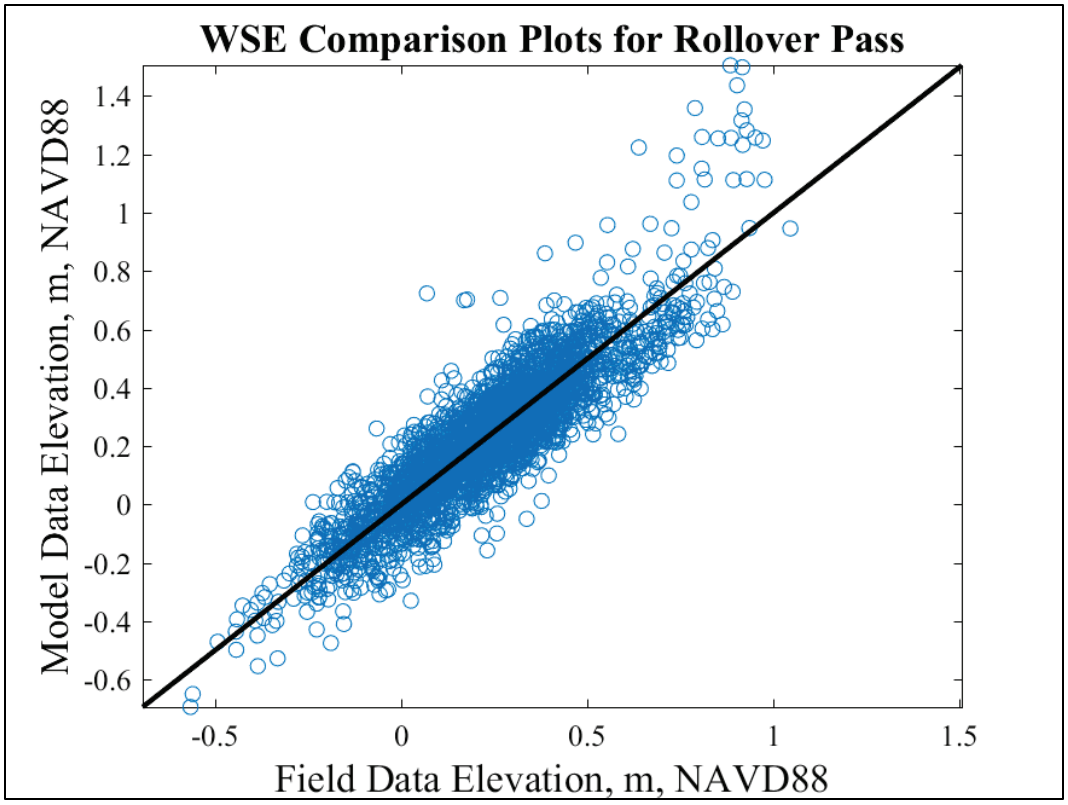
WSE Comparison Plots for Rollover Pass
Model Data Elevation, m, NAVD88
Field Data Elevation, m, NAVD88
1.4
1.2
1
0.8
0.6
0.4
0.2
0
-0.2
-0.4
-0.6
-0.5
0
0.5
1
1.5

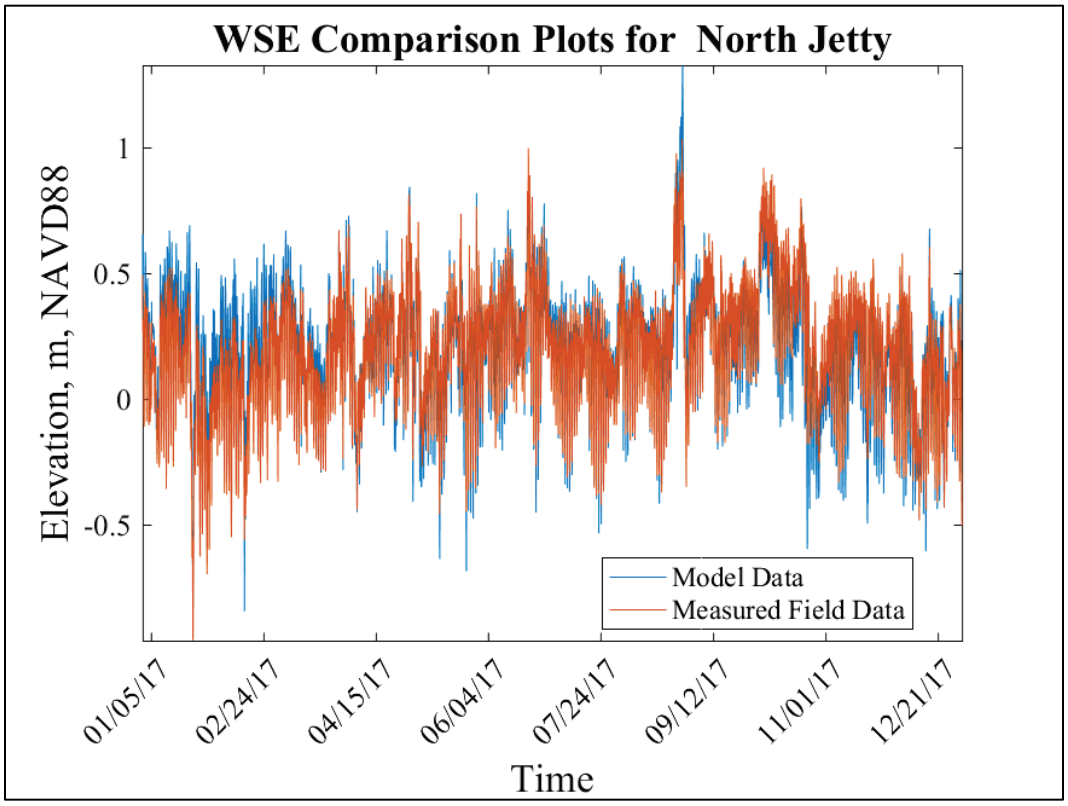
WSE Comparison Plots for North Jetty
Elevation, m, NAVD88
Time
Model Data
Measured Field Data
1
0.5
0
-0.5
01/05/17
02/24/17
04/15/17
06/04/17
07/24/17
09/12/17
11/01/17
12/21/17

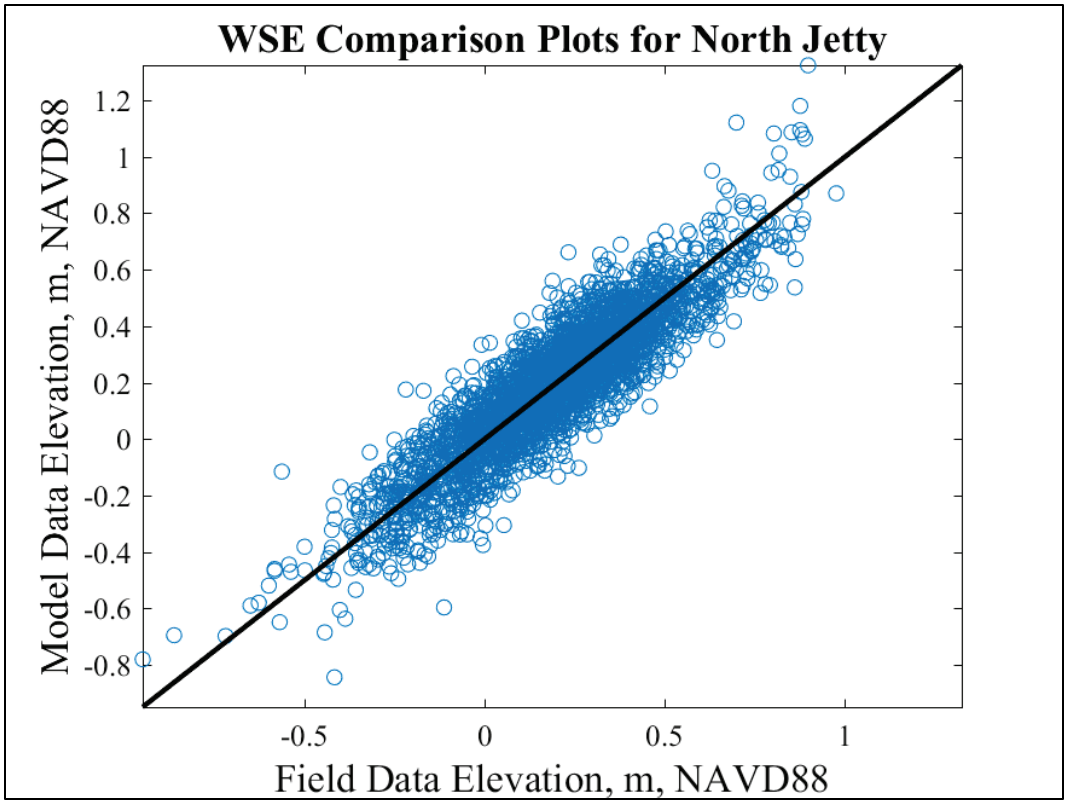
WSE Comparison Plots for North Jetty
Model Data Elevation, m, NAVD88
1.2
1
0.8
0.6
0.4
0.2
0
-0.2
-0.4
-0.6
-0.8
-0.5
0
0.5
1
Field Data Elevation, m, NAVD88

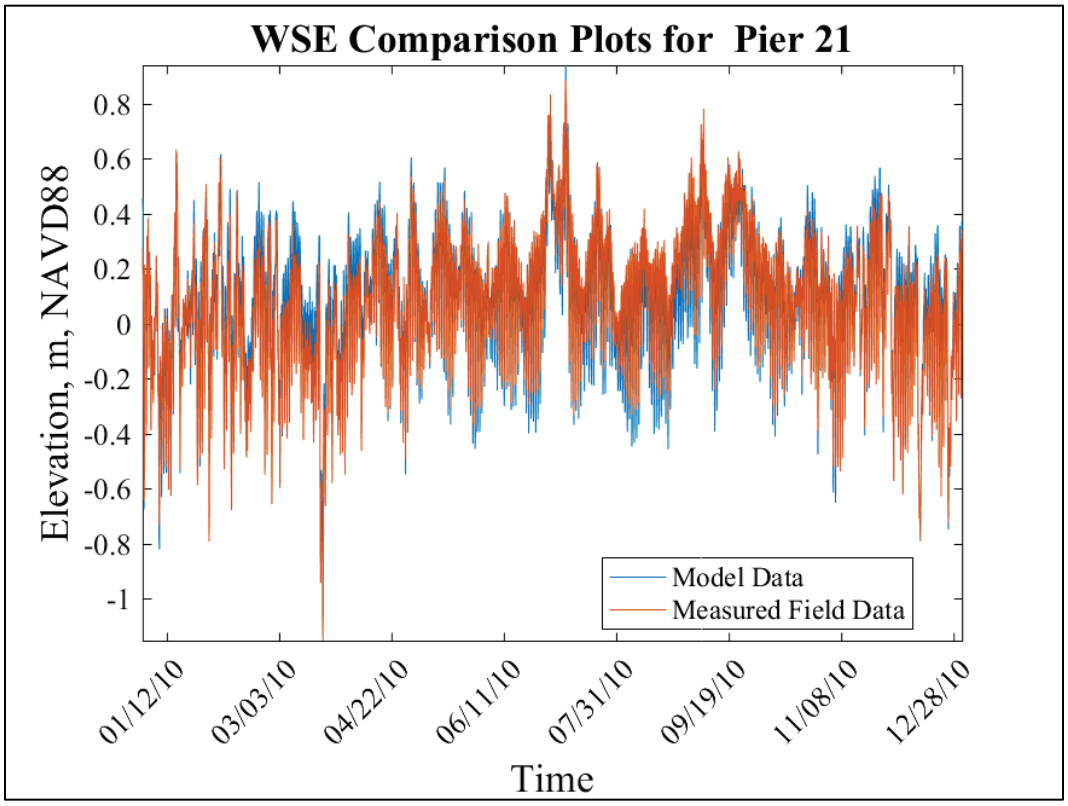
WSE Comparison Plots for Pier 21
Elevation, m, NAVD88
0.8
0.6
0.4
0.2
0
-0.2
-0.4
-0.6
-0.8
-1
Model Data
Measured Field Data
01/12/10
03/03/10
04/22/10
06/11/10
07/31/10
09/19/10
11/08/10
12/28/10
Time

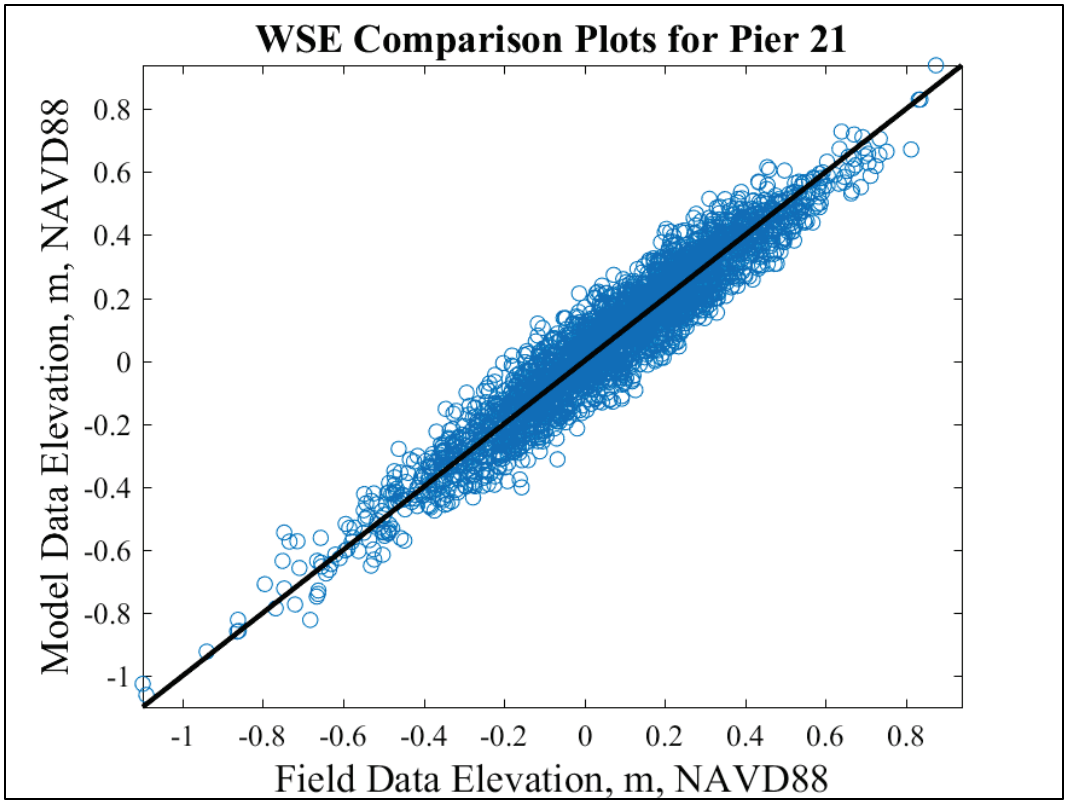
WSE Comparison Plots for Pier 21
Model Data Elevation, m, NAVD88
Field Data Elevation, m, NAVD88
0.8
0.6
0.4
0.2
0
-0.2
-0.4
-0.6
-0.8
-1
-1
-0.8
-0.6
-0.4
-0.2
0
0.2
0.4
0.6
0.8

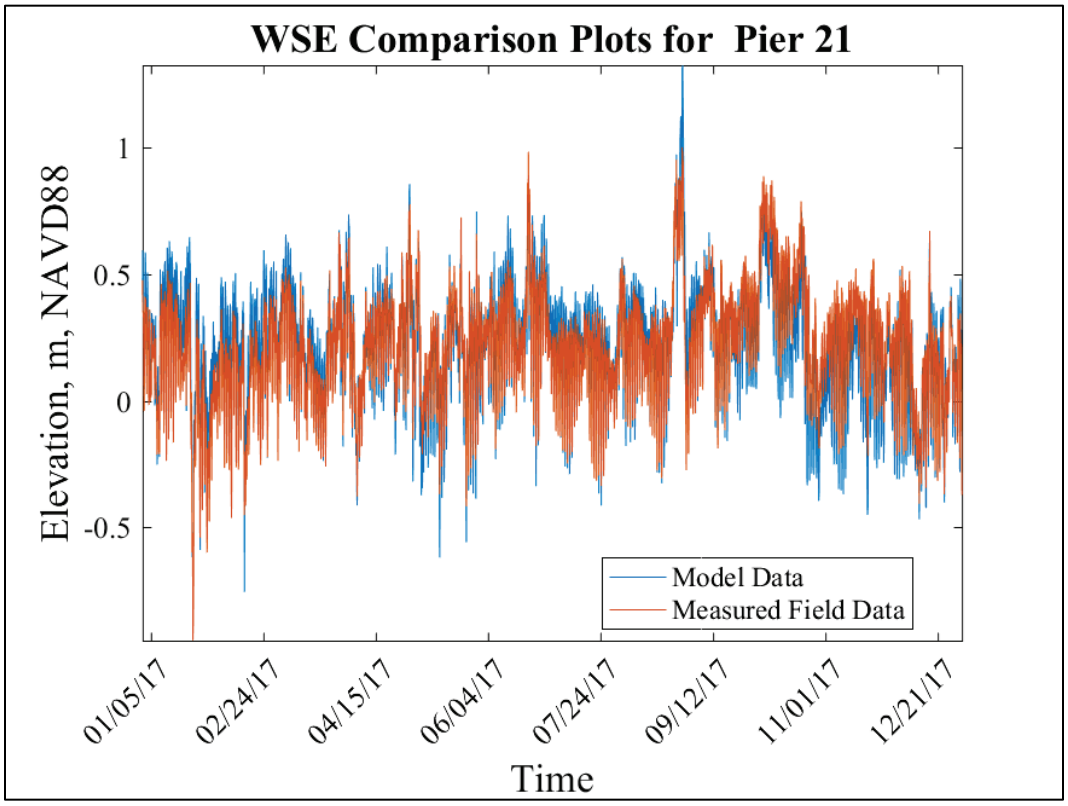
WSE Comparison Plots for Pier 21
Elevation, m, NAVD88
Time
1
0.5
0
-0.5
Model Data
Measured Field Data
01/05/17
02/24/17
04/15/17
06/04/17
07/24/17
09/12/17
11/01/17
12/21/17

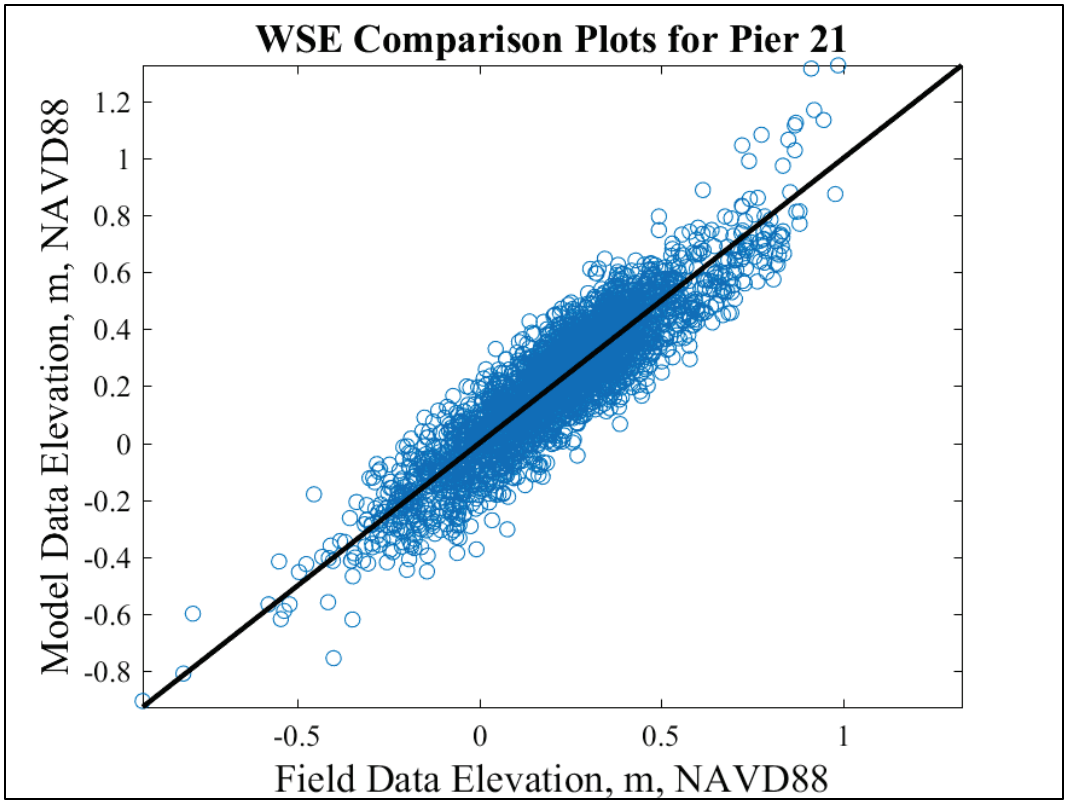
WSE Comparison Plots for Pier 21
Model Data Elevation, m, NAVD88
Field Data Elevation, m, NAVD88
1.2
1
0.8
0.6
0.4
0.2
0
-0.2
-0.4
-0.6
-0.8
-0.5
0
0.5
1

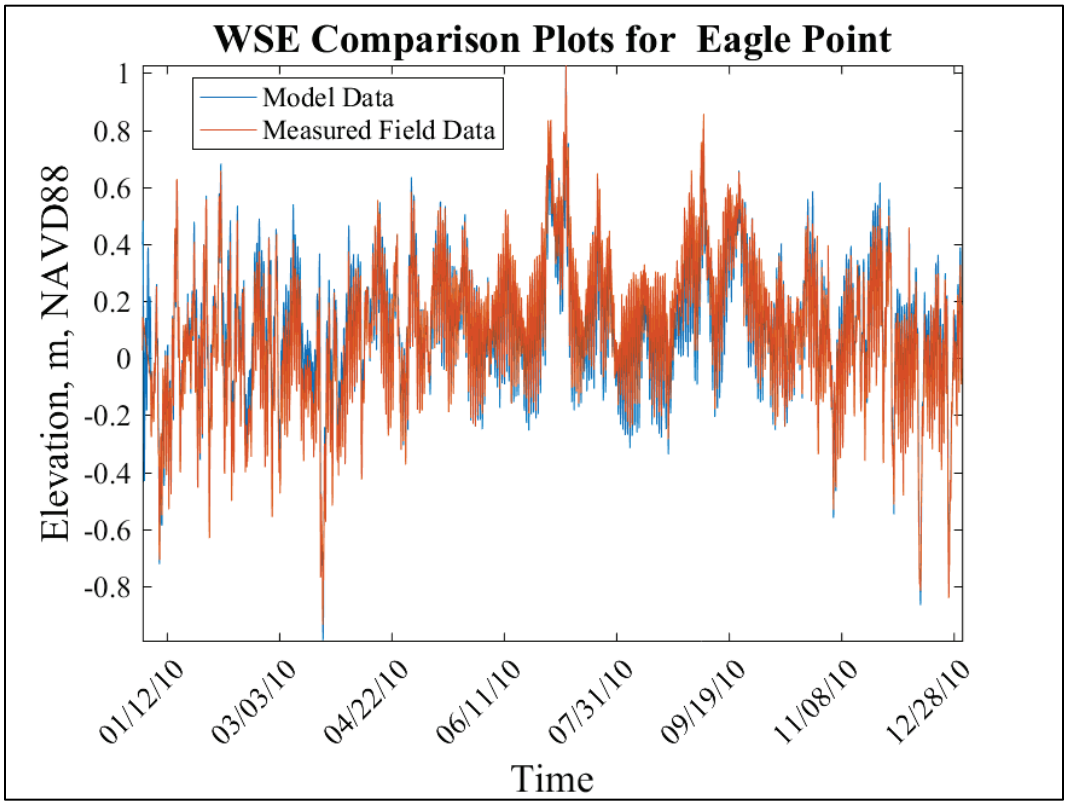
WSE Comparison Plots for Eagle Point
Model Data
Measured Field Data
Elevation, m, NAVD88
Time
1
0.8
0.6
0.4
0.2
0
-0.2
-0.4
-0.6
-0.8
01/12/10
03/03/10
04/22/10
06/11/10
07/31/10
09/19/10
11/08/10
12/28/10

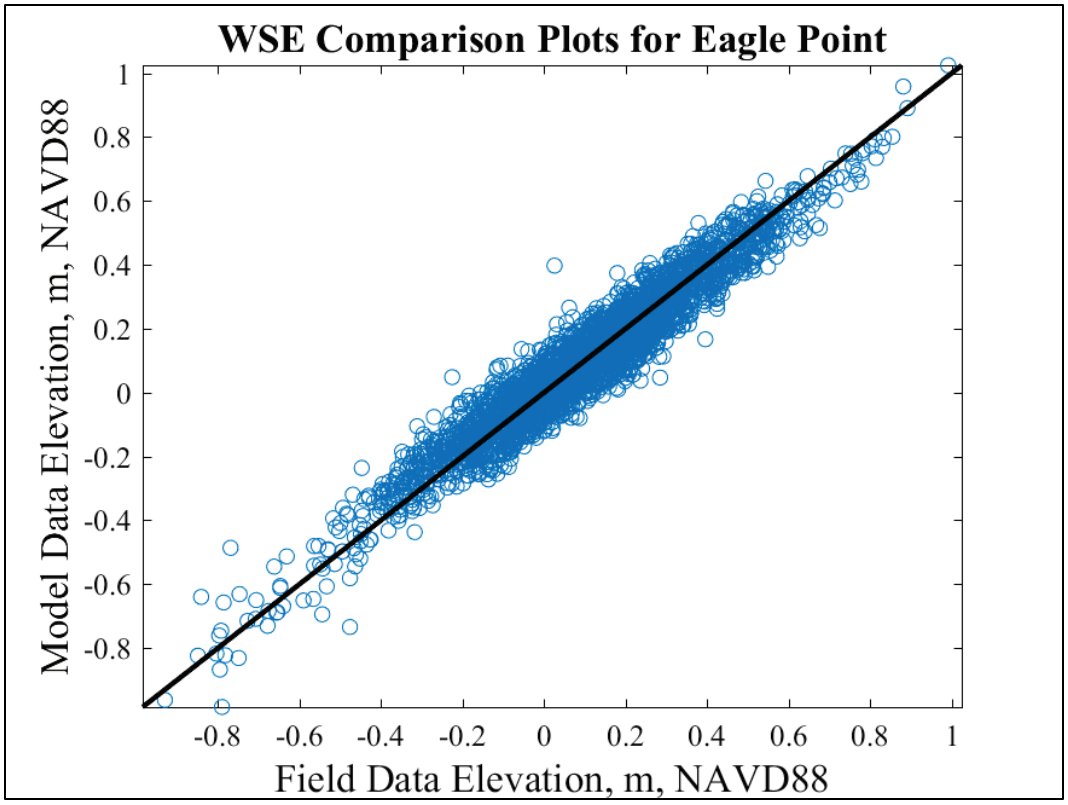
WSE Comparison Plots for Eagle Point
Model Data Elevation, m, NAVD88
Field Data Elevation, m, NAVD88
1
0.8
0.6
0.4
0.2
0
-0.2
-0.4
-0.6
-0.8
-0.8 -0.6 -0.4 -0.2 0 0.2 0.4 0.6 0.8 1

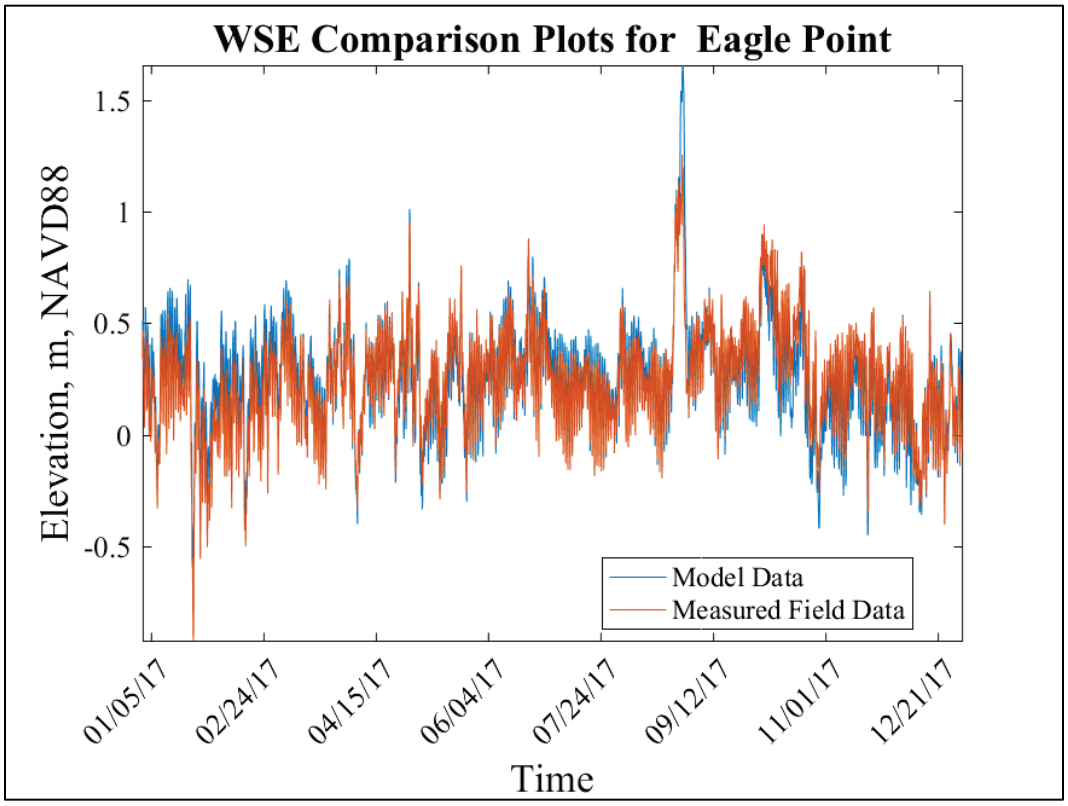
WSE Comparison Plots for Eagle Point
Elevation, m, NAVD88
Time
1.5
1
0.5
0
-0.5
Model Data
Measured Field Data
01/05/17
02/24/17
04/15/17
06/04/17
07/24/17
09/12/17
11/01/17
12/21/17

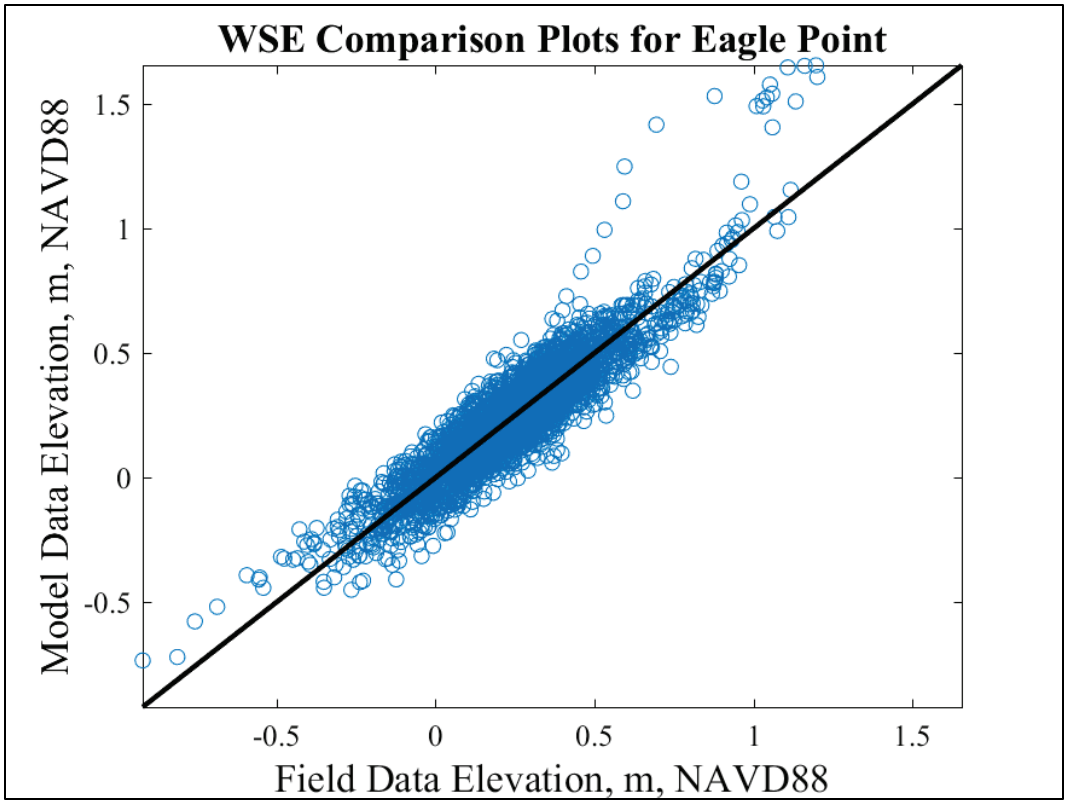
WSE Comparison Plots for Eagle Point
Model Data Elevation, m, NAVD88
Field Data Elevation, m, NAVD88
1.5
1
0.5
0
-0.5
-0.5
0
0.5
1
1.5

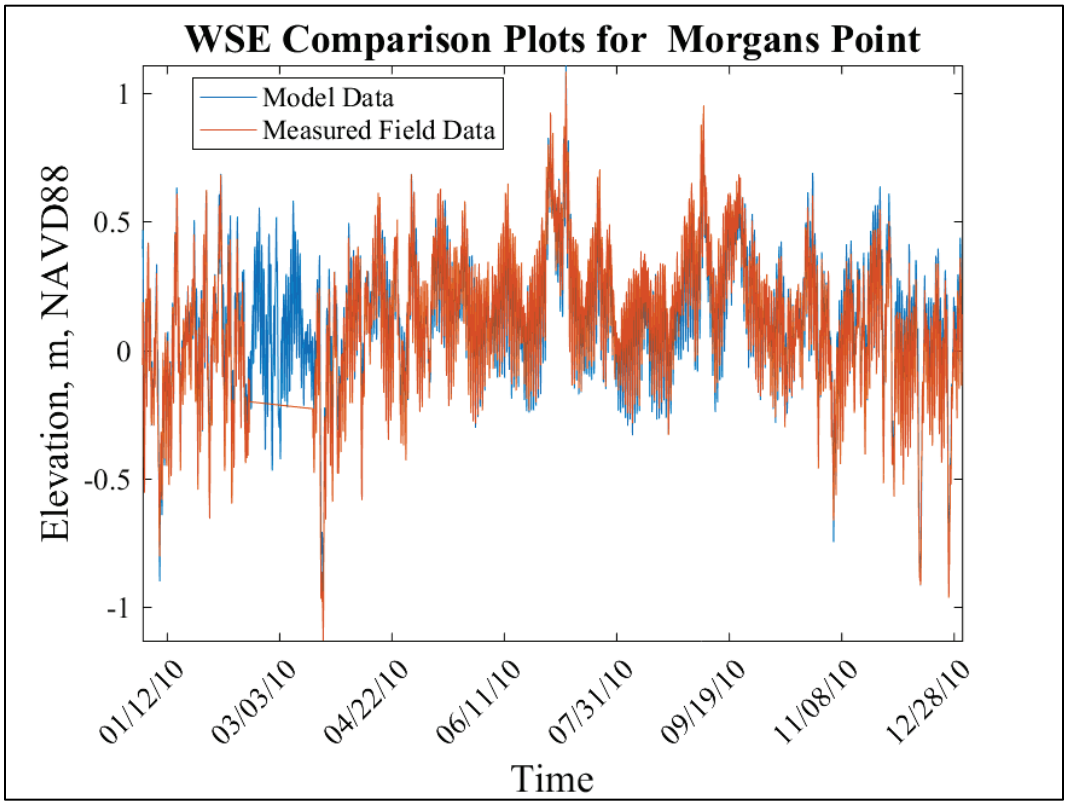
WSE Comparison Plots for Morgans Point
Model Data
Measured Field Data
Elevation, m, NAVD88
Time
1
0.5
0
-0.5
-1
01/12/10
03/03/10
04/22/10
06/11/10
07/31/10
09/19/10
11/08/10
12/28/10

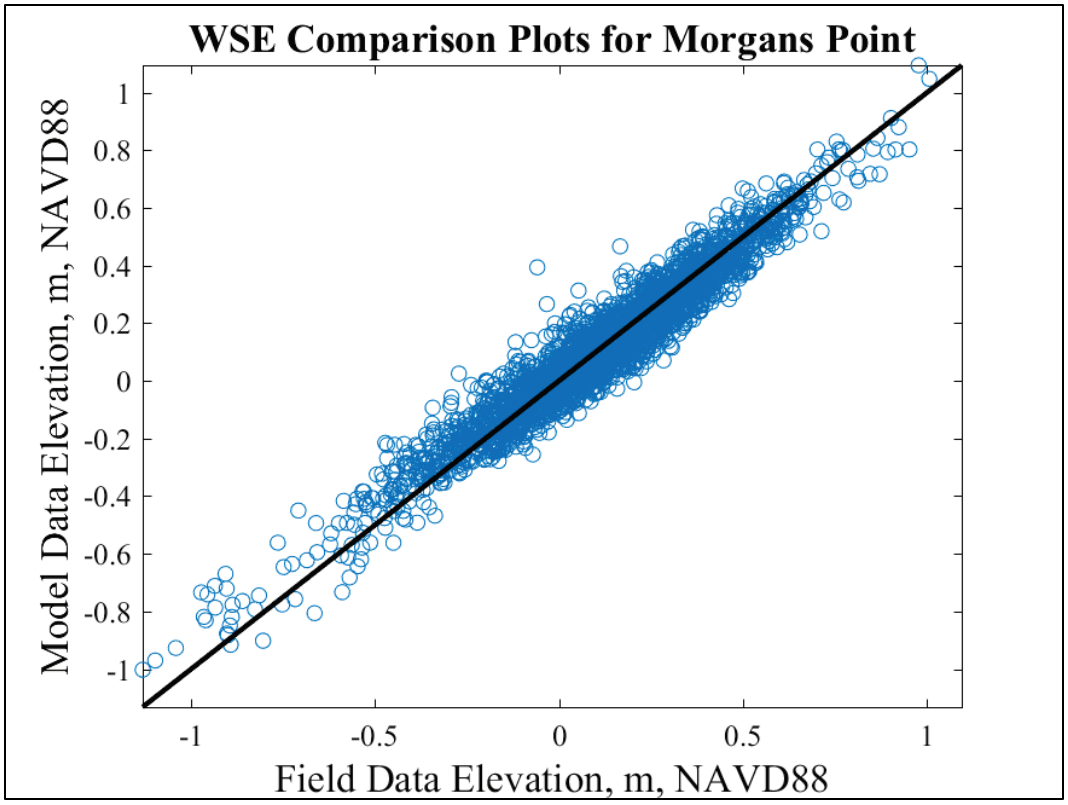
WSE Comparison Plots for Morgans Point
Model Data Elevation, m, NAVD88
Field Data Elevation, m, NAVD88
1
0.8
0.6
0.4
0.2
0
-0.2
-0.4
-0.6
-0.8
-1
-1
-0.5
0
0.5
1

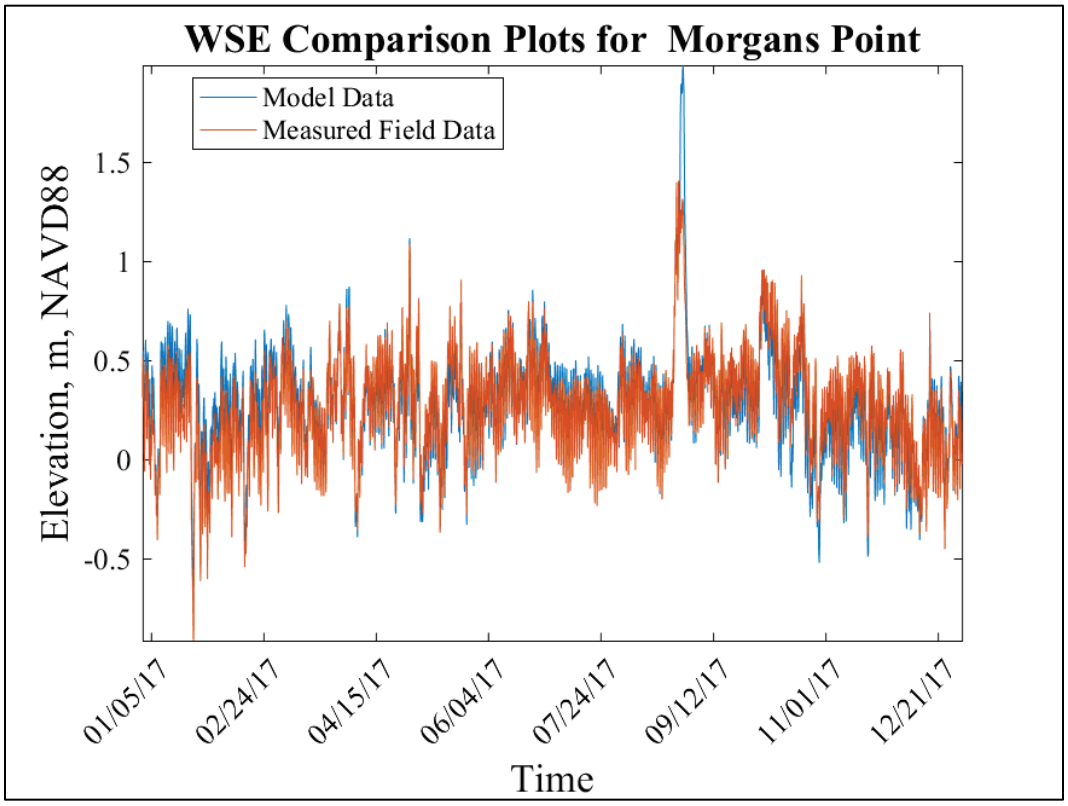
WSE Comparison Plots for Morgans Point
Model Data
Measured Field Data
Elevation, m, NAVD88
Time
1.5
1
0.5
0
-0.5
01/05/17
02/24/17
04/15/17
06/04/17
07/24/17
09/12/17
11/01/17
12/21/17

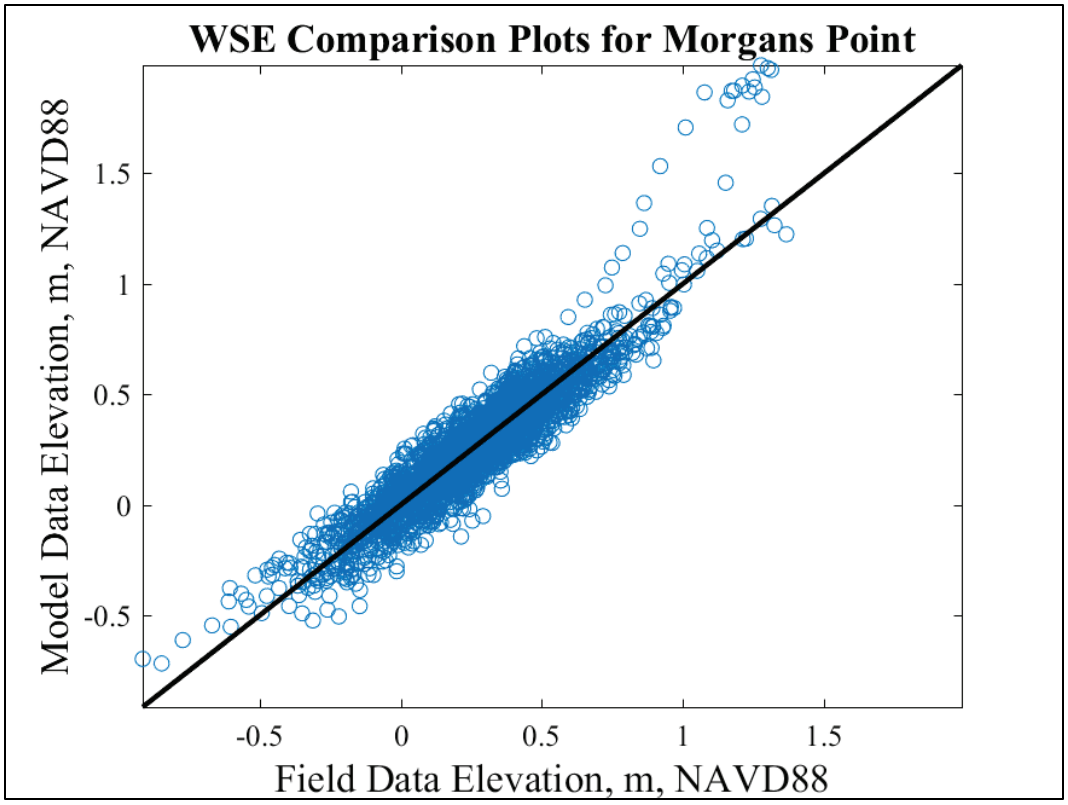
WSE Comparison Plots for Morgans Point
Model Data Elevation, m, NAVD88
Field Data Elevation, m, NAVD88
1.5
1
0.5
0
-0.5
-0.5
0
0.5
1
1.5

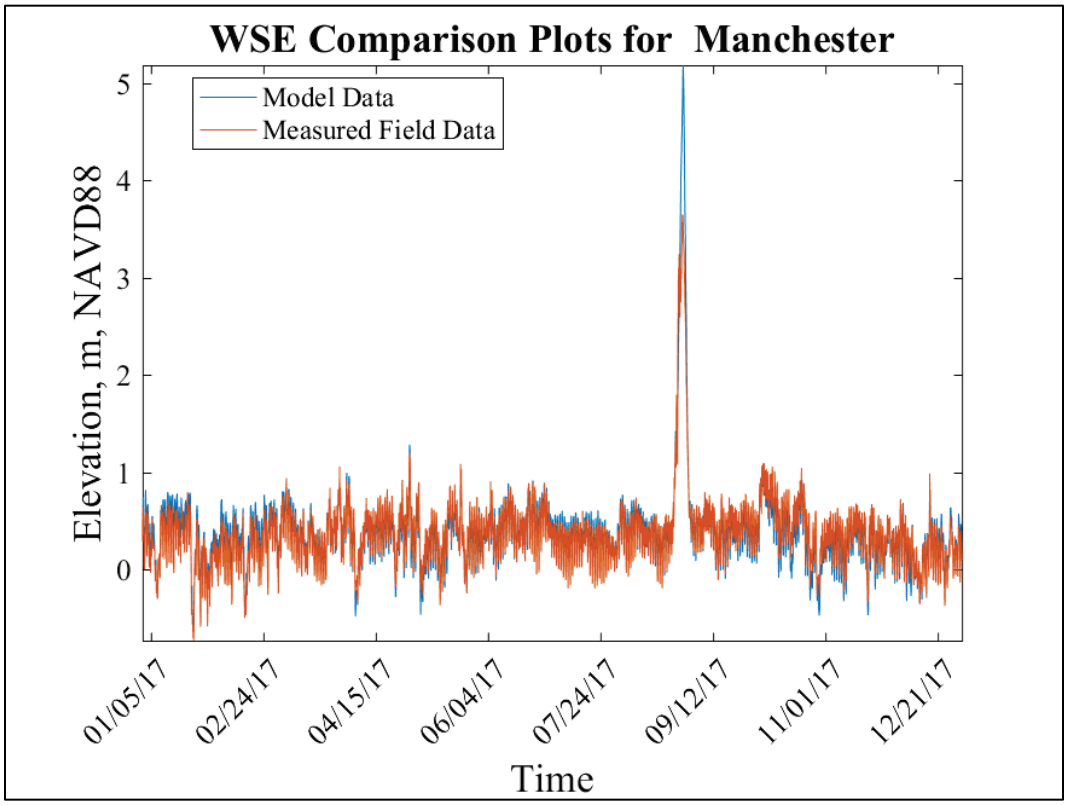
WSE Comparison Plots for Manchester
Model Data
Measured Field Data
Elevation, m, NAVD88
Time
5
4
3
2
1
0
01/05/17
02/24/17
04/15/17
06/04/17
07/24/17
09/12/17
11/01/17
12/21/17

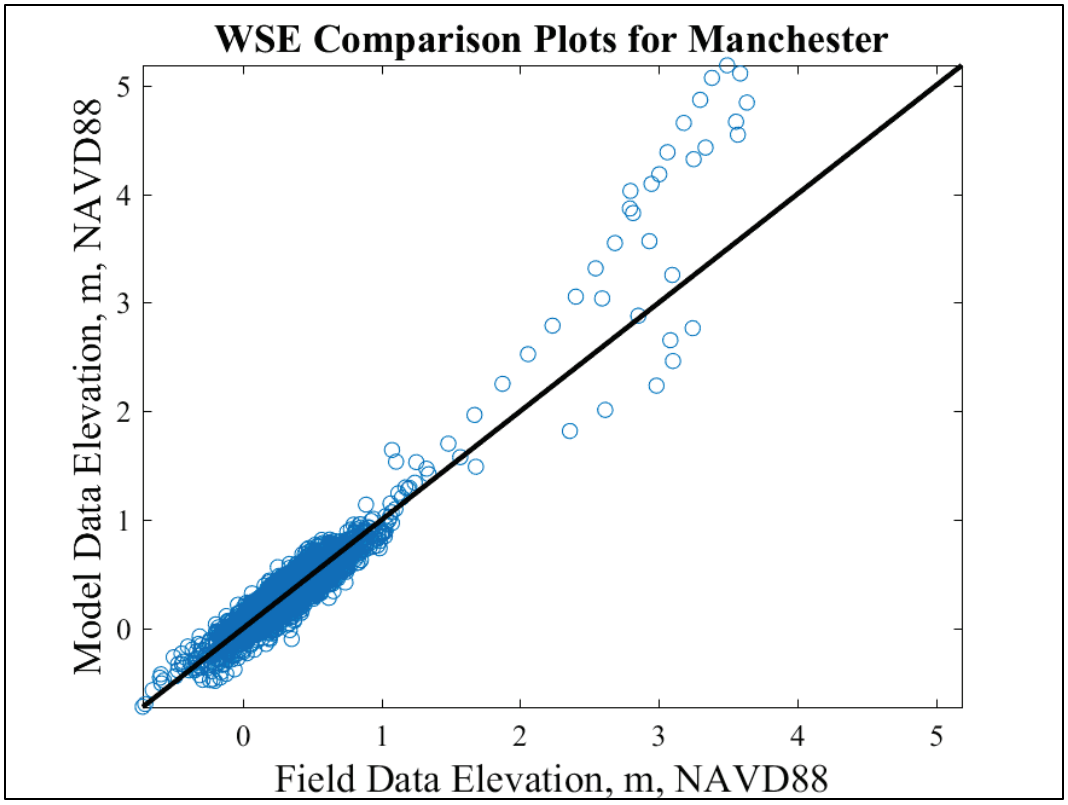
WSE Comparison Plots for Manchester
Model Data Elevation, m, NAVD88
Field Data Elevation, m, NAVD88
0
1
2
3
4
5

Appendix B: Salinity Comparisons

The following plots include all of the model-to-field comparisons for the available field data during the two comparison years—2010 and 2017. Data are not available for both years at all sites. Figure 49 through Figure 52 in the main text show the locations of all salinity-comparison sites. The *black dots* represent the measured field data. These data are defined as *near surface* for several of the sites, but many others do not define the vertical location of the samples. The model-computed surface salinity is given by the *blue line* and the model computed bottom salinity by the *red line*. In deep, stratified regions, the bottom salinity is larger than the surface salinity. In well-mixed regions, the two should be approximately equal.

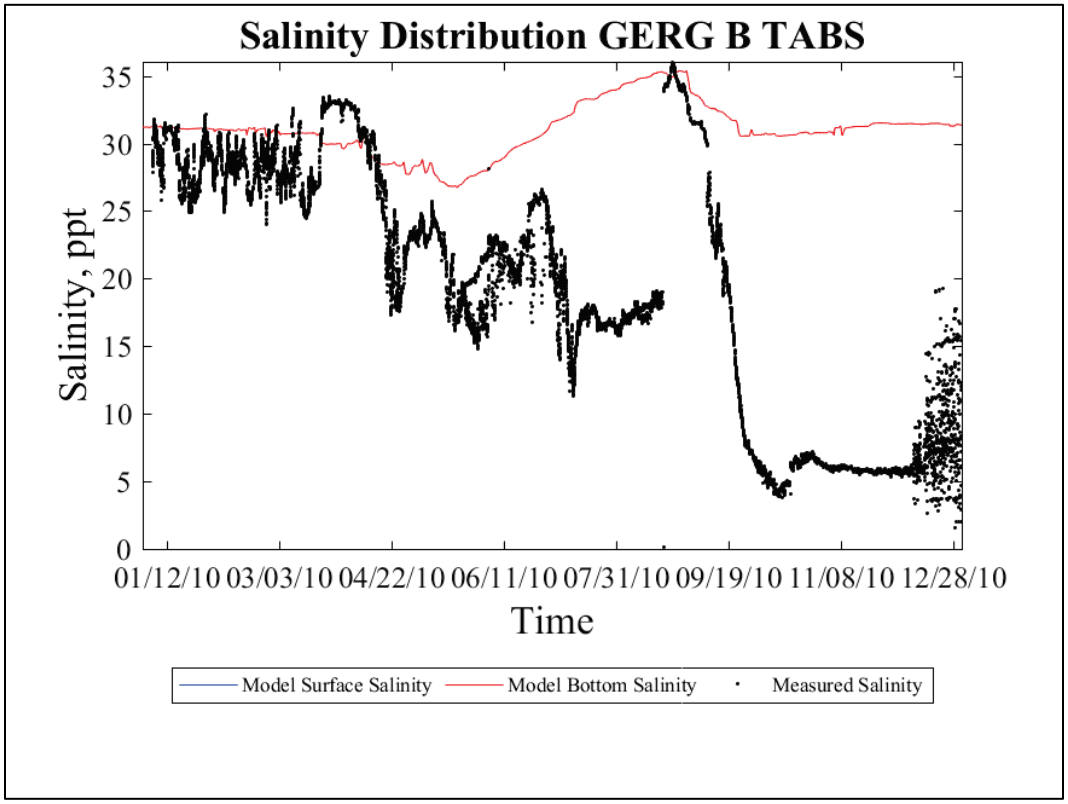

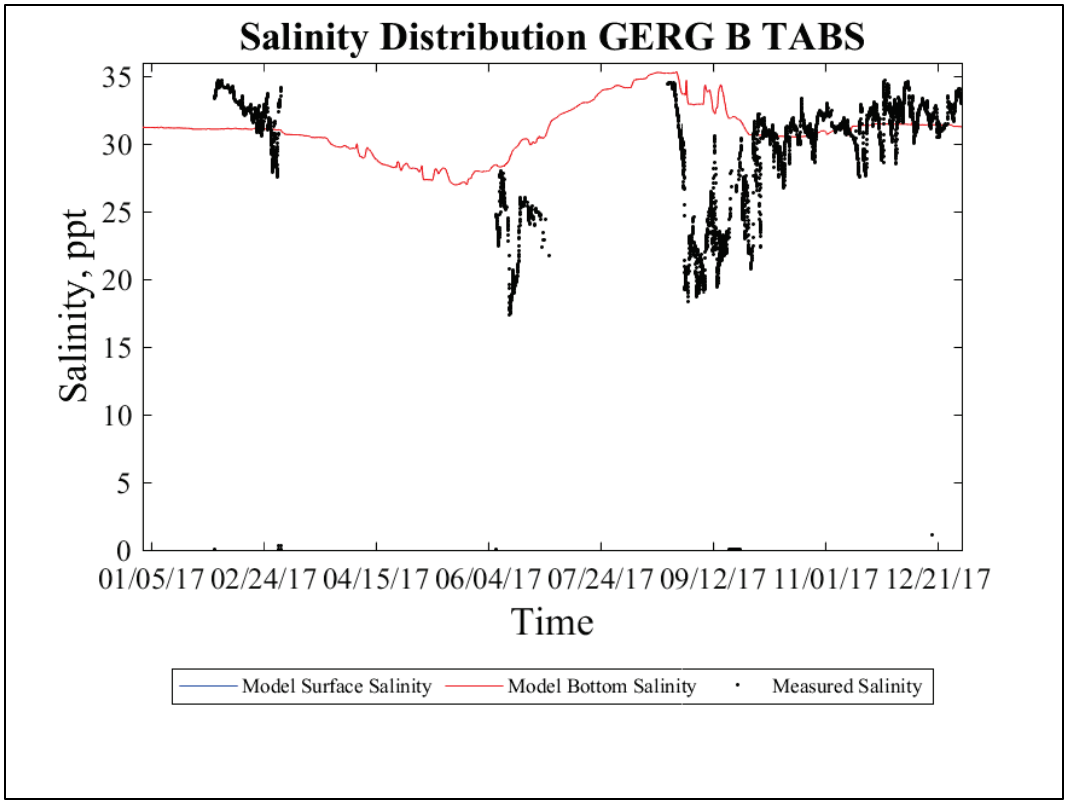
Salinity Distribution GERG B TABS
Salinity, ppt
0
5
10
15
20
25
30
35
01/05/17 02/24/17 04/15/17 06/04/17 07/24/17 09/12/17 11/01/17 12/21/17
Time
Model Surface Salinity
Model Bottom Salinity
Measured Salinity

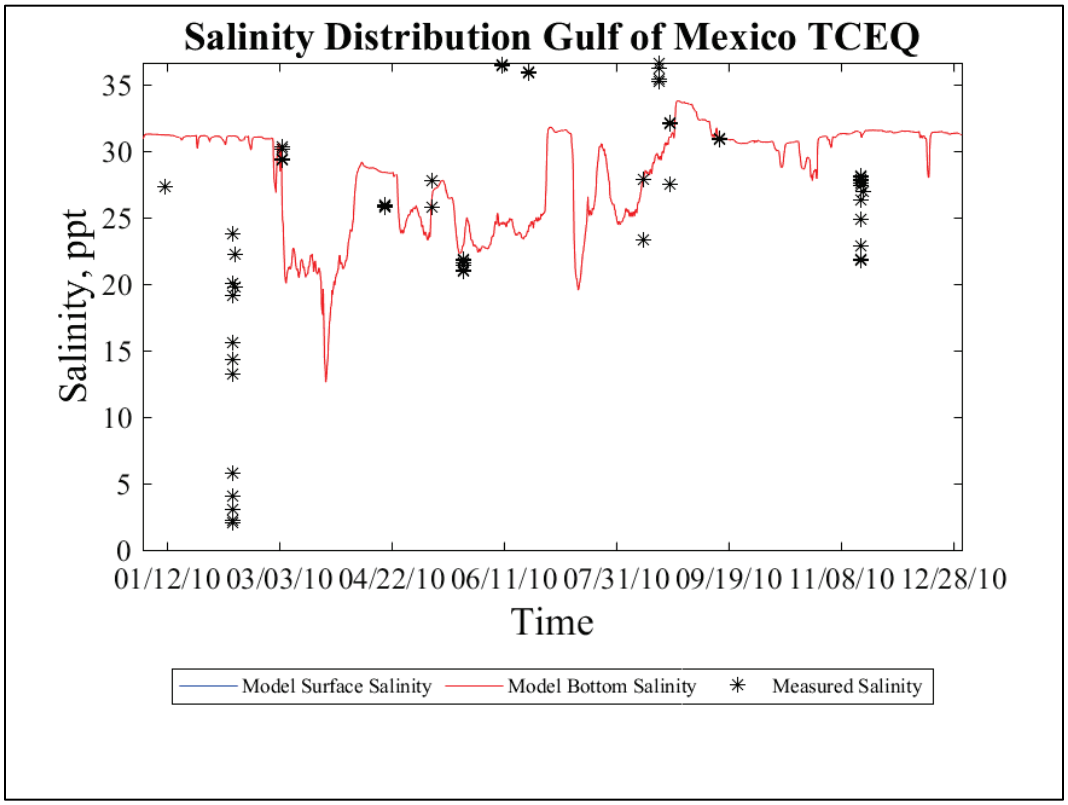
Salinity Distribution Gulf of Mexico TCEQ
Salinity, ppt
0
5
10
15
20
25
30
35
01/12/10 03/03/10 04/22/10 06/11/10 07/31/10 09/19/10 11/08/10 12/28/10
Time
Model Surface Salinity
Model Bottom Salinity
Measured Salinity

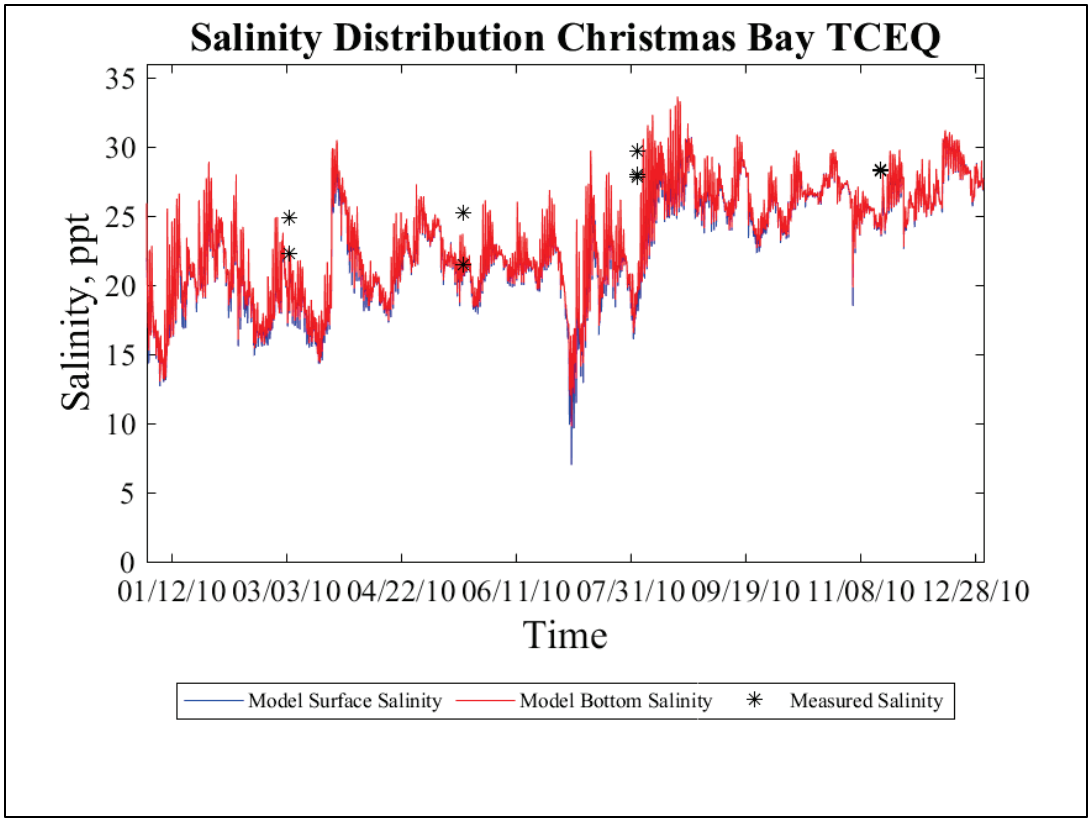
Salinity Distribution Christmas Bay TCEQ
Salinity, ppt
0
5
10
15
20
25
30
35
01/12/10 03/03/10 04/22/10 06/11/10 07/31/10 09/19/10 11/08/10 12/28/10
Time
Model Surface Salinity
Model Bottom Salinity
Measured Salinity

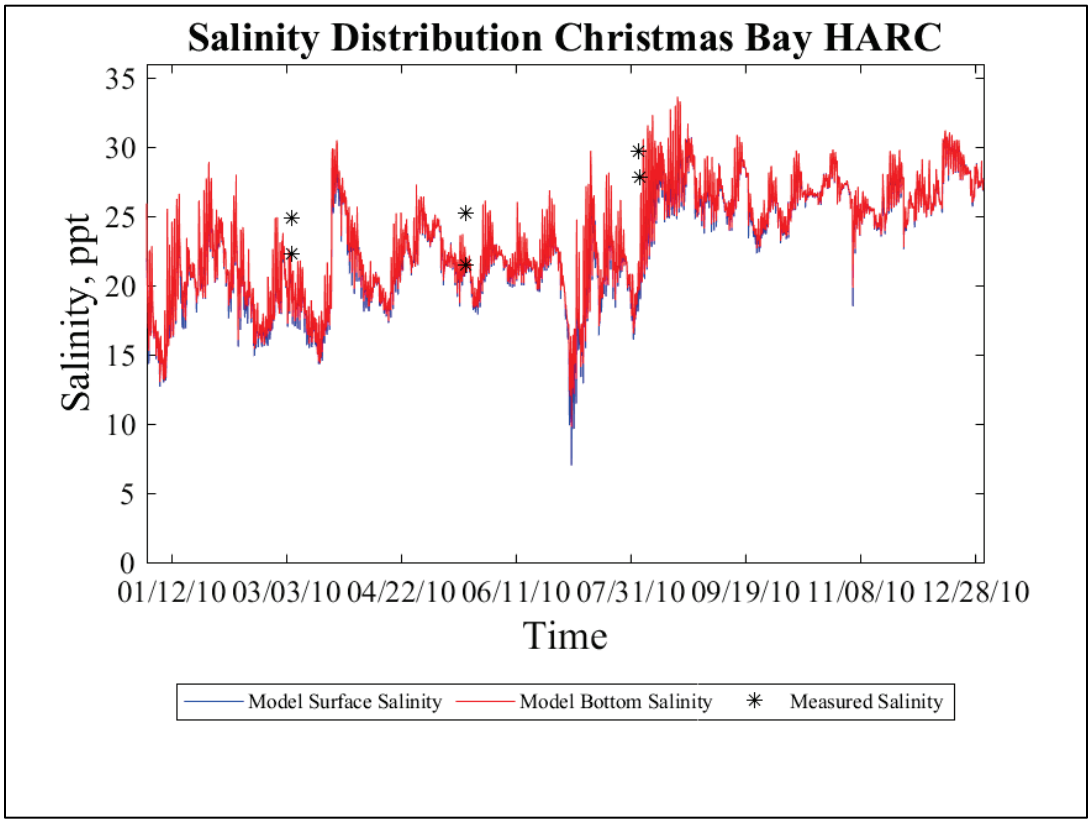
Salinity Distribution Christmas Bay HARC
Salinity, ppt
0
5
10
15
20
25
30
35
01/12/10 03/03/10 04/22/10 06/11/10 07/31/10 09/19/10 11/08/10 12/28/10
Time
Model Surface Salinity
Model Bottom Salinity
Measured Salinity

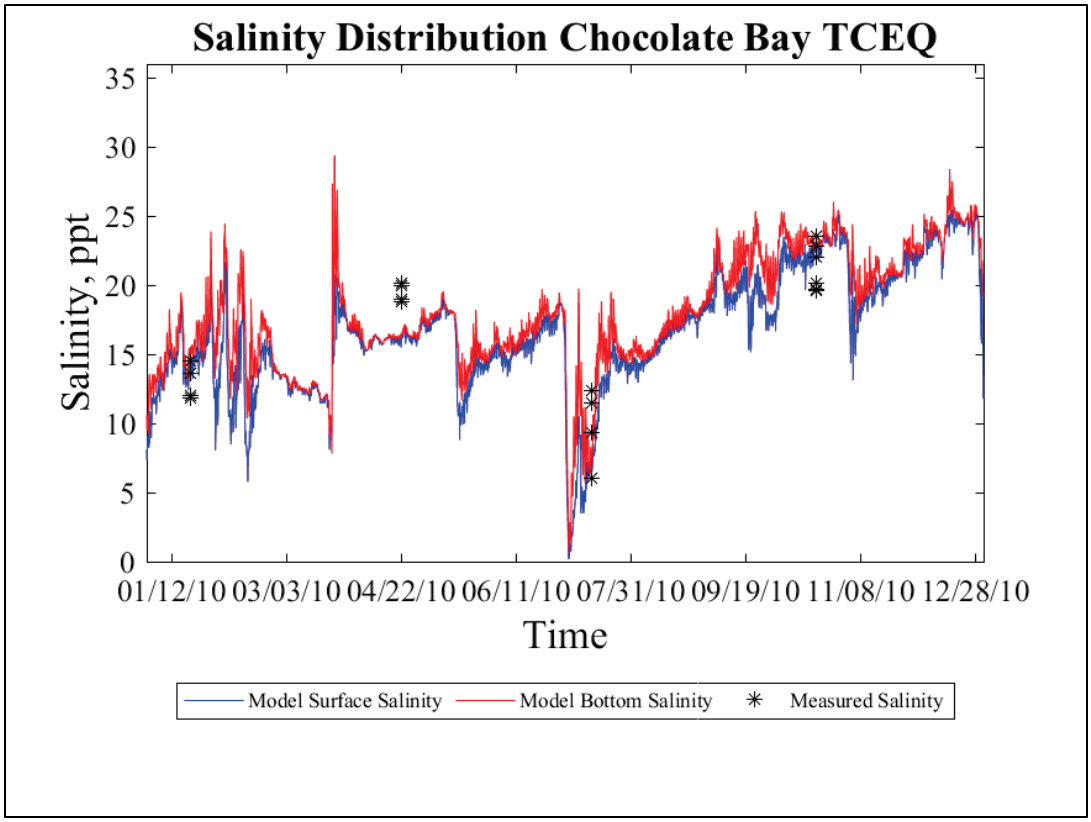
Salinity Distribution Chocolate Bay TCEQ
Salinity, ppt
0
5
10
15
20
25
30
35
01/12/10 03/03/10 04/22/10 06/11/10 07/31/10 09/19/10 11/08/10 12/28/10
Time
Model Surface Salinity
Model Bottom Salinity
Measured Salinity

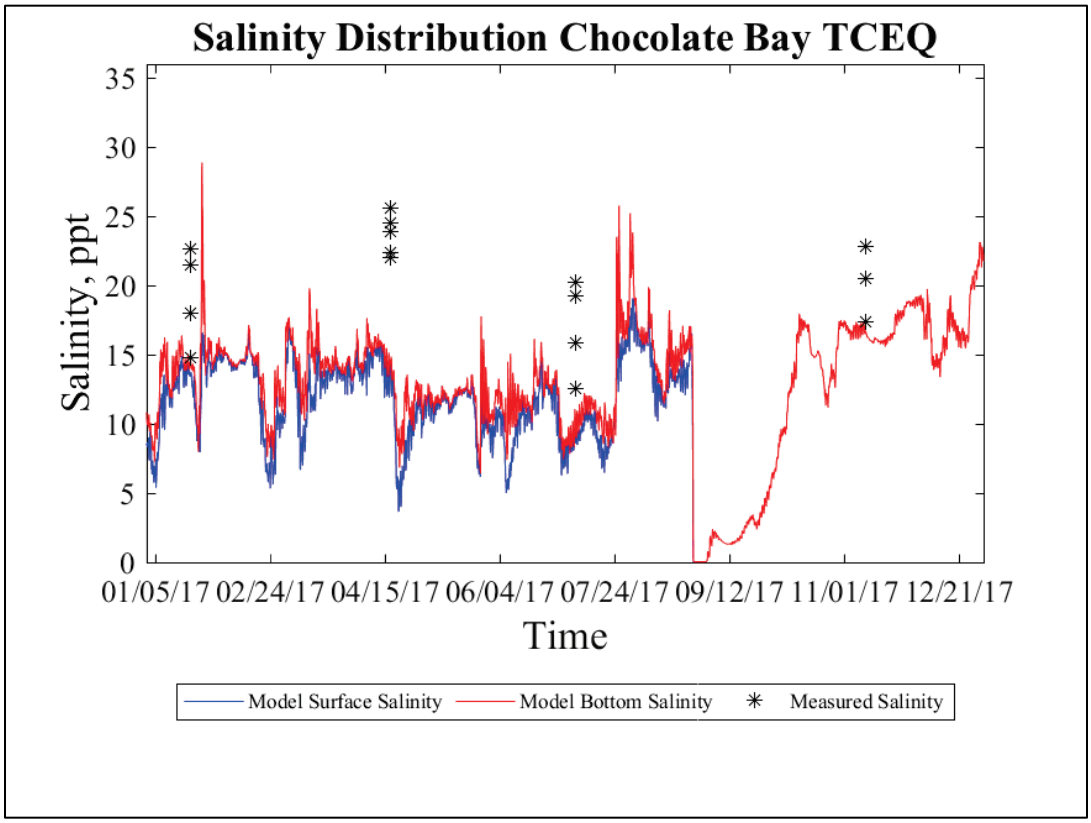
Salinity Distribution Chocolate Bay TCEQ
Salinity, ppt
0
5
10
15
20
25
30
35
01/05/17 02/24/17 04/15/17 06/04/17 07/24/17 09/12/17 11/01/17 12/21/17
Time
Model Surface Salinity
Model Bottom Salinity
Measured Salinity

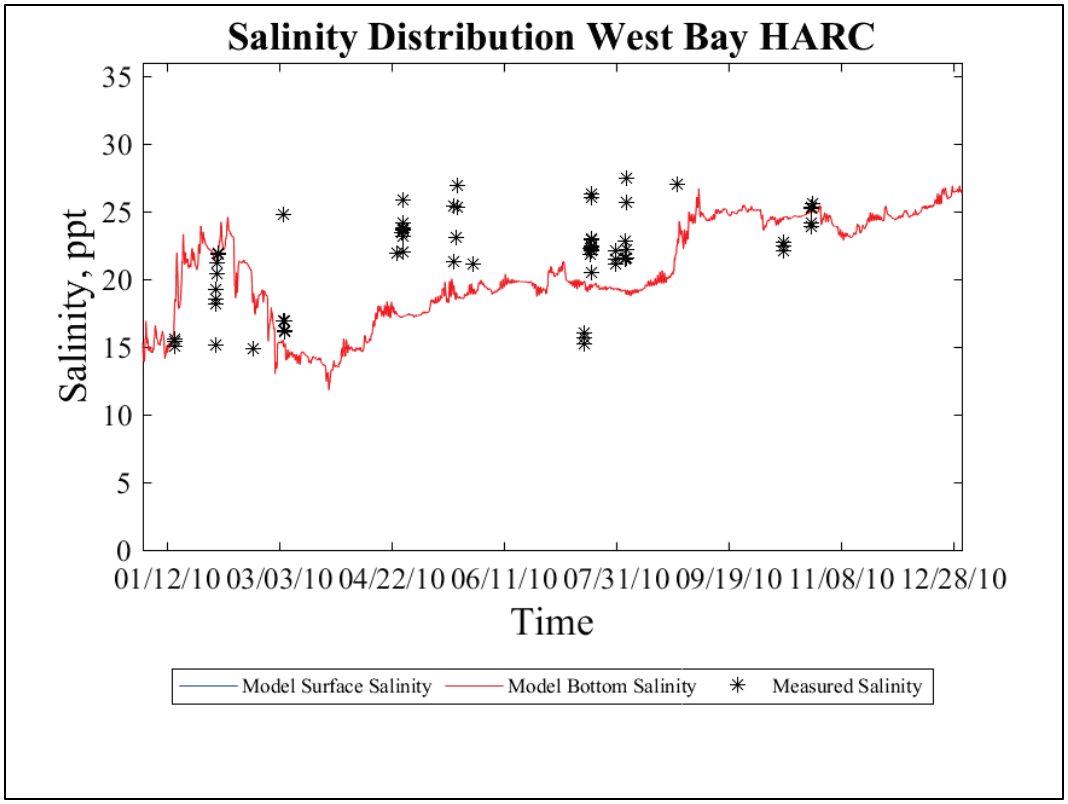
Salinity Distribution West Bay HARC
Salinity, ppt
0
5
10
15
20
25
30
35
01/12/10 03/03/10 04/22/10 06/11/10 07/31/10 09/19/10 11/08/10 12/28/10
Time
Model Surface Salinity
Model Bottom Salinity
Measured Salinity

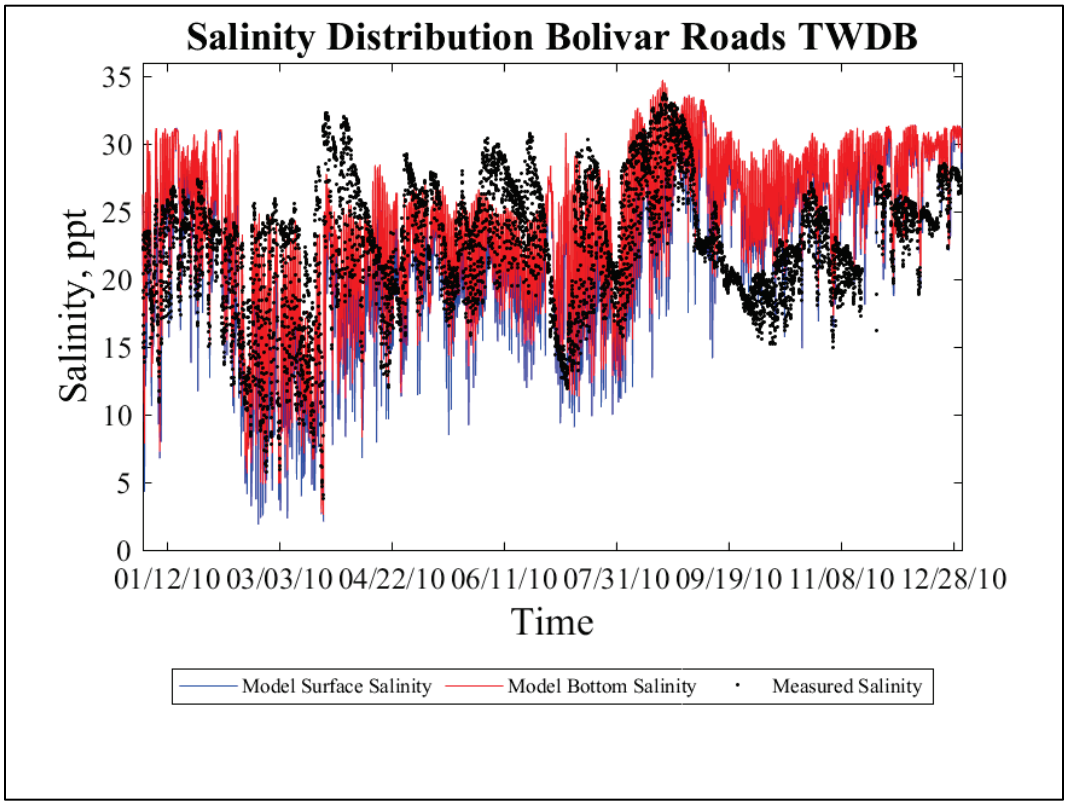
Salinity Distribution Bolivar Roads TWDB
Salinity, ppt
0
5
10
15
20
25
30
35
01/12/10 03/03/10 04/22/10 06/11/10 07/31/10 09/19/10 11/08/10 12/28/10
Time
Model Surface Salinity
Model Bottom Salinity
Measured Salinity

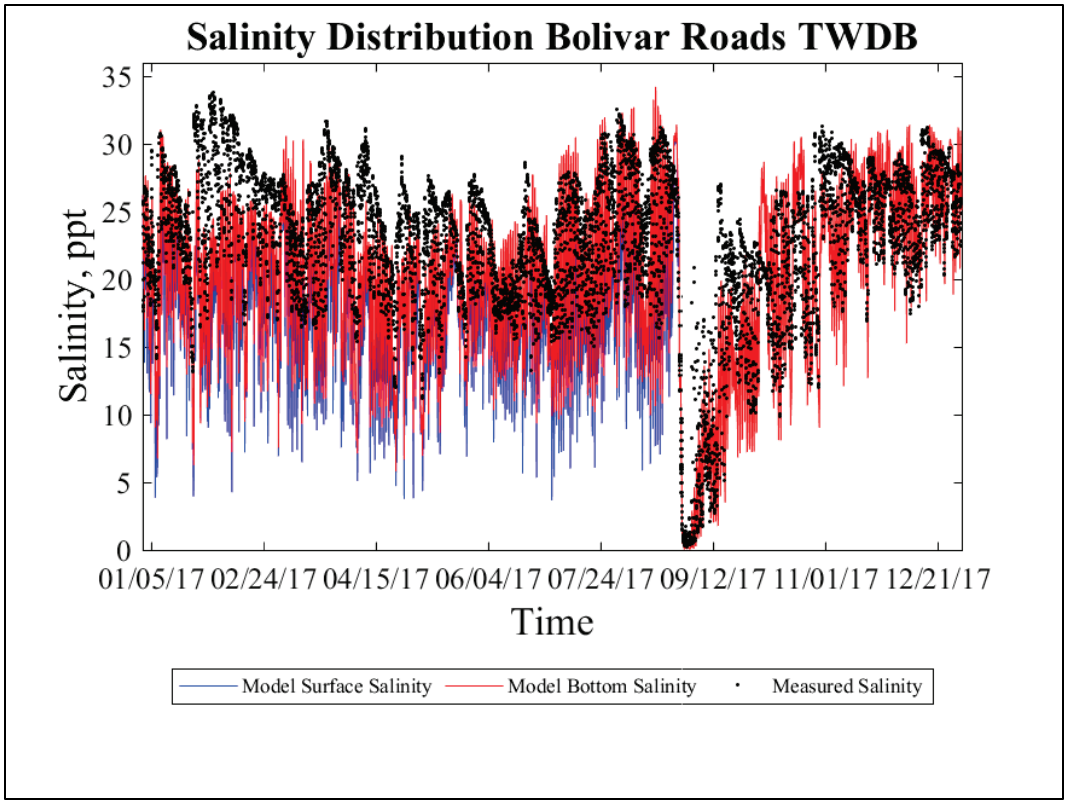
Salinity Distribution Bolivar Roads TWDB
Salinity, ppt
0
5
10
15
20
25
30
35
01/05/17 02/24/17 04/15/17 06/04/17 07/24/17 09/12/17 11/01/17 12/21/17
Time
Model Surface Salinity
Model Bottom Salinity
Measured Salinity

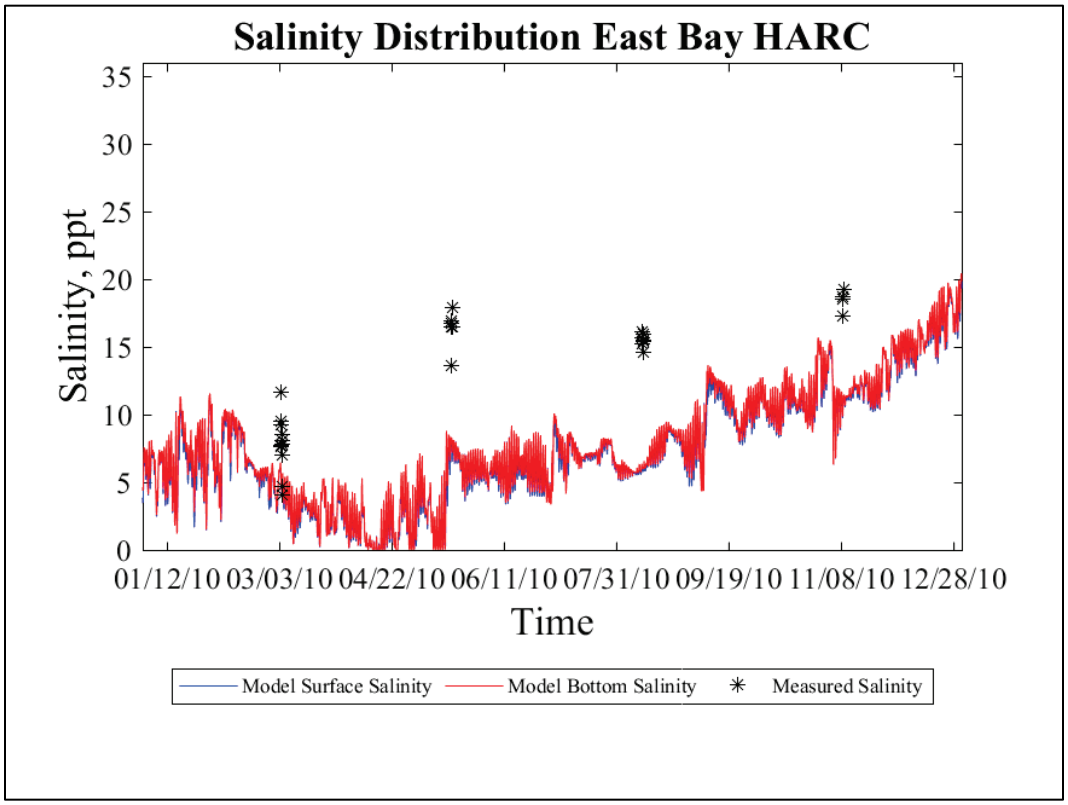
Salinity Distribution East Bay HARC
Salinity, ppt
0
5
10
15
20
25
30
35
01/12/10 03/03/10 04/22/10 06/11/10 07/31/10 09/19/10 11/08/10 12/28/10
Time
Model Surface Salinity
Model Bottom Salinity
Measured Salinity

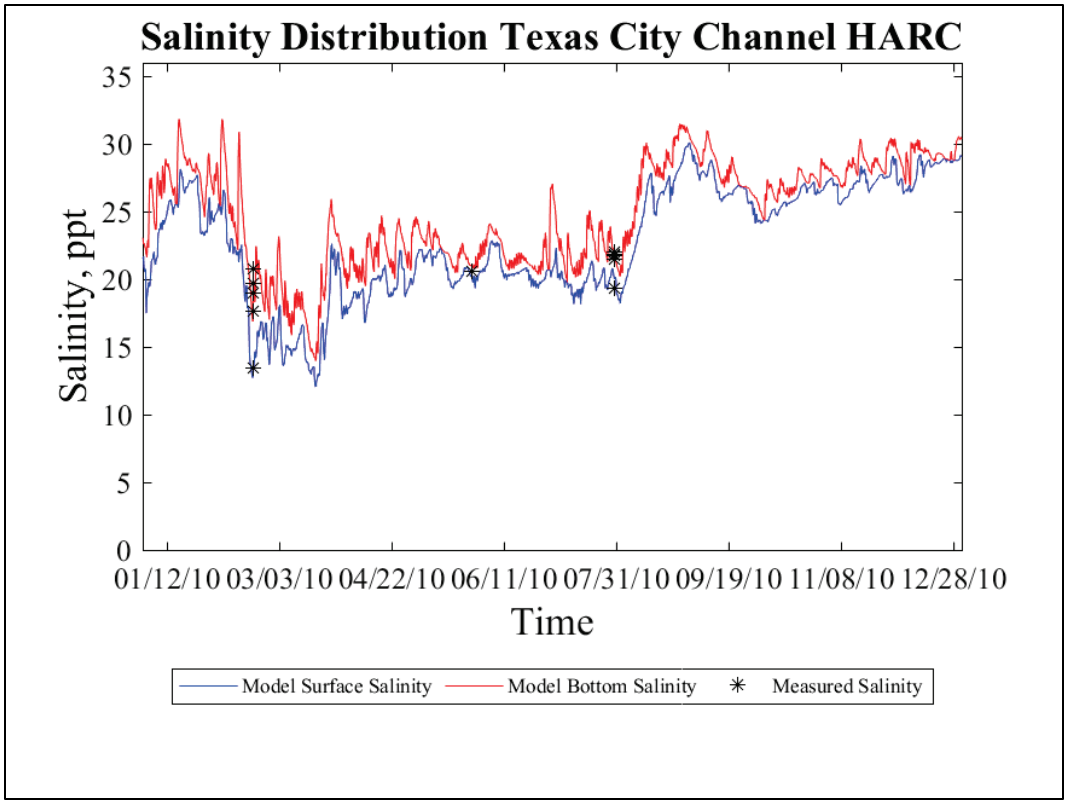
Salinity Distribution Texas City Channel HARC
Salinity, ppt
0
5
10
15
20
25
30
35
01/12/10 03/03/10 04/22/10 06/11/10 07/31/10 09/19/10 11/08/10 12/28/10
Time
Model Surface Salinity
Model Bottom Salinity
Measured Salinity

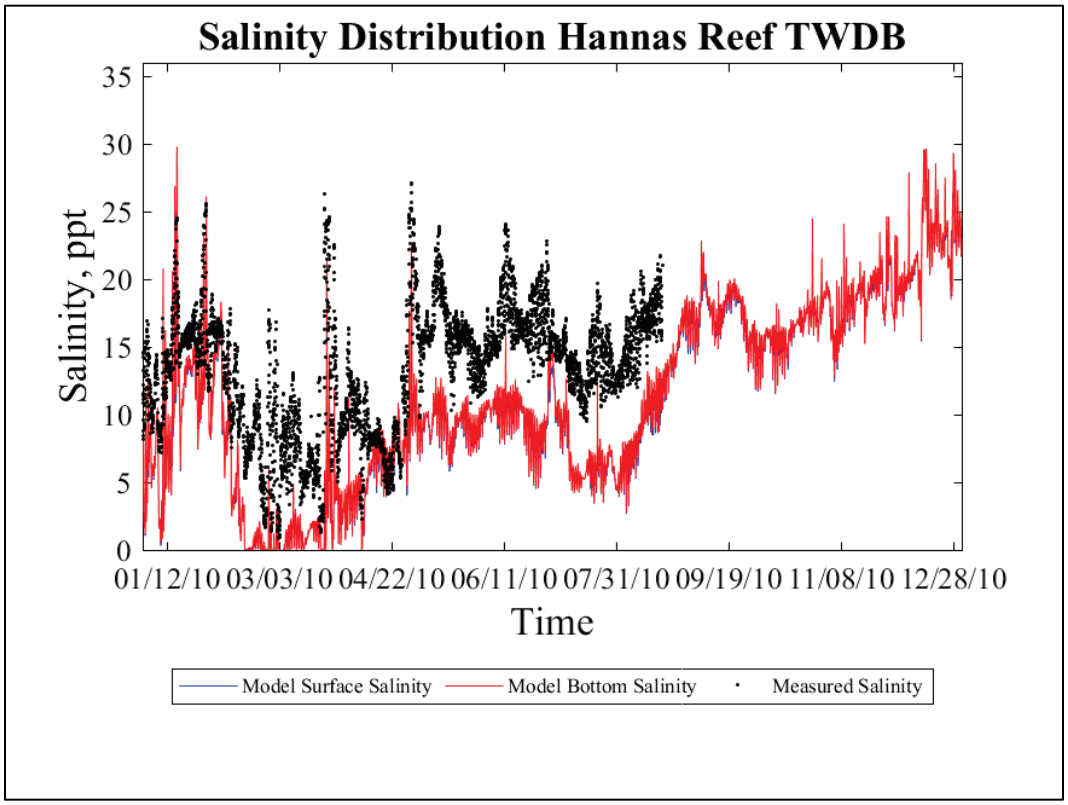
Salinity Distribution Hannas Reef TWDB
Salinity, ppt
0
5
10
15
20
25
30
35
01/12/10 03/03/10 04/22/10 06/11/10 07/31/10 09/19/10 11/08/10 12/28/10
Time
Model Surface Salinity
Model Bottom Salinity
Measured Salinity

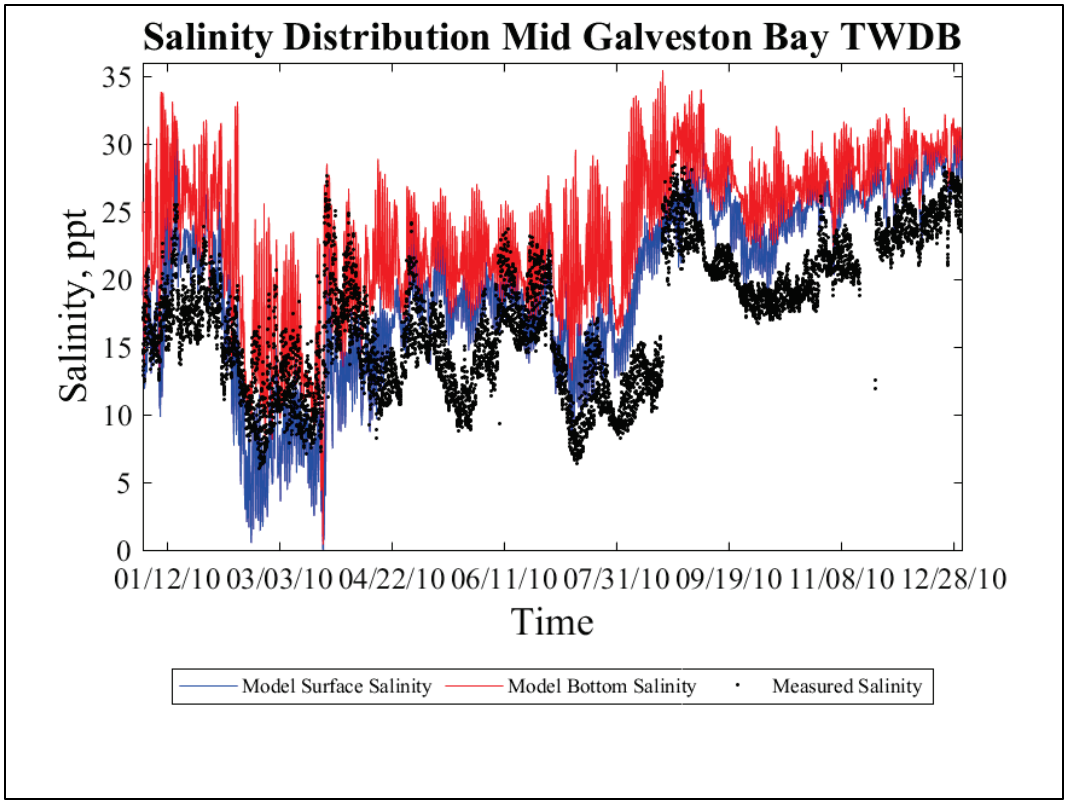
Salinity Distribution Mid Galveston Bay TWDB
Salinity, ppt
0
5
10
15
20
25
30
35
01/12/10 03/03/10 04/22/10 06/11/10 07/31/10 09/19/10 11/08/10 12/28/10
Time
Model Surface Salinity
Model Bottom Salinity
Measured Salinity

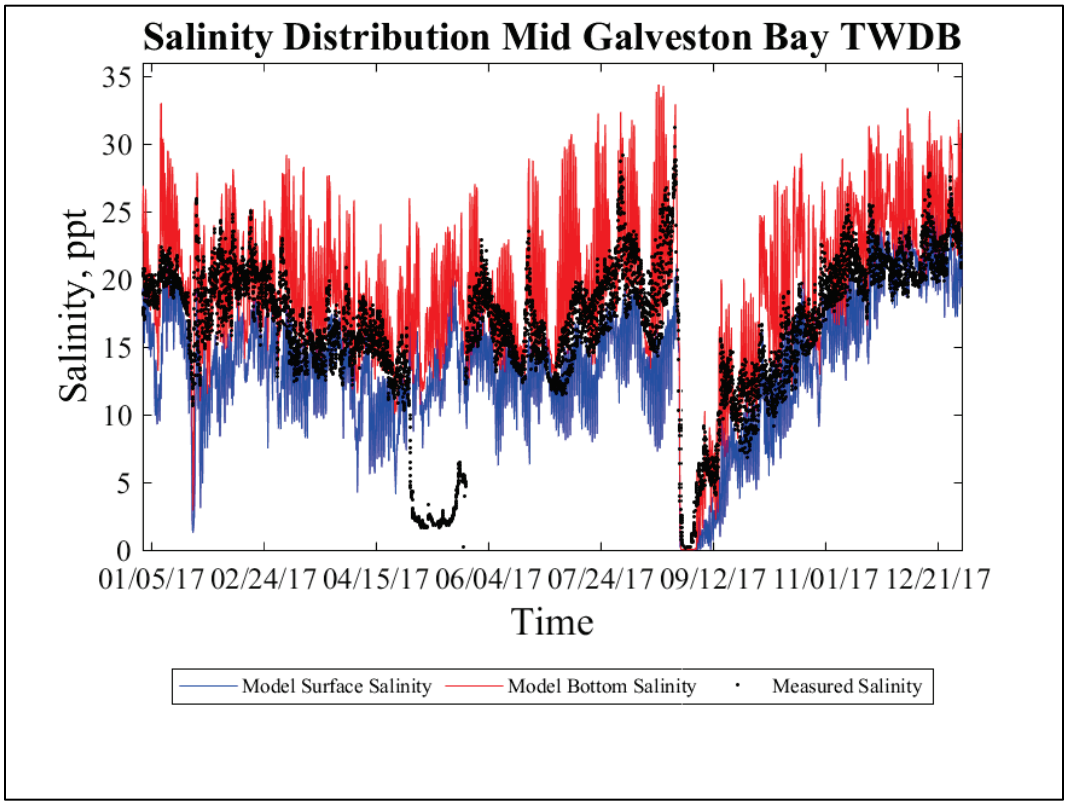
Salinity Distribution Mid Galveston Bay TWDB
Salinity, ppt
0
5
10
15
20
25
30
35
01/05/17 02/24/17 04/15/17 06/04/17 07/24/17 09/12/17 11/01/17 12/21/17
Time
Model Surface Salinity
Model Bottom Salinity
Measured Salinity

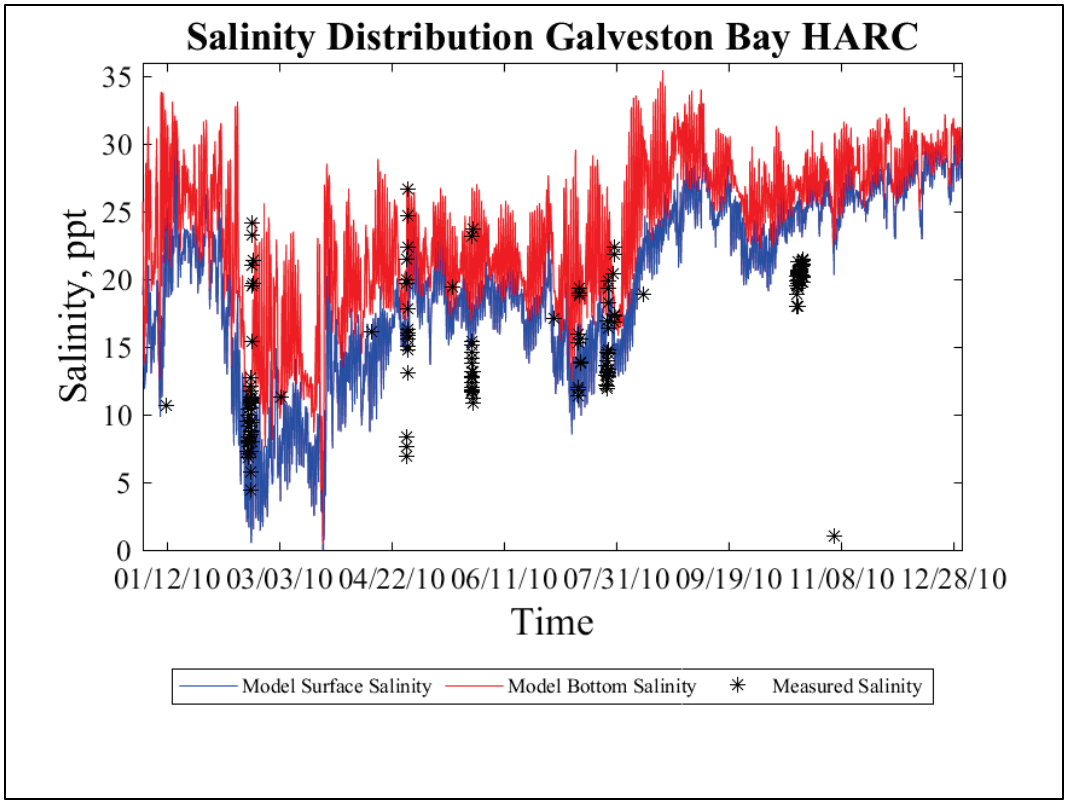
Salinity Distribution Galveston Bay HARC
Salinity, ppt
0
5
10
15
20
25
30
35
01/12/10 03/03/10 04/22/10 06/11/10 07/31/10 09/19/10 11/08/10 12/28/10
Time
Model Surface Salinity
Model Bottom Salinity
Measured Salinity

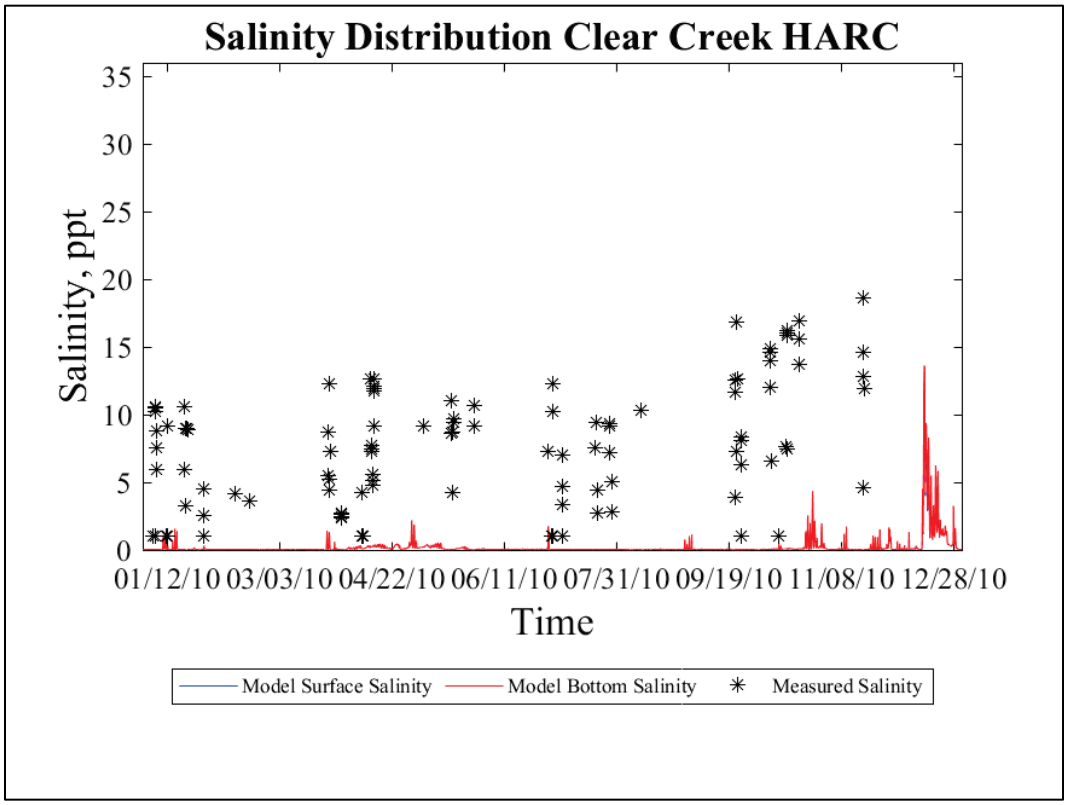
Salinity Distribution Clear Creek HARC
Salinity, ppt
0
5
10
15
20
25
30
35
01/12/10 03/03/10 04/22/10 06/11/10 07/31/10 09/19/10 11/08/10 12/28/10
Time
Model Surface Salinity
Model Bottom Salinity
Measured Salinity

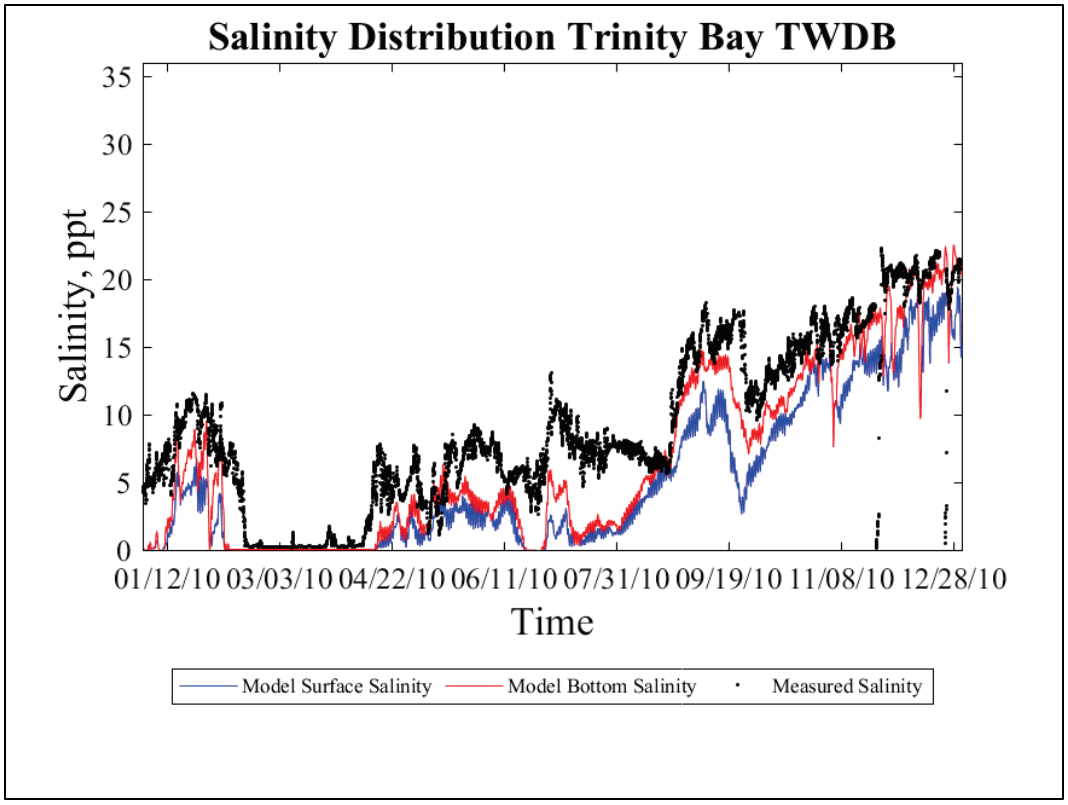
Salinity Distribution Trinity Bay TWDB
Salinity, ppt
0
5
10
15
20
25
30
35
01/12/10 03/03/10 04/22/10 06/11/10 07/31/10 09/19/10 11/08/10 12/28/10
Time
Model Surface Salinity
Model Bottom Salinity
Measured Salinity

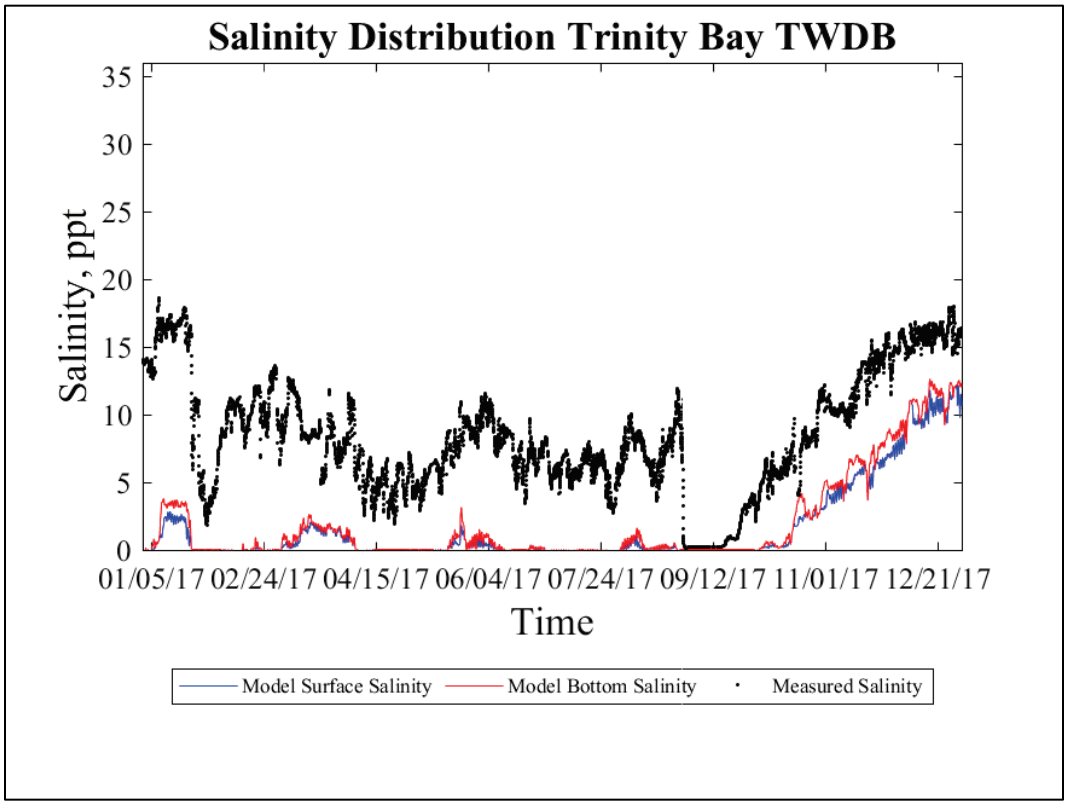
Salinity Distribution Trinity Bay TWDB
Salinity, ppt
0
5
10
15
20
25
30
35
01/05/17 02/24/17 04/15/17 06/04/17 07/24/17 09/12/17 11/01/17 12/21/17
Time
Model Surface Salinity
Model Bottom Salinity
Measured Salinity

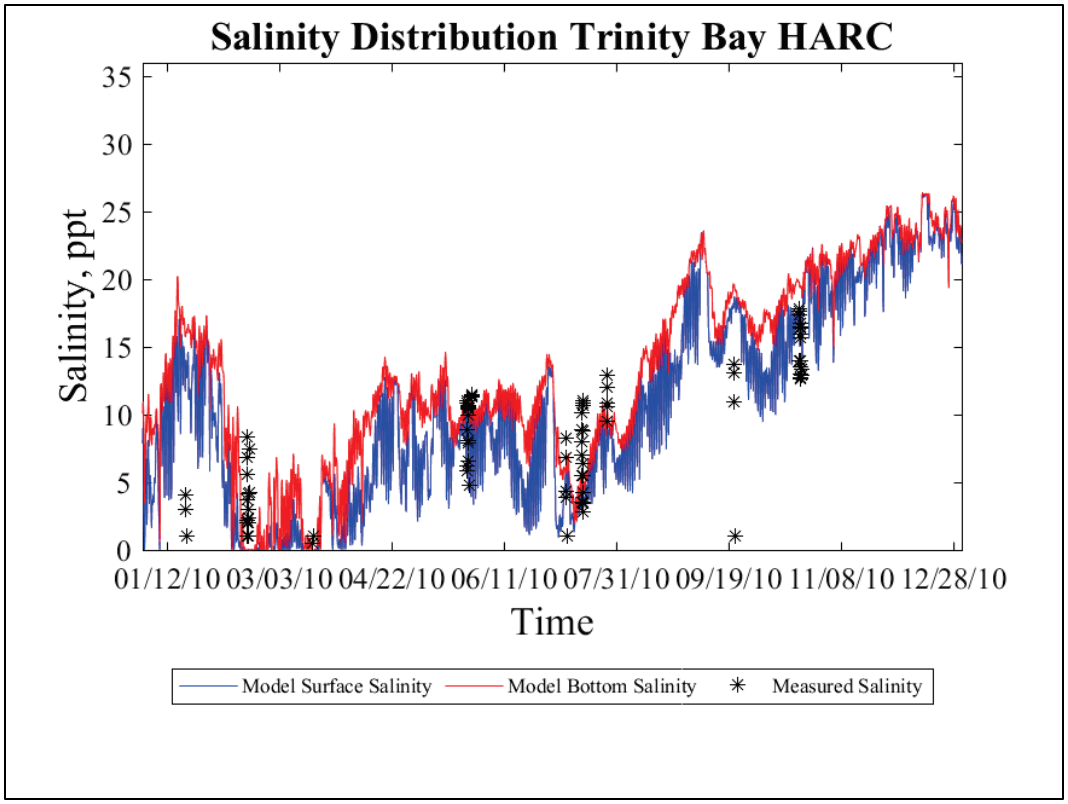
Salinity Distribution Trinity Bay HARC
Salinity, ppt
0
5
10
15
20
25
30
35
01/12/10 03/03/10 04/22/10 06/11/10 07/31/10 09/19/10 11/08/10 12/28/10
Time
Model Surface Salinity
Model Bottom Salinity
Measured Salinity

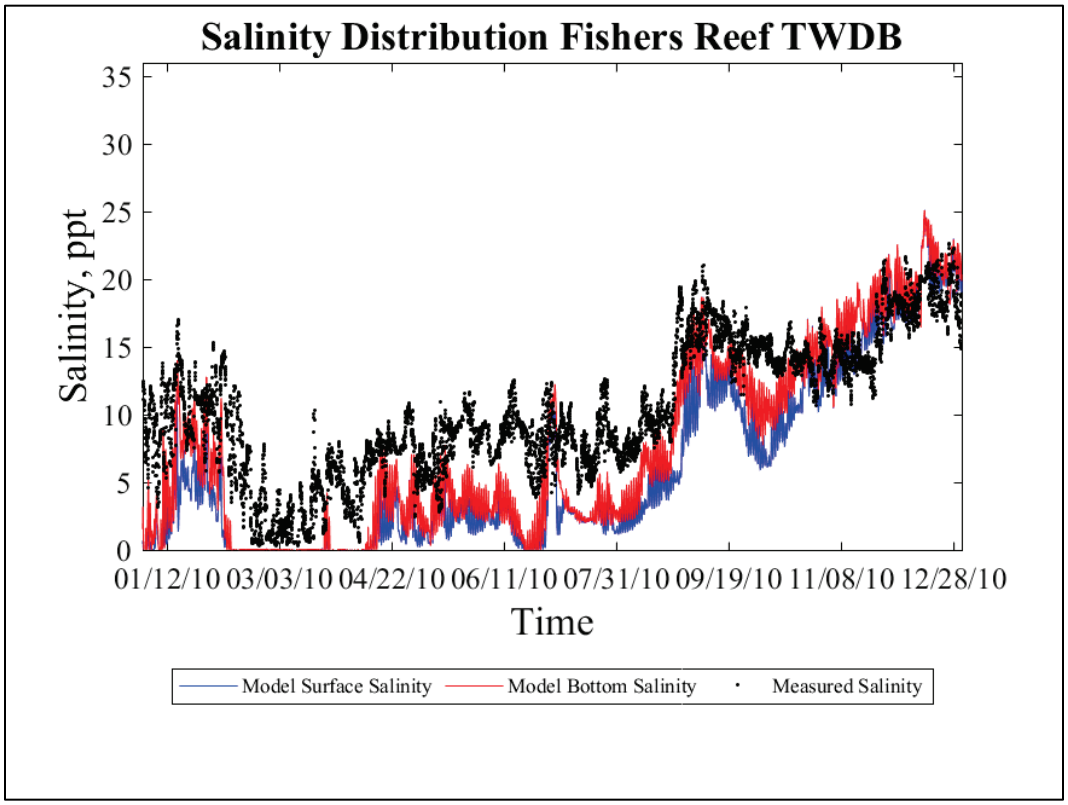
Salinity Distribution Fishers Reef TWDB
Salinity, ppt
0
5
10
15
20
25
30
35
01/12/10 03/03/10 04/22/10 06/11/10 07/31/10 09/19/10 11/08/10 12/28/10
Time
Model Surface Salinity
Model Bottom Salinity
Measured Salinity

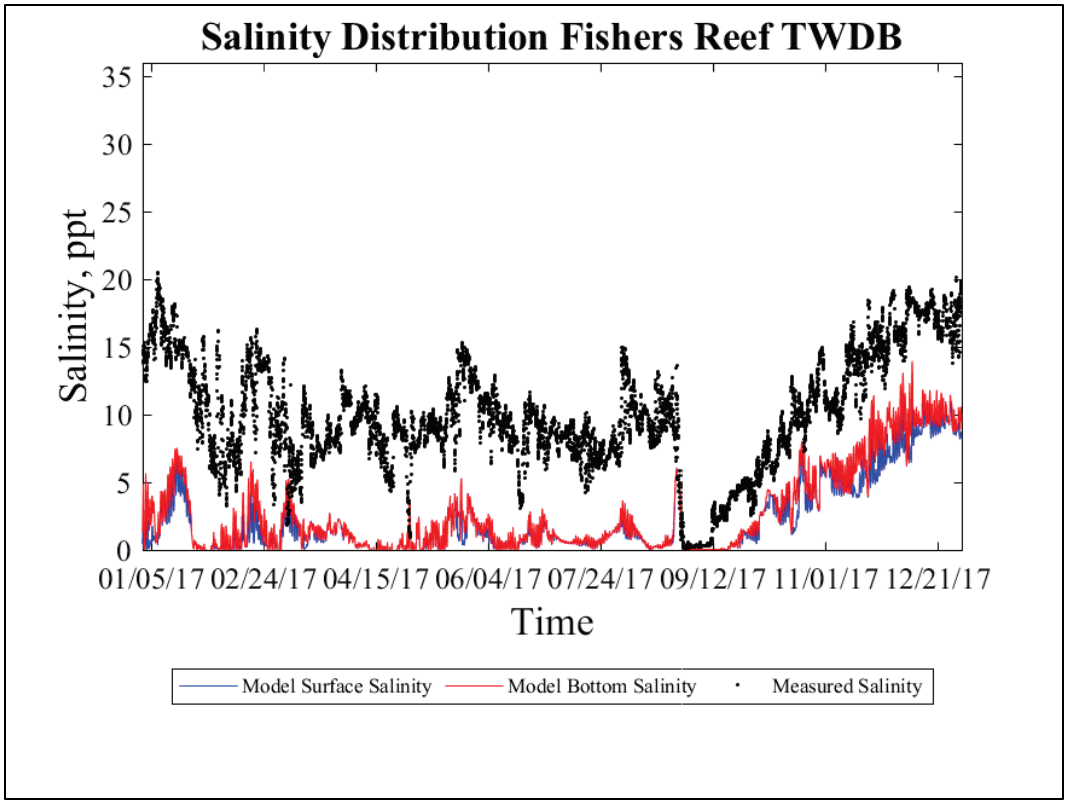
Salinity Distribution Fishers Reef TWDB
Salinity, ppt
35
30
25
20
15
10
5
0
01/05/17 02/24/17 04/15/17 06/04/17 07/24/17 09/12/17 11/01/17 12/21/17
Time
Model Surface Salinity
Model Bottom Salinity
Measured Salinity

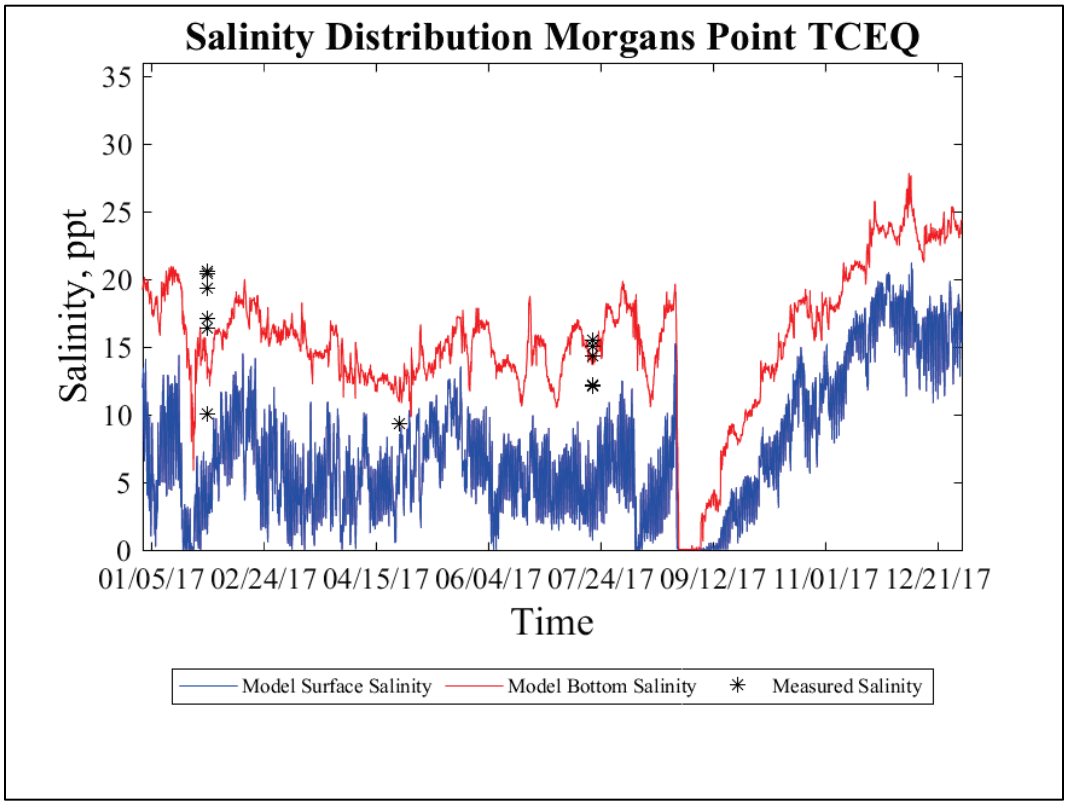
Salinity Distribution Morgans Point TCEQ
Salinity, ppt
35
30
25
20
15
10
5
0
01/05/17 02/24/17 04/15/17 06/04/17 07/24/17 09/12/17 11/01/17 12/21/17
Time
Model Surface Salinity
Model Bottom Salinity
Measured Salinity

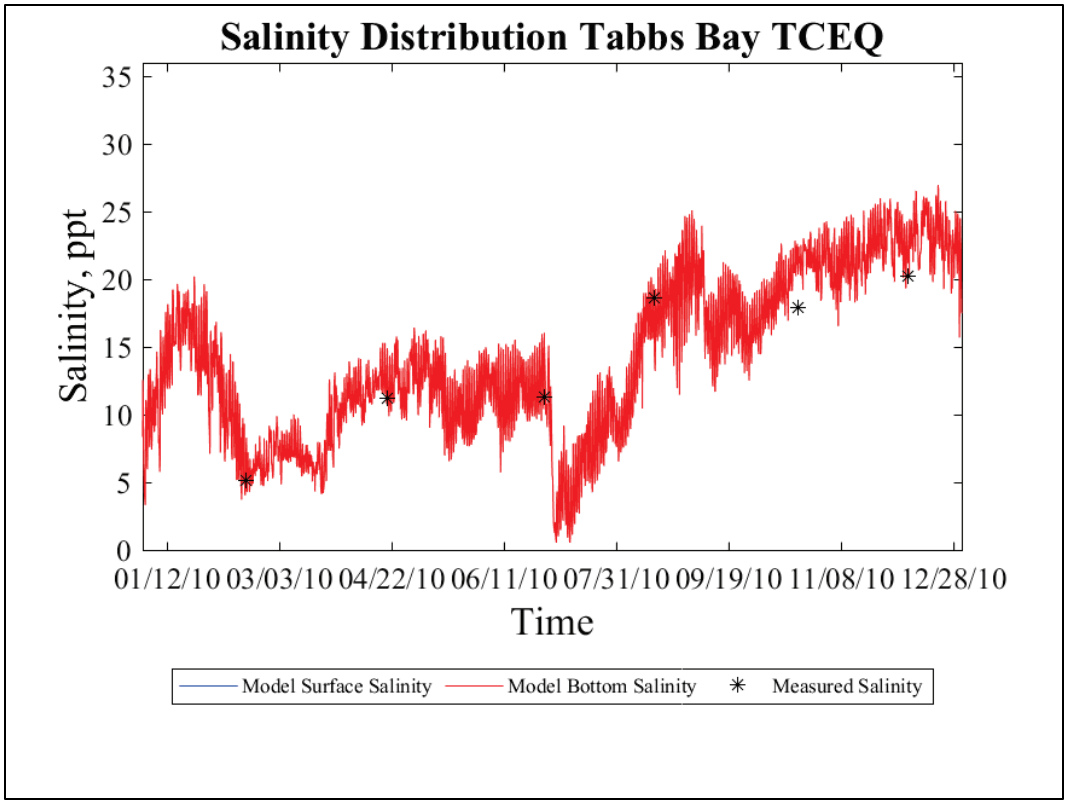
Salinity Distribution Tabbs Bay TCEQ
Salinity, ppt
0
5
10
15
20
25
30
35
01/12/10 03/03/10 04/22/10 06/11/10 07/31/10 09/19/10 11/08/10 12/28/10
Time
Model Surface Salinity
Model Bottom Salinity
Measured Salinity

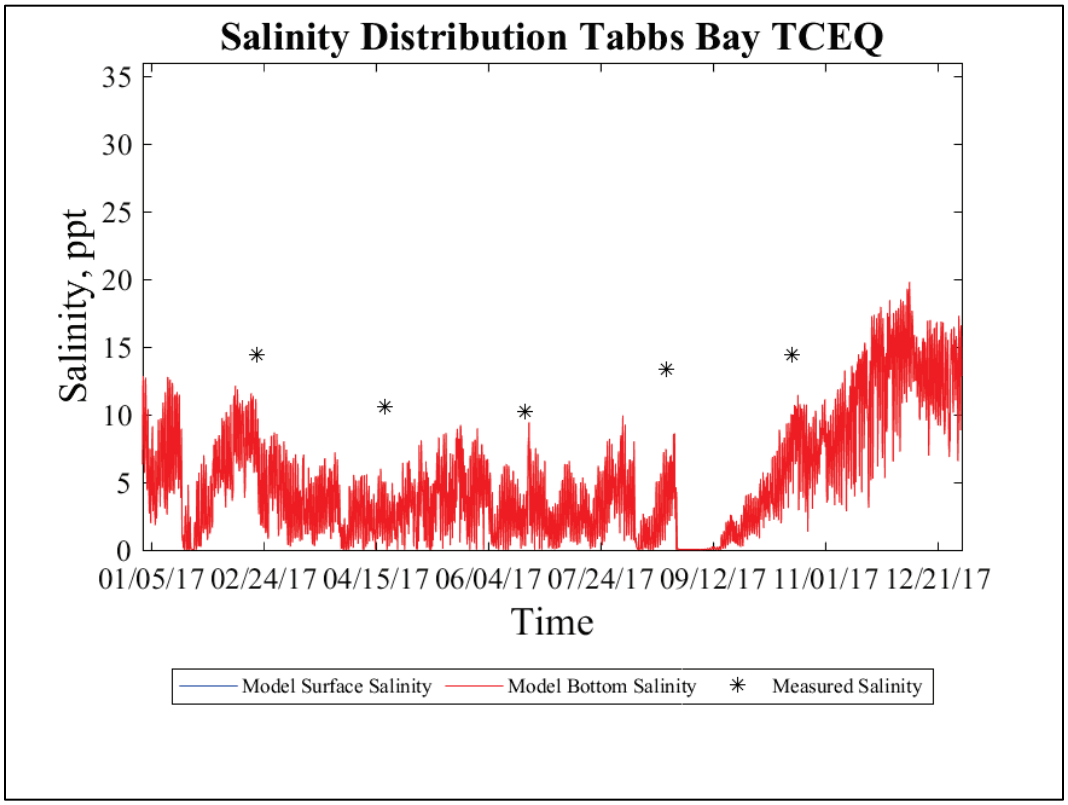
Salinity Distribution Tabbs Bay TCEQ
Salinity, ppt
0
5
10
15
20
25
30
35
01/05/17 02/24/17 04/15/17 06/04/17 07/24/17 09/12/17 11/01/17 12/21/17
Time
Model Surface Salinity
Model Bottom Salinity
Measured Salinity

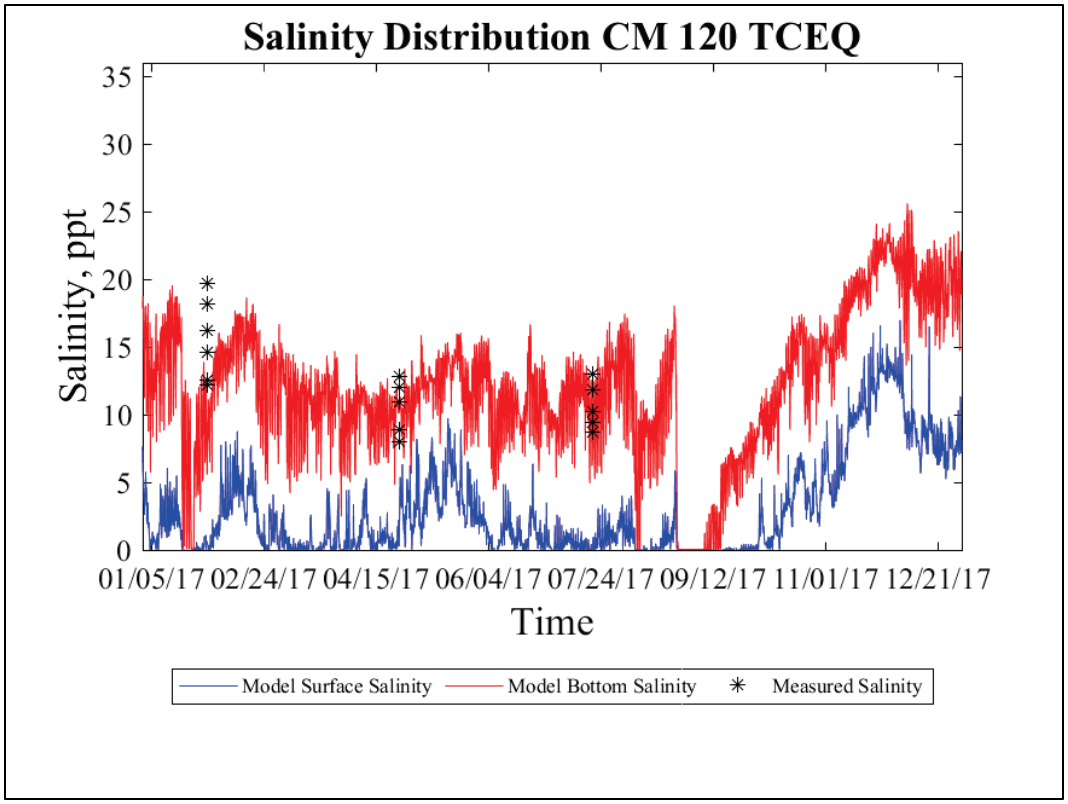
Salinity Distribution CM 120 TCEQ
Salinity, ppt
0
5
10
15
20
25
30
35
01/05/17 02/24/17 04/15/17 06/04/17 07/24/17 09/12/17 11/01/17 12/21/17
Time
Model Surface Salinity
Model Bottom Salinity
Measured Salinity

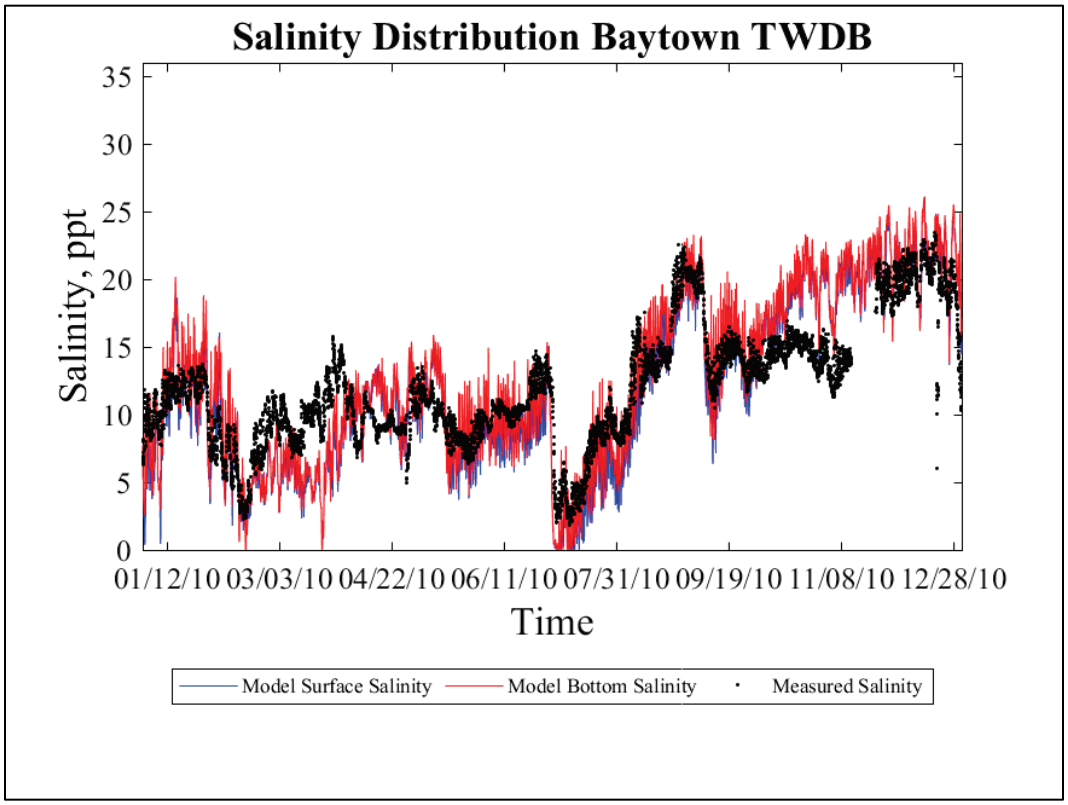
Salinity Distribution Baytown TWDB
Salinity, ppt
0
5
10
15
20
25
30
35
01/12/10 03/03/10 04/22/10 06/11/10 07/31/10 09/19/10 11/08/10 12/28/10
Time
Model Surface Salinity
Model Bottom Salinity
Measured Salinity

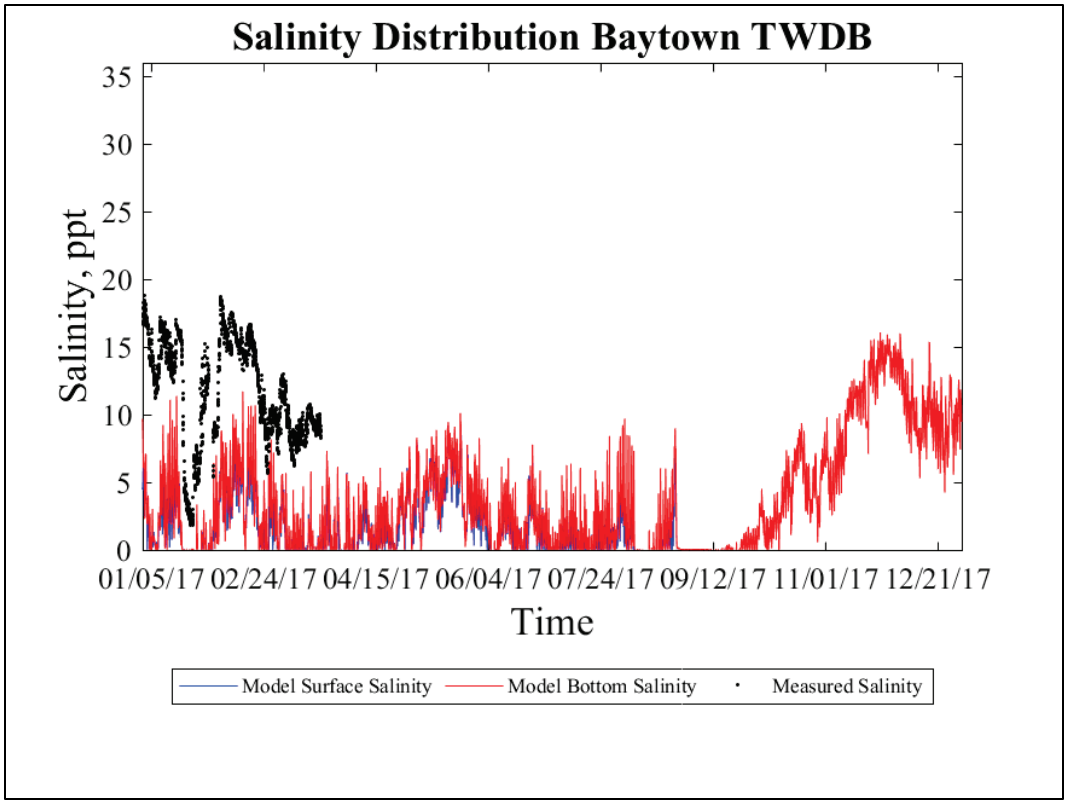
Salinity Distribution Baytown TWDB
Salinity, ppt
0
5
10
15
20
25
30
35
01/05/17 02/24/17 04/15/17 06/04/17 07/24/17 09/12/17 11/01/17 12/21/17
Time
Model Surface Salinity
Model Bottom Salinity
Measured Salinity

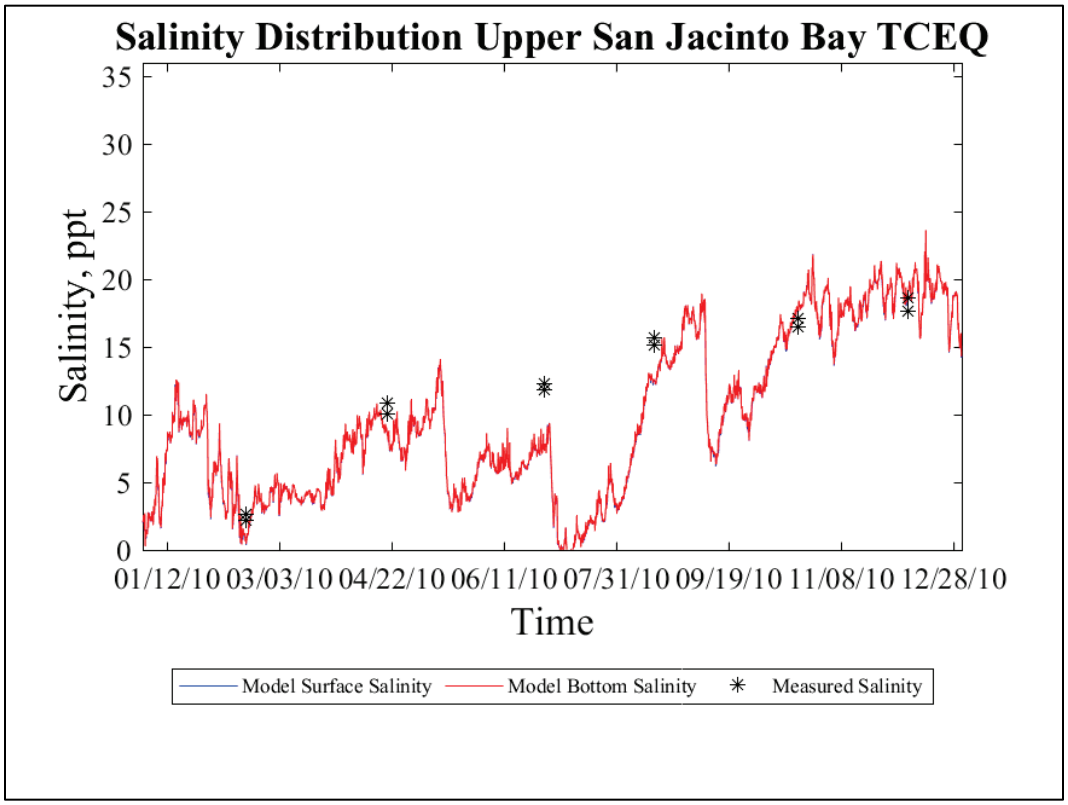
Salinity Distribution Upper San Jacinto Bay TCEQ
Salinity, ppt
0
5
10
15
20
25
30
35
01/12/10 03/03/10 04/22/10 06/11/10 07/31/10 09/19/10 11/08/10 12/28/10
Time
Model Surface Salinity
Model Bottom Salinity
Measured Salinity

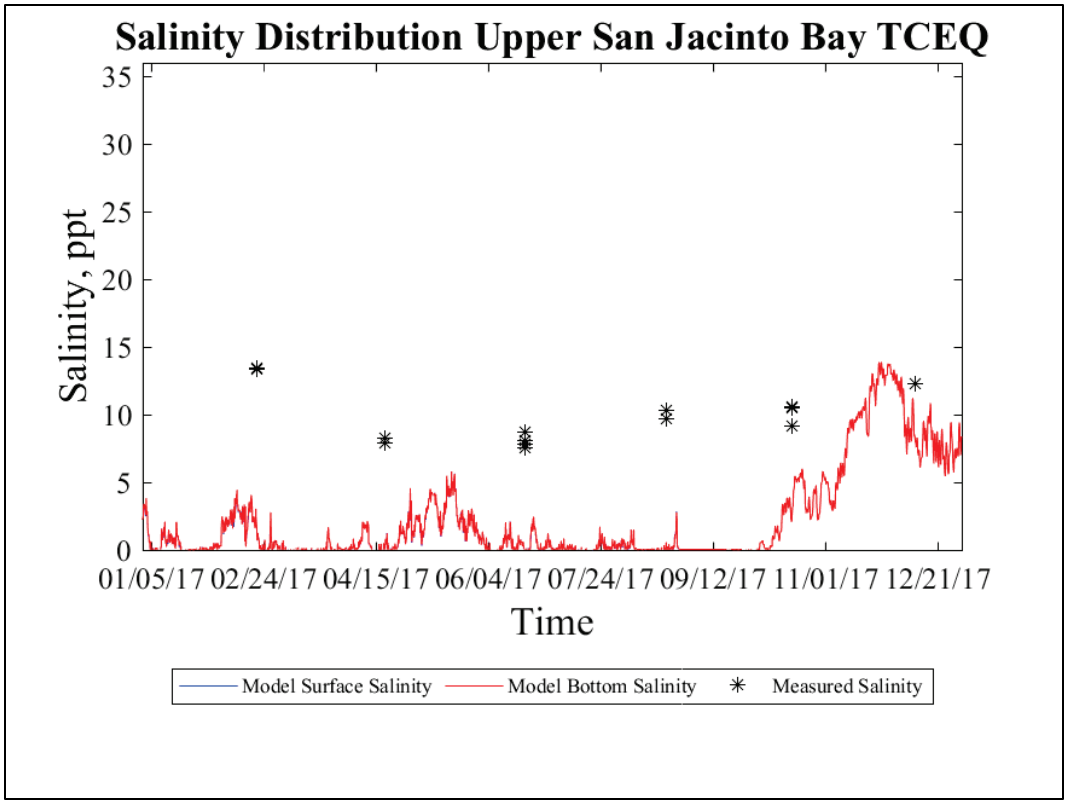
Salinity Distribution Upper San Jacinto Bay TCEQ
Salinity, ppt
0
5
10
15
20
25
30
35
01/05/17 02/24/17 04/15/17 06/04/17 07/24/17 09/12/17 11/01/17 12/21/17
Time
Model Surface Salinity
Model Bottom Salinity
Measured Salinity

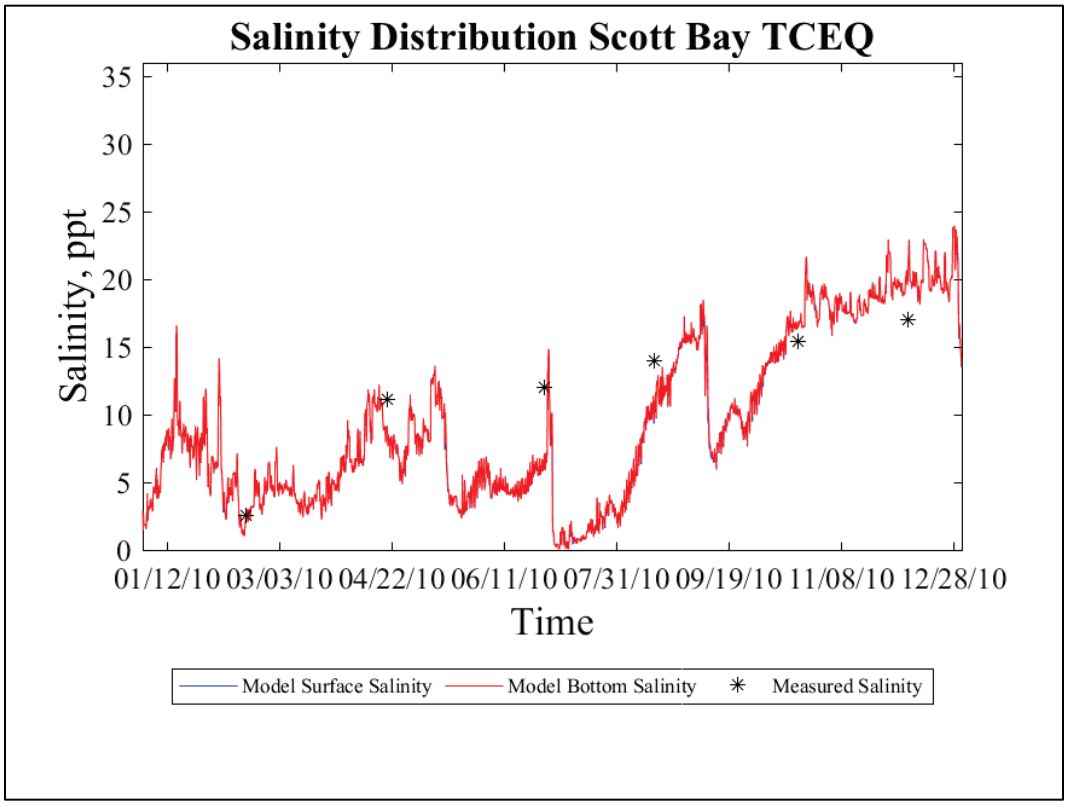
Salinity Distribution Scott Bay TCEQ
Salinity, ppt
0
5
10
15
20
25
30
35
01/12/10 03/03/10 04/22/10 06/11/10 07/31/10 09/19/10 11/08/10 12/28/10
Time
Model Surface Salinity
Model Bottom Salinity
Measured Salinity

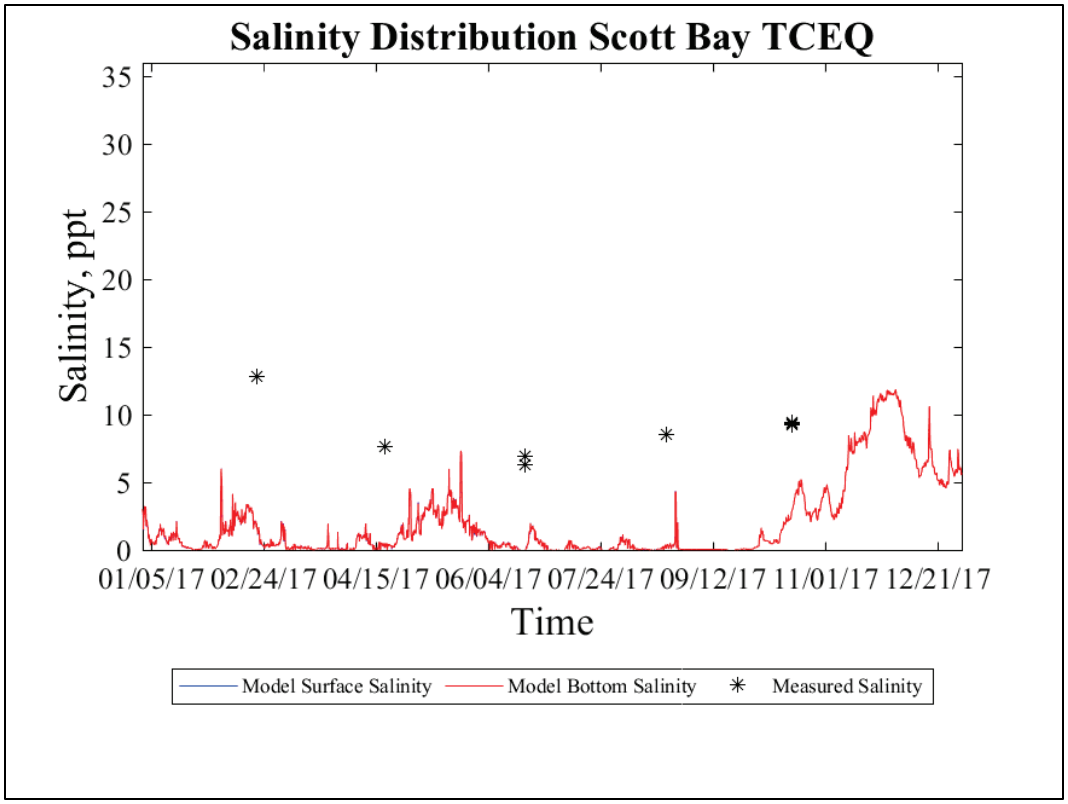
Salinity Distribution Scott Bay TCEQ
Salinity, ppt
0
5
10
15
20
25
30
35
01/05/17 02/24/17 04/15/17 06/04/17 07/24/17 09/12/17 11/01/17 12/21/17
Time
Model Surface Salinity
Model Bottom Salinity
Measured Salinity

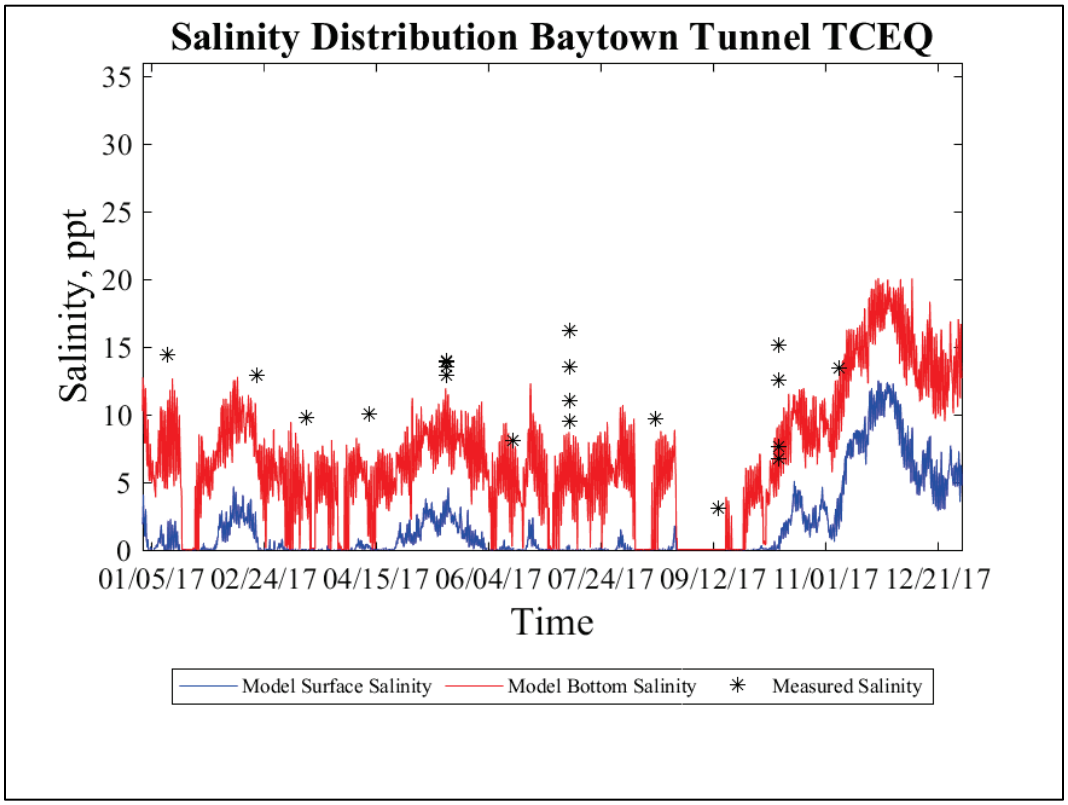
Salinity Distribution Baytown Tunnel TCEQ
Salinity, ppt
0
5
10
15
20
25
30
35
01/05/17 02/24/17 04/15/17 06/04/17 07/24/17 09/12/17 11/01/17 12/21/17
Time
Model Surface Salinity
Model Bottom Salinity
Measured Salinity

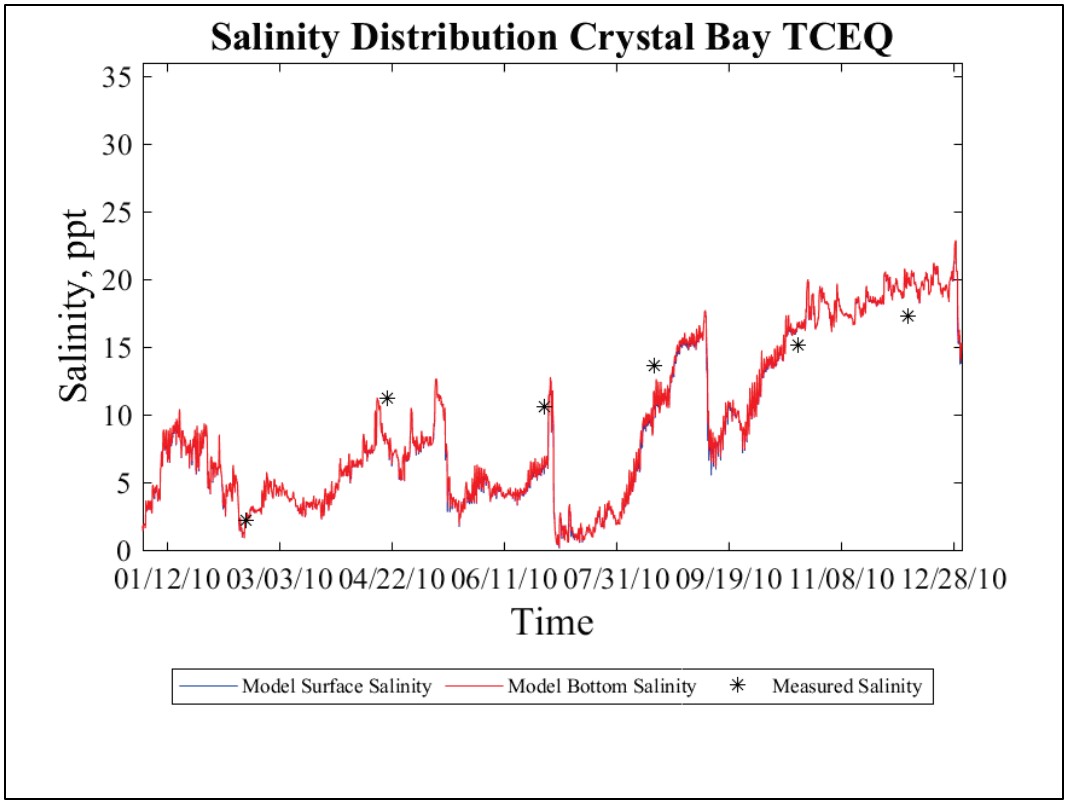
Salinity Distribution Crystal Bay TCEQ
Salinity, ppt
0
5
10
15
20
25
30
35
01/12/10 03/03/10 04/22/10 06/11/10 07/31/10 09/19/10 11/08/10 12/28/10
Time
Model Surface Salinity
Model Bottom Salinity
Measured Salinity

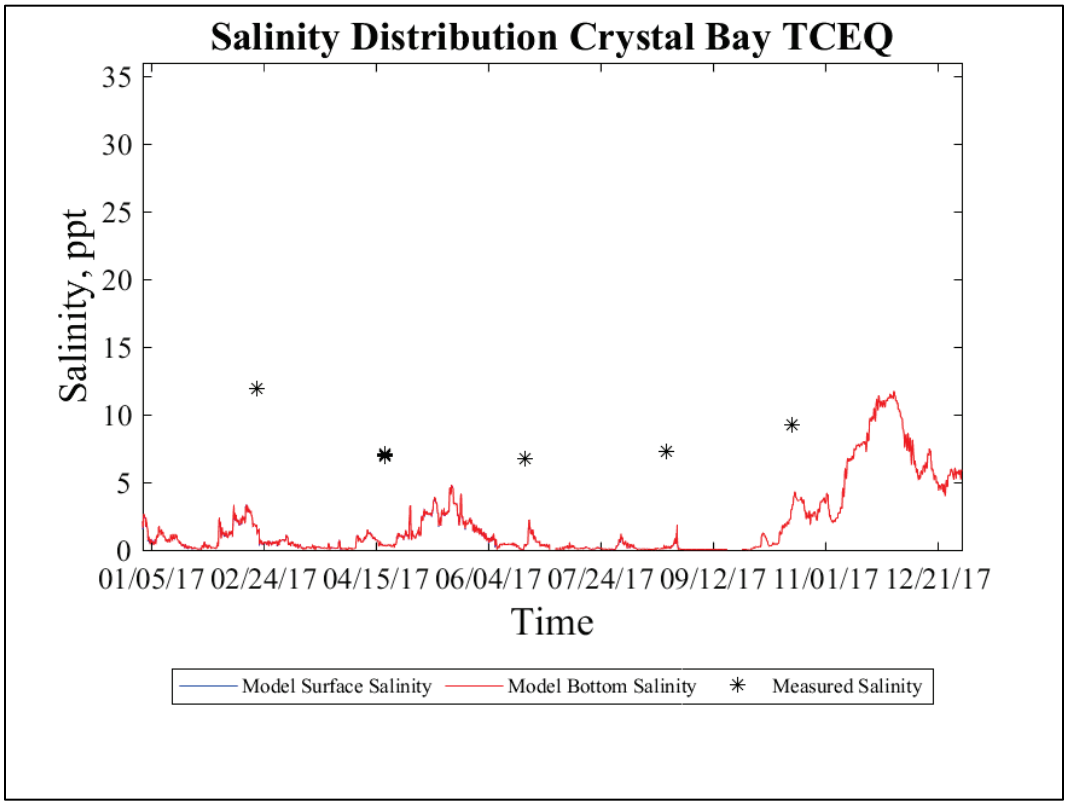
Salinity Distribution Crystal Bay TCEQ
Salinity, ppt
0
5
10
15
20
25
30
35
01/05/17 02/24/17 04/15/17 06/04/17 07/24/17 09/12/17 11/01/17 12/21/17
Time
Model Surface Salinity
Model Bottom Salinity
Measured Salinity

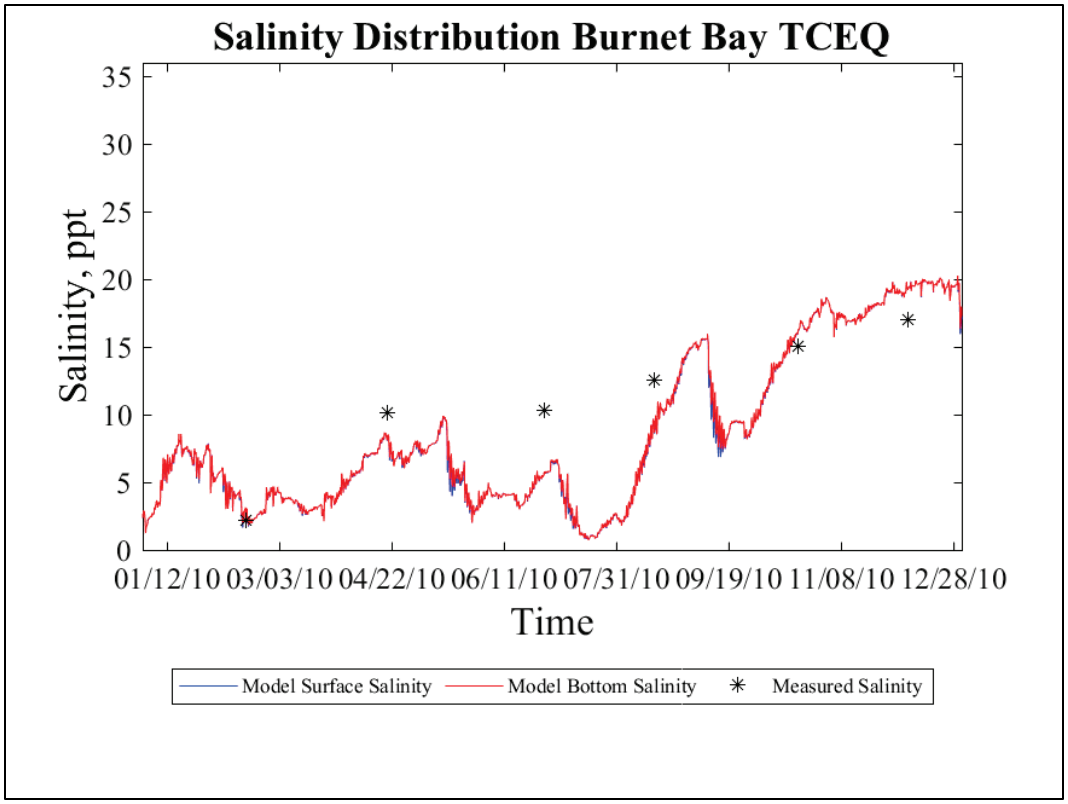
Salinity Distribution Burnet Bay TCEQ
Salinity, ppt
0
5
10
15
20
25
30
35
01/12/10 03/03/10 04/22/10 06/11/10 07/31/10 09/19/10 11/08/10 12/28/10
Time
Model Surface Salinity
Model Bottom Salinity
Measured Salinity

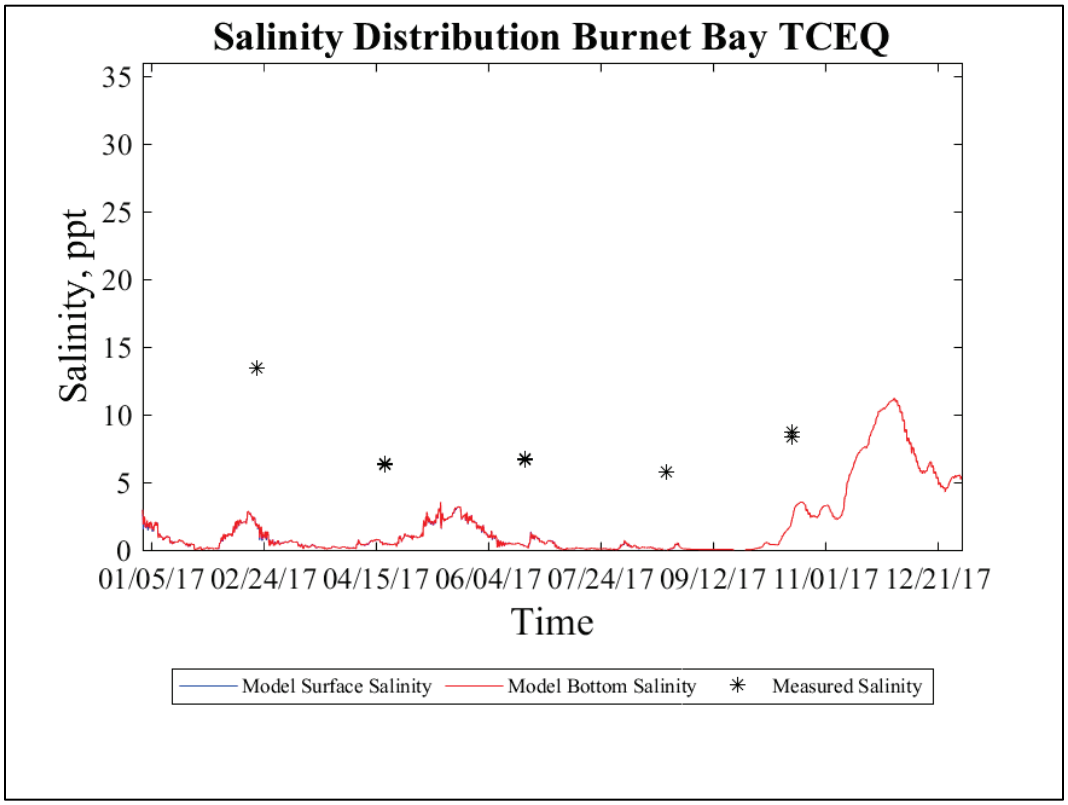
Salinity Distribution Burnet Bay TCEQ
Salinity, ppt
0
5
10
15
20
25
30
35
01/05/17 02/24/17 04/15/17 06/04/17 07/24/17 09/12/17 11/01/17 12/21/17
Time
Model Surface Salinity
Model Bottom Salinity
Measured Salinity

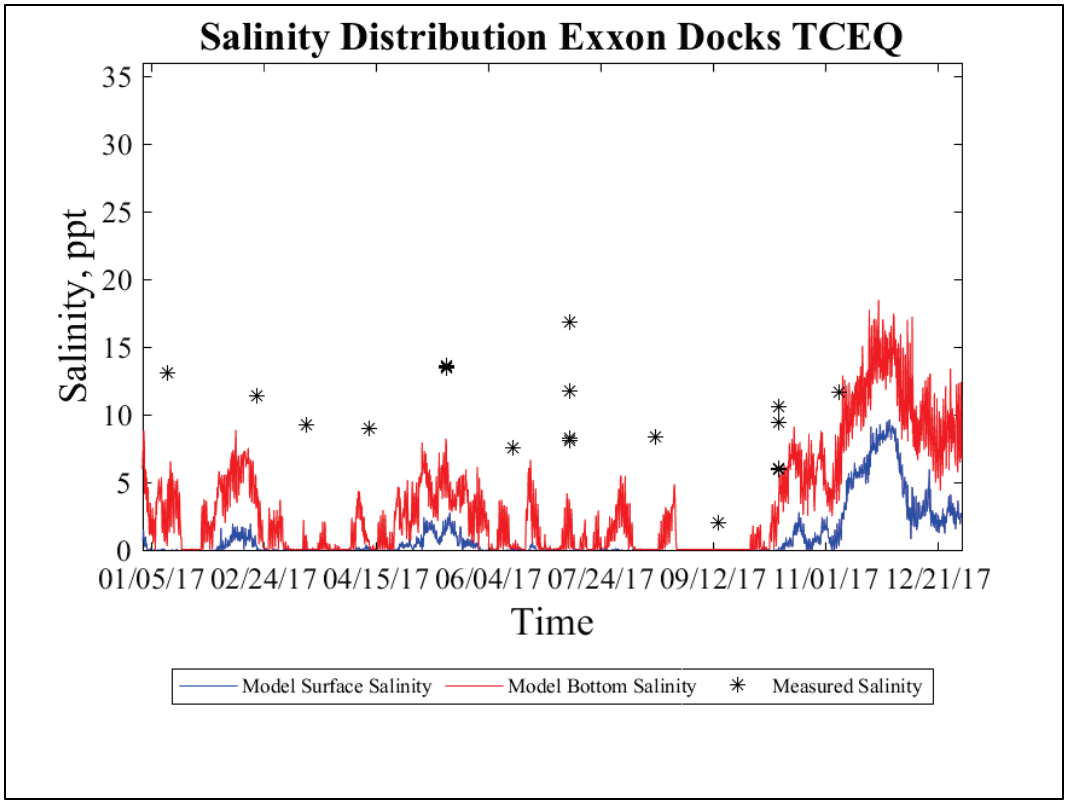
Salinity Distribution Exxon Docks TCEQ
Salinity, ppt
0
5
10
15
20
25
30
35
01/05/17 02/24/17 04/15/17 06/04/17 07/24/17 09/12/17 11/01/17 12/21/17
Time
Model Surface Salinity
Model Bottom Salinity
Measured Salinity

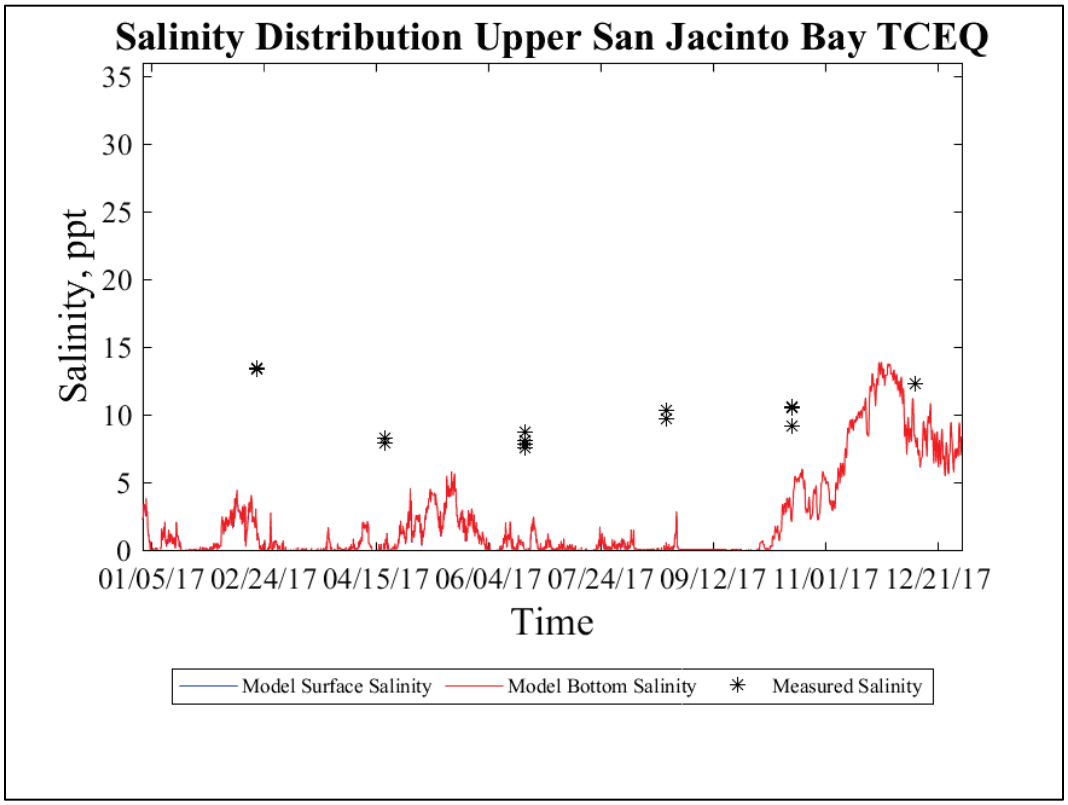
Salinity Distribution Upper San Jacinto Bay TCEQ
Salinity, ppt
0
5
10
15
20
25
30
35
01/05/17 02/24/17 04/15/17 06/04/17 07/24/17 09/12/17 11/01/17 12/21/17
Time
Model Surface Salinity
Model Bottom Salinity
Measured Salinity

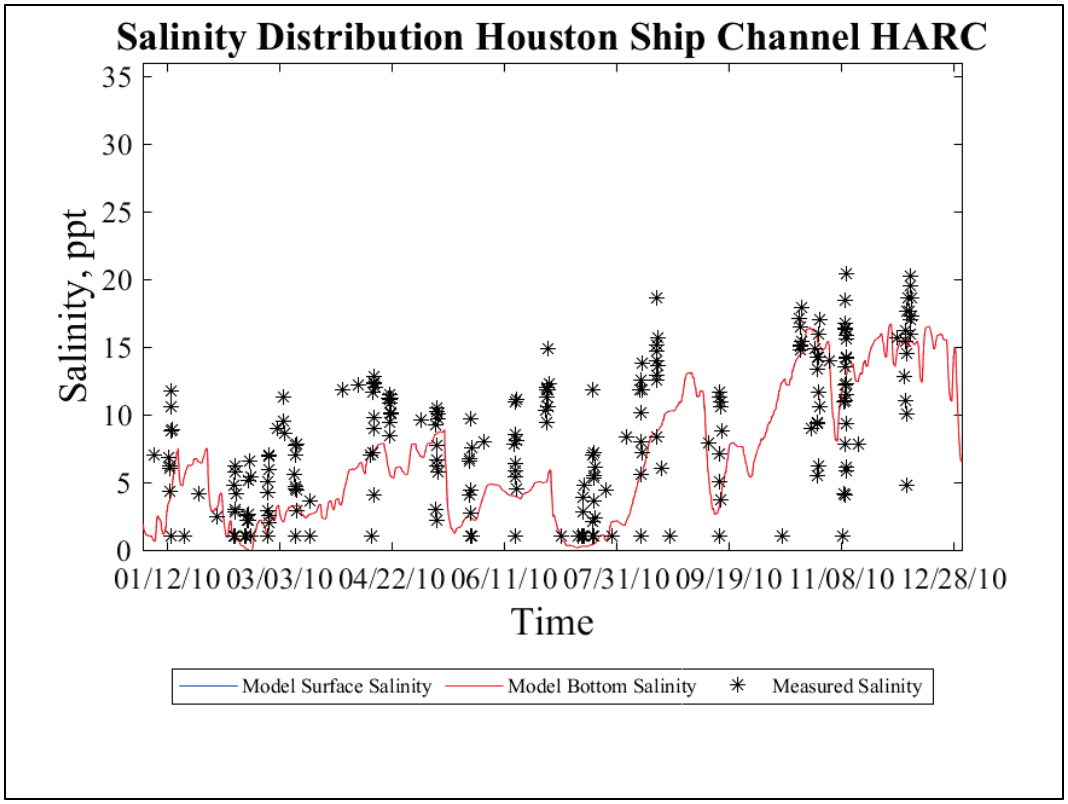
Salinity Distribution Houston Ship Channel HARC
Salinity, ppt
35
30
25
20
15
10
5
0
01/12/10
03/03/10
04/22/10
06/11/10
07/31/10
09/19/10
11/08/10
12/28/10
Time
Model Surface Salinity
Model Bottom Salinity
Measured Salinity

Abbreviations

ADCP	Acoustic Doppler current profiler
AdH	Adaptive Hydraulics
AGU	American Geophysical Union
BABUS	Bay Aquatic Beneficial Use System
CHL	Coastal and Hydraulics Laboratory
CSAT	Corps Shoaling Analysis Tool
ECIP	Expansion Channel Improvement Project
ERDC	US Army Engineer Research and Development Center
HARC	Houston Advanced Research Center
HSC	Houston Ship Channel
NAVD88	North American Vertical Datum of 1988
NOAA	National Oceanic and Atmospheric Administration
PHA	Port of Houston Authority
PORTS	Physical Oceanographic Real-Time System
SWG	Galveston District
TABS	Texas Automated Buoy System
TAMUG	Texas A&M University–Galveston
TCEQ	Texas Commission on Environmental Quality
TWDB	Texas Water Development Board
USGS	US Geological Survey
WIS	Wave Information Studies

REPORT DOCUMENTATION PAGE

1. REPORT DATE	2. REPORT TYPE	3. DATES COVERED	
		START DATE	END DATE
August 2023	Final report	FY21	FY23

4. TITLE AND SUBTITLE

Houston Ship Channel Numerical Model Update and Validation

5a. CONTRACT NUMBER	5b. GRANT NUMBER	5c. PROGRAM ELEMENT
5d. PROJECT NUMBER	**5e. TASK NUMBER**	**5f. WORK UNIT NUMBER**

6. AUTHOR(S)

Jennifer McAlpin and Cassandra Ross

7. PERFORMING ORGANIZATION NAME(S) AND ADDRESS(ES)

US Army Engineer Research and Development Center (ERDC)
Coastal and Hydraulics Laboratory (CHL)
3909 Halls Ferry Road
Vicksburg, MS 39180-6199

8. PERFORMING ORGANIZATION REPORT NUMBER

ERDC/CHL TR-23-9

9. SPONSORING/MONITORING AGENCY NAME(S) AND ADDRESS(ES)	10. SPONSOR/MONITOR'S ACRONYM(S)	11. SPONSOR/MONITOR'S REPORT NUMBER(S)
US Army Corps Engineers, Galveston District Galveston, TX 77550	USACE SWG	

12. DISTRIBUTION/AVAILABILITY STATEMENT

Distribution Statement A. Approved for public release: distribution is unlimited.

13. SUPPLEMENTARY NOTES

MIPR No. W45VAK11672077

14. ABSTRACT

The Houston Ship Channel (HSC) is one of the busiest deep-draft navigation channels in the United States and must be able to accommodate increasing vessel sizes. The US Army Corps of Engineers, Galveston District (SWG), requested the US Army Engineer Research and Development Center, Coastal and Hydraulics Laboratory, update and revalidate a previously developed three-dimensional Adaptive Hydraulics (AdH) hydrodynamic and sediment model of the HSC, Galveston, and Trinity Bays. The model is necessary for analyzing potential impacts on salinity, sediment, and hydrodynamics due to alternatives designed to reduce shoaling in the HSC.

SWG requested an updated validation of the previously developed AdH model of this area to calendar years 2010 and 2017, utilizing newly collected sediment data. Updated model inputs were supplied for riverine suspended sediment loads as well as for the ocean tidal boundary condition. The updated model shows good agreement to field data in most conditions but also indicates potential issues with freshwater flow inputs as well as the ocean salinity boundary condition.

15. SUBJECT TERMS

Coastal engineering--Mathematical models; Houston Ship Channel (Tex.); Hydrodynamics; Inland navigation; Sedimentation and deposition; Sediment transport

16. SECURITY CLASSIFICATION OF:			17. LIMITATION OF ABSTRACT	18. NUMBER OF PAGES
a. REPORT	b. ABSTRACT	C. THIS PAGE		
Unclassified	Unclassified	Unclassified	SAR	106

19a. NAME OF RESPONSIBLE PERSON	19b. TELEPHONE NUMBER (include area code)
Jennifer N. McAlpin	601-634-2511